Experimental Investigation of Silicon Dust Explosions in Pipes

Anders Bjørnsen

Master Thesis in Energy

University of Bergen

Department of Physics and Technology

Bergen, Norway

June 2023

Supervisor: Trygve Skjold

Co-Supervisor: Torfinn Buseth and Bjørn Johan Arntzen

Abstract

This thesis presents an experimental study of silicon dust explosions in different pipe configurations. The experimental configuration involved a 32-litre explosion vessel connected to pipes of different dimensions, specifically with inner diameters of 245, 157, and 62 mm and lengths ranging from 6 to 24 metres. The pipes could be connected by concentric crossovers, allowing for flexibility in the configurations.

Most of the experiments were conducted with two silicon dusts of different particle size distributions. Dust explosion parameters were decided in a 20-litre USBM explosion vessel.

The initial tests performed in single pipes gave rise to higher pressures when reducing the diameter of the pipe. Introducing crossovers to the configuration led to a significant increase in measured pressures. In the final configuration consisting of all pipes connected with gradually reducing the diameter, explosion pressures above 50 barg and shockwave velocities over 2000 m/s were observed. The significant pressures coupled with the shock velocities indicate that the propagation mechanism might be in the quasi-detonation regime or fast turbulent deflagration.

The observed pressure can be attributed to multiple contributing factors, such as compression caused by choked flow, flame acceleration resulting from flame stretching due to increased turbulence and shock interaction, and the influence of reducing diameters that intensify these effects. The presence of crossovers has been observed to enhance pre-compression, resulting in significantly higher pressures and faster pressure development.

Acknowledgements

I would like to offer my sincere gratitude to my supervisor, Trygve Skjold, for his enthusiasm and commitment throughout this project. His dedication and guidance, even during unconventional hours, have been invaluable. I am deeply grateful for my childhood friend Andreas Faye, for making this academic journey more enjoyable than one could even imagine. The countless good discussions and long hours in the workshop have been invaluable in shaping the outcome of this project.

Additionally, I would like to offer my profound thanks to Torfinn Buseth at Elkem ASA, for presenting the research problem that served as the foundation of this thesis, and his ability to address any questions throughout the project. The experiments could not have been conducted without Torfinn's involvement and Elkem's financial support. Roald and Charles at UiB deserve a heartfelt thanks for all their help, and for entrusting us with the use of the workshop. Furthermore, Mattheus van Wingerden deserves sincere gratitude for his assistance regarding instrumentation and data acquisition. As well as the staff at Gexcon Steinsland, for their warm welcome and their assistance in setting up the equipment.

Finally, I would like to express my deepest appreciation to my girlfriend and my family for their patience and unwavering support.

Disclaimer

The experimental work conducted for the thesis was so extensive that it was necessary to have two individuals collaborating on the experiments. For this reason, all experiments conducted in the pipes were carried out in collaboration with my fellow student, Andreas Faye. Including the experiments involving Si-1 in the 20-l apparatus. A total of three dusts were used during the experiments. The data obtained from one of the dust samples (Si-1) were shared, while the two others were individual.

As a result, it is expected that there will be substantial similarities in the method section of the thesis and identical results for experiments involving Si-1. The collaboration has allowed for more comprehensive experimental work.

Table of Contents

List of Tables

List of Figures

Nomenclature

Abbreviations

Barg	Bar gauge
CFD	Computational Fluid Dynamics
DESC	Dust Explosion Simulation Code, now FLACS - DustEX
LEL	Lower Explosive Limit
MIE	Minimum Ignition Energy
UEL	Upper Explosive Limit

Symbols

$D[1,0]$	Number mean diameter	m
$D[3,2]$	Sauter mean diameter	m
$D[4,3]$	Volume mean diameter	m
D_{50}	Mass median diameter	m
dc	Critical tube diameter	m
$(dP/dt)_m$	Maximum rate of pressure rise, single test	$bar \cdot s^{-1}$
$(dP/dt)_{max}$	Maximum rate of pressure rise, series of tests	$bar \cdot s^{-1}$
E_i	Ignition energy	J
K_{St}	Explosibility of dust	$bar \cdot m \cdot s^{-1}$
L/D	Length-to-diameter ratio	
M	Molar mass	$kg \cdot mol^{-1}$
P_{ci}	Pressure due to chemical igniters	bar
P_m	Maximum explosion pressure, single tests	bar
P_{max}	Maximum explosion pressure, series of tests	bar
R	Universal gas constant	$J \cdot mol^{-1} \cdot s^{-1}$
T	Absolute temperature	K
T_m	Melting temperature	K
T_b	Boiling temperature	K
$T_{adb,max}$	Adiabatic flame temperature	K
T_{pyr}	Pyrometric flame temperature	K
v	Velocity	$m \cdot s^{-1}$
c	Speed of sound	$m \cdot s^{-1}$
V	Volume	m^3
γ	Ratio of heat capacities	
λ	Detonation Cell size	m

1. Introduction

Dust explosions have been a known hazard in the process industries for over 200 years, dating back to the first recorded event in 1785 at an Italian bakery (Morozzo, 1795). Despite extensive research and significant technological advancements, dust explosions remain a persistent threat in many industries. The severe consequences of dust explosions, including loss of life, injuries, and property damage, emphasize the importance of continued research into the field of explosion safety.

1.1 Dust explosions

A dust explosion arises from the rapid combustion of finely divided flammable particles suspended in air. The intensity and speed of the combustion are highly dependent on the particle size. According to Eckhoff (2003), "*any solid material that can burn in air will do so with a violence and speed that increases with increasing degree of subdivision of the material*".

Figure 1-1 shows the fire triangle and the explosion pentagon. The fire triangle illustrates the three elements necessary for a fire – fuel, oxygen, and an ignition source. The explosion pentagon adds two additional elements, confinement, and dispersion, which are critical to understanding the dynamics of dust explosions. Confinement refers to the limited space in which a dust cloud is present or contained, such as a room, building, ventilation channel, or process equipment. Igniting a confined dust cloud can lead to a powerful explosion that generates high pressures and temperatures. Understanding the impact of confinement and dispersion is crucial in preventing dust explosions and ensuring safety in industrial settings. Many industries deal with flammable solid materials in finely divided forms, including agriculture, food processing, pharmaceuticals, chemicals, wood and paper production, textiles, mining and mineral processing, and the metalworking industries.

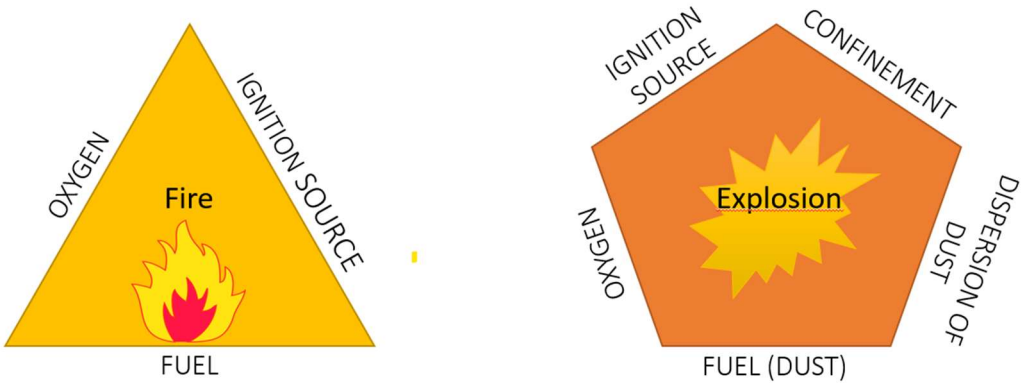

Figure 1-1: Fire triangle and the explosion pentagon (Kauffman, 1982).

1.2 Statistical records

Metal working industries is frequently impacted by dust explosions (Marmo et al., 2017). The increasing use of metal dusts in process industries has led to a rise in the number of incidents involving metal dust in recent decades (Taveau et al., 2015). Information about dust explosion accidents can be obtained from various sources, including government agency reports, organizations, and scientific publications. Several notable compilations of dust explosion incidents are mentioned below.

Beck and Jeske (1989, cited in Eckhoff, 2003, pp. 22-25) provided a comprehensive overview of reported dust explosions in Germany from 1965-1985, with 426 recorded incidents. Of these, 17.2% were associated with dust-collecting systems and 10.1% with conveying systems. It is important to note that the recorded incidents likely represent only a fraction of the incidents. Estimations suggest that recorded incidents only account for 15% of the total number of explosions, indicating that there might have been over 2400 incidents in the given timeframe.

The US Chemical Safety and Hazard Investigation Board (CSB) initiated a study on dust explosions following three deadly incidents in 2003, as documented in their report(CSB, 2006). The results were alarming, with 281 combustible dust incidents documented between 1980 and 2005, resulting in 119 fatalities, 718 injuries, and significant damage to facilities. They also found that dust collectors are the equipment most often involved in incidents.

Yuan et al. (2015) compiled a significant number of relevant dust explosion accidents. They concluded that more than 2500 incidents occurred between 1785 and 2012, which is arguably lower than the approximation made by Beck and Jeske (1989). Dust collection systems were involved in 17% of all the incidents, closely followed by conveying systems, indicating that equipment that frequently contains dust in suspended form is often involved in incidents.

Aryambayeva & van Hees (2020) researched dust explosions that involved dust collection systems in the US, Canada, and China for the past decade. Of the 143 incidents discovered, only 20 had enough information to be thoroughly investigated. The results indicated that the primary cause of physical damage was dust accumulation in production areas and within channels. The second most significant factor was issues with the dust collection systems, such as poor ventilation placement, limited options for cleaning, weak airflows, and the absence of detection systems.

The recurring frequency of dust explosions continues to pose a significant threat across various industries. Reports highlight a disturbingly high number of incidents, particularly those involving dust collection and conveying systems. Considering the dangers these events pose, the frequency of such

incidents must decrease. To achieve this, one must continue the research on dust explosions. Eckhoff (2020) highlights several areas that warrant further investigation, including:

- Dust cloud formation processes
- Dust cloud ignition processes
- Flame propagation processes in dust clouds
- Dust explosion prevention methods
- Dust explosion mitigation methods
- National and international standards

Exploring these topics in depth can give a better understanding of the underlying causes of dust explosions and could help the industries to develop more effective strategies for preventing them.

1.3 Case histories

1.3.1 Bremanger, Norway

In 1972, Elkem experienced a devastating accident at its plant in Bremanger, resulting in the loss of five lives, injuries to four others, and extensive property damage (Eckhoff, 2003). The milling section in the silicon plant had been shut down for maintenance, but the dust extraction system was still operational. The explosion caused most of the process equipment to bend or crack, and almost all the panel walls in the factory were blown out. Witnesses reported a bright, almost white light, with people over 100 meters away suffering burns. The explosion was consistent with the combustion of silicon, which burns at a very high flame temperature.

Investigation revealed that the explosion originated in a pipe that transported silicon powder from the screens to a silo. It is assumed that the pipe's interior was not cleaned before the work began, and it was most likely covered with a layer of silicon dust on the inside. The leading hypothesis is that a cutting torch dispersed and ignited the dust layer. The initial explosion suspended accumulated dust and caused subsequent explosions that propagated throughout the plant.

The accident at Elkem underscores the importance of regular cleaning of equipment and the necessity of safety protocols to prevent such incidents from occurring.

1.3.2 Kunshan, China:

On August 2, 2014, one of the most catastrophic dust explosions of modern times occurred in Kunshan, China, where 146 people lost their lives, and 114 got injured in a factory where various metallic components were polished (Li et al., 2016). The incident occurred in the morning after the workday had started and resulted in an economic loss of approximately 351 million Yuan, or nearly 500 million NOK.

The primary explosion started in one of the eight dust filters, propagated through ventilation ducts, and caused secondary explosions throughout the factory. According to the investigation following the accident, the explosion was caused by aluminium dust generated during polishing operations. The ignition source was likely due to self-heating in the dust collector under one of the filter units. The particle sizes had a D50 equal to 19 µm. The extensive propagation of the dust explosion throughout the factory would not have been possible unless considerable amounts of dust had been allowed to accumulate over time throughout the plant. It is recommended that regular and efficient removal of accumulated dust should be implemented in any plant facing a dust explosion risk.

1.4 Dust extraction systems

Dust extraction systems are a combination of different equipment, intended to remove airborne dusts from the environment, by capturing and conveying it to dust collectors. Typically, an extraction system consists of hoods, ducts, pipes, filters, and a fan package. However, a significant concern regarding dust extraction systems, which may explain their involvement in numerous incidents, is that they inherently support two sides of the explosion pentagon – confinement and dispersion.

Dust extraction systems typically consist of intricate networks of ductwork or piping of different dimensions, crossover sections, and bends to change directions. Figure 1-2 illustrate a typical dust extraction type.

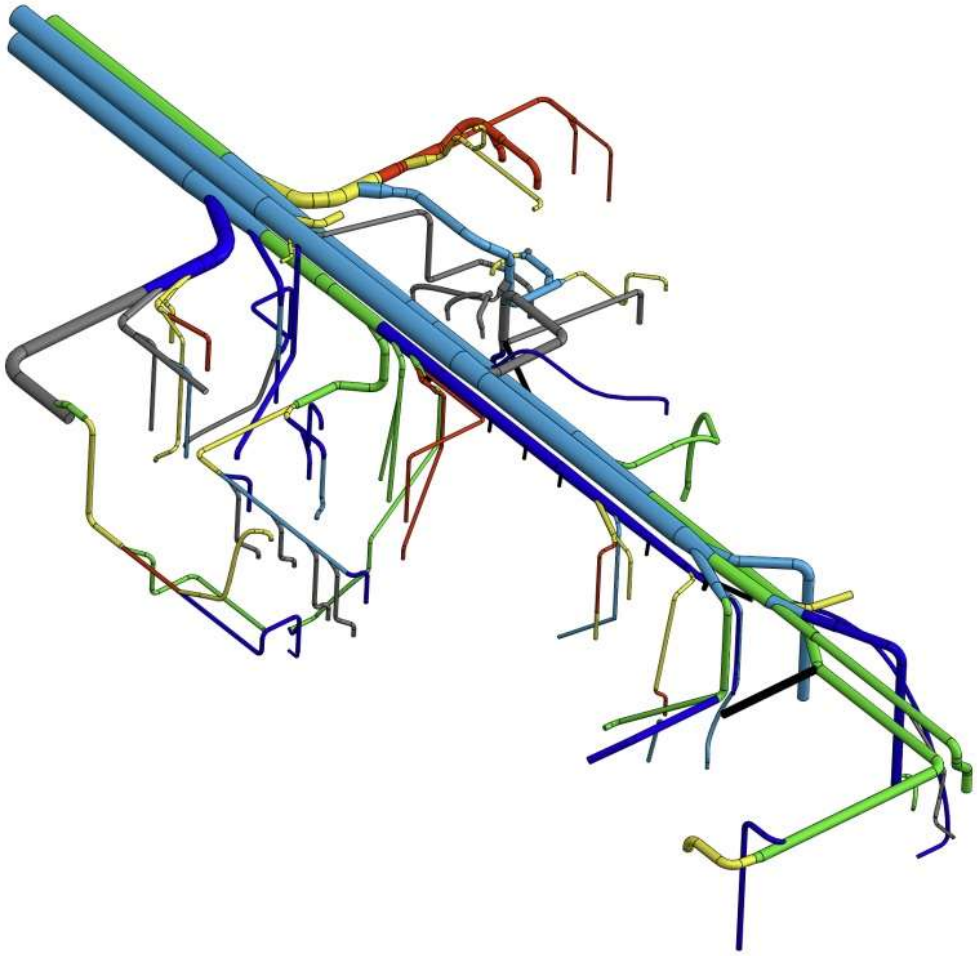

Figure 1-2: Illustration of dust extraction ducting, which consists of piping for three different filters. The system is composed of a vast amount of different pipe dimensions, lengths, bends, and crossovers.

NFPA 72 (2012) provides comprehensive recommendations for equipment design and explosion protection and prevention systems for industrial process plants. Including dust extraction and conveying systems. Some recommendations apply to general conveying design, such as maximum allowed concentration of 25 % of the LEL of the material within the pipes, and sufficient conveying velocity to prevent accumulation of dust. Additionally, it describes measures for explosion prevention, protection systems, such as, isolation, venting and suppression systems.

Similarly, in Europe, comparable design requirements are covered by European Standards. For instance, NS-EN 14491:2012 (2012), is part of a series that represents the concept of dust explosion venting. A common factor between NFPA and the European Standards, is that they utilize the explosion properties of the dusts, conveying velocities, as well as the geometry to determine the necessary safety measures.

1.5 Objective

Following the high number of accidents involving dust extraction systems, this thesis aims to investigate silicon dust's explosion characteristics in pipes. The research investigates how different pipe configurations influence the explosion behavior of silicon dust with varying particle sizes. Specifically analyzing the effects of pipe diameters, lengths, and crossovers on the explosion characteristics.

Standards to determine safety measures in dust extraction systems do not adequately consider the complex network of varying-sized piping systems. It is essential to consider the dust extraction systems' complex dynamics and configurations, not only the explosion indices of the materials involved. Explosion indices, pipe dimensions, reducers, expanders, and their interaction may result in a more robust approach to explosion protection.

In addition, conducting large-scale experiments might provide empirical data that can be used to validate and improve dust explosion simulation codes, such as FLACS – DustEX (formerly known as DESC), as highlighted by Skjold (2007). Improving simulation tools play a crucial role in enhancing the accuracy of explosion predictions, consequently making risk assessment more reliable.

2. Theory and previous work

2.1 Concepts and definitions

2.1.1 Combustion

Combustion is a complex phenomenon that involve several simultaneous chemical reactions. Combustion is a fast oxidation reaction, where the atoms in fuel react with an oxidizer (e.g., oxygen in the air), releasing heat and often light. The reaction takes place within a thin zone known as the combustion wave, where the flame might be thought of as the visible manifestation of the combustion. A common way to characterize a combustion involves three categories; the system's degrees of mixing, the systems flow conditions, and the phases present in the reaction (Glassman, 2008; Ragland, 2011; Turns, 2000; Warnatz et al., 2006).

i. Premixed vs non-premixed combustion:

In non-premixed combustion, the fuel and oxidizer are separated prior to the reaction. The reaction is driven by the diffusion of fuel and oxidizer into the reaction zone, where continuous mixing takes place during the reaction.

In premixed combustion, fuel and oxidizer are mixed on a molecular level before reacting. Dust explosions are a combination of the above and are called an intermediate system (dust clouds are both premixed and non-premixed at the same time).

ii. Laminar vs turbulent combustion.

Laminar combustion is a type of combustion that occurs in a smooth, orderly, and predictable flow pattern. Chaotic and unpredictable flow patterns characterize turbulent combustion.

iii. Homogenous vs heterogenous combustion

Homogenous combustion refers to a reaction when the fuel and oxidizer are in the same phase, such a flammable gas combustion in air.

Heterogenous combustion refers to a reaction where there are more than one phases present, like the combustion of particles in air.

Combustion of dust

The characteristic of the dust flame can be split into two types of flames, the Nusselt flame and the volatile flame (Cassel, 1964, as sited in Eckhoff, 2003, p. 268).

Nusselt flame – Is a heterogenous reaction that is controlled by the diffusion of oxygen to the surface of the particles.

Volatile flame – When heated, the particles release volatiles (vapours), mixing with the air, followed by a homogenous reaction which burns almost as a premixed flame. Depending on the material in question, three mechanisms have been suggested for the combustion of particles in volatile flames (Bardon & Fletcher, 1983, sited in Rockwell & Rangwala, 2013, p. 22);

i. Devolatilization and burning of volatiles followed by combustion of a solid residue, typical for carbonous materials.
ii. Melting is followed by evaporation and vapor phase burning, typical for plastics.
iii. Evaporation through a solid oxide shell followed by combustion of the vapor, typical for metals.

Glassman (1960), suggested that combustion of metal particles behave differently based on the boiling points of the metal and its oxides. A way to categorize the combustion mechanism of metal particles is based on the volatility of the metal in relation to the flame temperature, the volatility of the metal oxides formed during combustion, and the solubility of metal oxide species in the metal (Ogle, 2017; Yetter & Dryer, 2001).

i. *Low temperature oxidation:* When the adiabatic flame temperature is lower than the boiling points of the metal and its oxides.
ii. *Surface combustion*: When the adiabatic flame temperature is close to the metal oxide's boiling point, but lower than the metal's boiling point.
iii. *Vapor phase combustion*: When the adiabatic flame temperature of the is higher than the metal's melting point, but lower than the boiling point of the metal oxide.

Heat of combustion

The heat of combustion is the amount of heat released when one mole of fuel completely reacts with an oxidizer (e.g., oxygen) at a constant pressure. Every substance inhabits an individual heat of combustion. Thus, materials release different amounts of heat during combustion. During constant pressure combustion, the adiabatic flame temperature is the highest temperature theoretically possible to achieve with a complete reaction, without heat losses from the vessel.

The heat of combustion is closely related to the flame temperature. When comparing different materials, it is useful to consider the heat of combustion per mole of oxygen consumed in the reaction. Explosions often occur in confined spaces, with a limited amount of oxygen available for the combustion process, limiting the amount of heat the reaction release (Eckhoff, 2016).

Combustion of silicon

Silicon inhabits the properties of both metals and nonmetals. As such, it belongs to a group of elements called metalloids. Due to its material properties, it is a vastly used component in solar cells, transistors, and other electronic devices (Martin, 2013).

With a heat of combustion of 830 kJ/mol O_2, silicon is among the substances with a high heat of combustion per mole O_2 and is shown to result in high flame temperatures compared to flames of organic dust (Eckhoff, 2003). Table 2-1 illustrate selected material properties of silicon and silicon dioxide and silicon monoxide.

Table 2-1: Selected material properties. Si and SiO_2 properties are gathered from (Rumble et al., 2022), SiO from, adiabatic and pyrometric flame temperature collected from (Cashdollar & Zlochower, 2007)

Substance		**Si**	**SiO_2**	**SiO**
M	[g/mol]	28.085	60.085	44.085
T_m	[K]	1687	1986	N/A
T_b	[K]	3538	3223	N/A
$T_{adb,\,max}$	[K]	3240	N/A	N/A
T_{pyr}	[K]	2300 ± 100	N/A	N/A

Where M, T_m, T_b, $T_{adb,max}$, *and* T_{pyr} are molar mass, melting point, boiling point, adiabatic flame temperature and calorimetric flame temperature, respectively. Combustion of silicon can yield two balanced reaction equations:

$$Si\ (s) + O_2\ (g) \rightarrow SiO_2(s) \tag{1-1}$$

$$2Si\ (s) + O_2(g) \rightarrow 2SiO(g) \tag{1-2}$$

Knowing that for every O_2 in air there is $\frac{79}{21}$ N_2, the balanced reaction equations become:

$$Si\ (s) + [O_2 + \frac{79}{21}N_2]\ (g) \rightarrow SiO_2(s) + \frac{79}{21}N_2(g) \tag{1-3}$$

$$Si\ (s) + [O_2 + \frac{79}{21}N_2]\ (g) \rightarrow 2SiO(g) + \frac{79}{21}N_2(g) \tag{1-4}$$

Using the ideal gas law to find the amount of silicon per cubic metre, then calculating the amount of O_2 needed for stoichiometric combustion, leads to a stoichiometric dust concentration of 241 g/m^3 for Eq. (1-3). At the same time, the stoichiometric concentration for Eq. (1-4) is 482 g/m^3.

According to Skjold (2003), combustion of silicon in air is best described by Eq. (1-3), yet some of the reacting dust can react according to Eq. (1-4) and further react as:

$$2SiO\ (s) \rightarrow Si\ (s, brown) + SiO_2(s, white) \tag{1-5}$$

In which some of the products changes colour from grey to brown/dark yellow.

Given the material properties of silicon, the combustion mechanism of the particles is likely to be a surface combustion, based on the condition of Eq. (1-6) and the categorization criteria from (Ogle, 2017; Yetter & Dryer, 2001).

$$T_{adb} \sim T_{b,ox} < T_{b,Si} \tag{1-6}$$

This is supported by Matsuda (1995) who indicate that the combustion mechanism occurs at the particles surface. If temperature is above the melting point of Si, the reaction occurs on the liquid surface of the particle.

Due to the many steps involved in particle combustion, the rates of transport and kinetics happen at a slower pace. Because of the slower burning rate, part of the fuel remains unburned after the deflagration wave has passed. Thus, maximum explosion pressures for dusts are typically found at a concentration vastly larger than stoichiometric concentrations (Nagy and Verakis, 1983, cited in Ogle, 2017, p. 13).

2.1.3 Explosions

A dust explosion is initiated when a suspended cloud of combustible dust is ignited within a confined space, resulting in an increase of pressure. Due to the inherent presence of suspended dust, primary explosions are likely to occur inside process equipment (e.g., dust collectors, grinders, dryers, and conveyors). These primary explosions have the potential to escalate through secondary explosions, pressure piling, flame acceleration and detonations.

Secondary explosions

Secondary explosions arise when the blast wave emitted by the primary explosion, or the rupture of the process equipment, suspends otherwise settled dust in the surrounding areas. The flame from the primary explosion then ignites the suspended dust cloud, which leads to a secondary explosion. This sequence of events can lead to a chain reaction, creating multiple explosions that cause vast amounts of damage.

Pressure piling

It is well established that the final pressure from an explosion within an enclosed vessel is directly proportional to its initial pressure (Eckhoff, 2003; Ogle, 2017). If several vessels are interconnected via pipes or ducts, this phenomenon can give rise to considerable explosion pressures given the right conditions. Suppose an explosion is initiated in one vessel connected to another. In that case, the expansion of hot combustion gases will result in a compression wave that compresses the unburnt mixture in front of the combustion wave. The pressure will gradually rise to pressures above atmospheric conditions within the vessel. When the combustion wave catches up and ignites the unburnt mixture, it can generate significant pressures within the system. This phenomenon can also be seen in long pipes and situations of choked flow.

Turbulence induced flame acceleration

Turbulence is an essential property of dust combustion. Without turbulence, the dust would not be dispersed, creating a combustible cloud. It is often distinguished amongst two origins of turbulence, initial turbulence and turbulence generated after ignition (Eckhoff, 2016). The initial turbulence significantly impacts the ignition of the dust cloud. More turbulence tends to cool down the ignition zone, thus increasing the energy one needs to ignite the dust cloud. Lower turbulence might not suspend the dust nor mix it sufficiently with air to make an explosive mixture.

Turbulence generated after ignition is highly dependent on the geometry of the confinement. Walls, obstacles, openings, and changes in the area all act as turbulence generators. During flame acceleration in a pipe, turbulence is generated by wall friction and pressure waves that interact with the flame front. The turbulence stretches and folds the flame so that a larger area of the flame surface is subjected to “fresh” reaction products. This increases heat release in the reaction, subsequently increasing the burning rate and velocities. Increasing the burning velocity will increase the pressure waves, which increase the convective flow and stretch the flame even more. This acts as a positive feedback mechanism that accelerates the deflagration.

Deflagrations

When the flame propagates through the dust–air mixture at subsonic velocities, it is called a deflagration. The propagation mechanism of a deflagration is sustained by turbulence, which mixes the burning part of the cloud with the unburnt part of the cloud. The enhanced mixing significantly increase the combustion rate of the dust cloud.

Detonation

A detonation is a supersonic combustion wave propagating through the mixture, which can result in very high pressures. The heat transfer in the flame front does not happen through conduction, convection, or thermal radiation but by compression of the unburnt mixture ahead of the combustion wave, propagating at supersonic speed (Eckhoff, 2016).

Detonation fronts have been known to exhibit instabilities, manifesting as transverse shock waves in the detonation front, propagating in the direction normal to the leading shock. The intersection, or "collision," of these shock waves gives rise to areas of heightened temperatures and pressures, accelerating the leading shock. The interaction of these shockwaves can be observed on sooted foils after a detonation and is known as the detonation cell size (λ) (Lee, 2008).

A correlation between the cell size of a detonation and critical tube diameter (d_c) was discovered in the early '80s, suggesting a limitation of the ability to sustain a stable detonation in pipes with a diameter smaller than the critical tube diameter (Borissov, 1991). Cell sizes are commonly used to measure a substance's likelihood of detonation sensitivity (Lee, 1984). The reactivity of a substance directly affects its cell size - substances with low reactivity inhabit larger cell sizes, thus requiring larger geometries to sustain a stable detonation (Hussaini et al., 1992).

The Chapman–Jouguet (C-J) detonation velocity is a simplified model used to describe self-sustained detonations and is closely coupled with the materials thermochemistry. The C-J velocity is only dependent on the total amount of chemical energy release from the reaction and is typically a place between 5-10 % larger than experimental values (Shepherd & Lee, 1992).

Detonations in dust-air mixtures

Due to the slower combustion processes between dust particles and their oxidizer, the transverse wave spacing, or cell sizes of dust detonations, are substantially larger than for gas detonations. Consequently, dust explosions require a larger tube diameter and tube lengths to transition to a self-sustained detonation. Nevertheless, several researchers have shown that detonations in dust-air mixtures can be initiated given the right conditions (Proust, 1996).

Zhang et al. (2001) investigated DDT and detonation waves from experimental results done by Zhang and Grönig in 1991 and 1992. Their work indicates that stable detonations can occur in pipes ranging from 0.1 m to 1 m in diameter for dusts with K_{St} values between 400 to 40 bar·m/s. By assuming that the minimum pipe diameter for propagation of a self-sustained detonation is given by $d_{min} \cong \lambda / \pi$, they found minimum pipe diameters as shown in Table 2-2.

Table 2-2: Experimental minimum tube diameter and K_{St} (Zhang et al., 2001).

Dust	**Particle size** [µm]	**K_{St}** [bar·m/s]	**d_{min}** [m]
Cornstarch	10	160	0.3
Anthraquinone	22 × 6 × 6	274	0.14
Aluminum	36×36×1	365	0.12

Experiments done by Zhang et al. (2010), show that quasi-detonations can be observed for aluminium dust in pipes, with semi-steady shock velocities nearly 40% below the theoretical CJ value. The shockwaves and subsequent retonation waves are similar to those of a self-sustaining detonation. However, they will not accelerate further because of the heat loss due to the smaller diameter pipes.

Deflagration to detonation transition

Flame propagation in pipes can give rise to high pressures and flame velocities under certain circumstances. Suppose a dust explosion is initiated in an open end of an otherwise closed pipe. In that case, the explosion will propagate with a low flame velocity and result in weak pressures in the closed end, independent of the diameter of the pipe. If the explosion is initiated on the opposite end, the flame velocities and maximum pressures increase with the propagation length.

The initial shock created by the ignition induce a convective flow which can suspend layers of dust if present. Suspended dust further fuels the flame, which is further stretched by turbulence and shock interaction, increasing acceleration. With every change in heat or velocity, compression waves are created, which propagate towards the open end. Due to adiabatic compression, the unburnt mixture ahead of the deflagration wave is heated, so every compression wave is slightly faster than the previous one. These waves eventually catch up to the leading shock, creating a strong leading shock front. If the deflagration accelerates sufficiently and catches up to the leading shock wave, the flame propagation mechanism can transition from turbulence-induced diffusion to shock-induced ignition (Eckhoff, 2003).

Fast turbulent deflagration and quasi-detonations

Fast turbulent deflagrations can propagate with high supersonic speeds before detonating, usually referred to as the transition period. Quasi-detonations are detonations that propagate at lower speeds, like in pipes with a rough surface (Lee, 2008).

Unstable fast deflagrations have been found hard to differ from quasi-detonations due to the similar velocities of flame propagation and the induced pressure waves (Chan & Greig, 1989). The work done by Chan & Greig discovered that though hard to differentiate, there is a clear difference between their reaction mechanisms. It is assumed that fast deflagrations are sustained by turbulent diffusion,

amplified by shock and flame front interaction, increasing the reaction rate. Quasi-detonations, on the other hand, have the same reaction mechanism as detonations – shock heating of the unburnt mixture, increasing the temperatures to levels of autoignition.

The transition from deflagration to detonation is a complex process involving several physical elements, such as shock waves, boundary layers, reflections of shock waves, turbulence, and the interactions between them all.

Explosion parameters

Maximum explosion pressure (P_{max}), maximum rate of pressure rise $(dp/dt)_{max}$ and K_{St}, are characteristics used to define the hazard of combustible dust. They are found using standardized test equipment, like the 20-l Siwek test apparatus, and are decided in accordance with NS-EN 14034-1:2006+A1:2011 and NS-EN 14034-2:2006+A1:2011 (2011a, 2011b).

The maximum pressure of an explosion is a measure of its severity, and higher pressures tend to inflict more damage to the surroundings then lower pressures. Maximum pressures are directly related to the amount of heat released in the explosion, thus the average temperatures in the test vessel (Ogle, 2017).

Maximum rate of pressure rise is highly dependent of the mass burning rate of the fuel and varies greatly with the degree of dispersion or amount of heat losses to the walls of the vessel. These factors are directly influenced by the size and shape of the test apparatus.

The normalized rate of pressure rise, the K_{St}, is a measure of the relative explosion severity of the dust, compared to other dusts. A higher K_{St} value indicates that the dust has the potential for more severe explosions, as illustrated in Table 2-3.

Table 2-3. The classification of dusts based on their K_{St} value (Barton, 2002).

Dust explosion class	**K_{St} [Bar·m/s]**	**Characteristic**
St 0	0	No explosion
St 1	>0 and ≤ 200	Weak explosion
St 2	>200 and ≤ 300	Strong explosion
St 3	> 300	Very strong explosion

Since $(dP/dt)_{max}$ is dependent on the volume of the test vessel, scaling laws must be employed. The cube-root-law states that the K_{St} value should be constant under specific conditions, and is one of the most used scaling laws (Bartknecht, 1971; Eckhoff, 2003).The K_{St} value is calculated as the maximum rate of pressure rise $(dP/dt)_{max}$ normalized by the cube root of the volume, as presented in Eq.(1-7).

$$K_{St} = dP/dt_{max} * V^{\frac{1}{3}} \quad (1\text{-}7)$$

$$K_{St} = dP/dt_{max} * V^{\frac{1}{3}} = Constant \quad (1\text{-}8)$$

As pointed out by Eckhoff (2003), the "cube-root-law" is only valid in geometrically similar vessels, with negligible flame thickness and identical burning velocity. Most test methods do not fulfil these conditions, making experimental K_{St} values a relative measurement of dust explosion violence, strongly influenced by the experimental conditions in the test methods used.

Ignition sensitivity and explosion sensitivity

Several parameters influence a dust cloud explosion property, such as the dust concentration in the cloud, chemical composition, particle sizes, and turbulence. These parameters strongly influence the explosion's severity and the necessary precautions to take. The most significant parameters are mentioned below, and are collected from Eckhoff (2003). The ones that are not, are otherwise mentioned.

1. *Material properties*
   - i. *Particle size* – Smaller particle sizes have a lower minimum ignition energy (MIE) but yield higher maximum pressures. The surface area available for reaction in the cloud is highly increased when particle sizes are reduced. Thus, more of the surface can react, so more heat can be liberated in the same amount of time, giving rise to more violent explosions.
   - ii. *Particle shape* – A particle that is not spherical has a larger surface area. When the surface area increases, more of the surface can participate in the reaction.
   - iii. *Chemical composition* – In adiabatic constant volume combustion, the pressure rise in the system depends solely on the amount of heat generated during the reaction. The heat of combustion per mole of oxygen varies based on the chemical composition of the material, with some substances having a higher heat of combustion than others. Non-organic materials, such as magnesium, aluminium, and silicon, are substances with a high heat of combustion and exhibit higher flame temperatures than organic materials.
   - iv. *Moisture content* – reduces both the explosion violence and the ignition sensitivity of the dust cloud. It also prevents the dispersion of particles by increasing the interparticle cohesion forces. Heating the water acts as an inert heat sink; when evaporated, the water vapour makes the gas mixture less reactive by mixing with the pyrolysis gases.

2. *Properties of the oxidizer*

   i. *Initial pressure* – increasing initial pressure leads to a proportional increase of the maximum explosion pressure and the minimum explosion concentration.

   ii. *Initial temperature* – increasing the initial temperature decreases the maximum explosion pressure, the lower explosive limit (LEL), and the oxygen limit concentration(1987)

   iii. *Oxidant concentration* – the maximum pressure and maximum rate of pressure rise are closely coupled with oxygen concentration, leading to a linear decrease when the concentration decreases (Ogle, 2017).

3. *Dust cloud*

   i. *Concentration of dust cloud* – the dust cloud will only be able to propagate a flame if the concentration is within LEL and UEL. Unlike flammable gases which has clear limits of concentrations, dust do not have a clear limit for UEL. The concentrations can vary from 50 g/m^3 to several kg/m^3 (Abbasi & Abbasi, 2007).

   ii. *Degree of dispersion* – a poorly dispersed dust cloud is likely to consist of agglomerates of clusters of particles, giving a larger effective particle size than the actual particles. This will give a lower specific surface area, lower combustion speeds and lower maximum pressures. The opposite goes for a perfectly dispersed dust cloud.

   iii. *Turbulence* – we distinguish between two separate types of turbulence, initial turbulence and turbulence created during combustion. The initial turbulence distributes the dust concentration more evenly, and gives the particles surface more access to oxygen, greatly increasing the burning rate of the cloud. The second type is caused when expansion of the burnt mixture induces a flow of unburnt mixture ahead of the flame. The geometric constrictions and obstacles govern the amount of turbulence created during combustion.

3. *Radiative heat transfer*

   i. *Flame temperature* – the effects of radiative heat transfer might be considered intuitive, as the minimum ignition energy needed to ignite a singular particle decreases with increasing initial temperature. Increasing the heat radiated from a particle result in increased pre heating of adjacent particles, reducing the time needed for them to ignite. As such the influence of thermal radiation might play a large role to flame propagation in dust clouds (Bidabadi et al., 2013).

   ii. Combustion of light metal dust (e.g., aluminium, magnesium, and silicon) occurs at considerably higher temperatures compared to that of organic dusts. Recent studies have suggested that thermal radiation play a larger role in the flame propagation mechanism, and

that ordinary 20-litre experiments underestimate the severity of light metallic dust explosions (Taveau et al., 2019). Thus, special care should be taken when designing explosion protection systems for processes that involve light metallic dusts.

2.1.4 Prevention and mitigation

The risk of a process is determined by the likelihood of an incident occurring, and the consequence of that incident. The issue of explosion protection is built up in the same way, prevention, and mitigation. Prevention is the systems in place to reduce the likelihood of an incident to occur, whilst mitigation aims to reduce the consequence if an incident has occurred. The following discussion of prevention and mitigation is explained in detail by Eckhoff (2016).

Prevention, can be divided into two focus areas:

1. *Prevention of explosive dust clouds*

   Dust explosions commonly occur inside process equipment due to their predisposition to inhabit a dust cloud. To prevent this, equipment should be designed to diminish dust accumulation. Where this is not possible, the atmosphere of equipment can be inerted (injecting N2 or CO2), suppressing the oxygen needed for combustion. Alternatively, the process could be optimized to reduce the amount of dust concentration below the explosible range, continually measuring the concentration, and using adequate dust extraction systems. General housekeeping routines of removing accumulated dust in the process plant, as well as in channels and equipment, are crucial for preventing dust explosions.

2. *Prevention of ignition sources*

   Some ignition sources are easy eliminate. Open flames and hot work should be restricted, and their use should only be allowed with the release of work permits. Electrical installations should be designed according to regulations, and the use of EX-systems should be implemented in areas in risk of having an explosive atmosphere. Several other ignition sources should be considered (e.g., heat from mechanical impacts and hot surfaces).

   If an incident has occurred, *mitigation* aims to reduce the consequences of the incident. Reducing the amount of accumulated dust will inherently reduce the probability and severity of secondary explosions. Process design can help achieve this by reducing the formation of dust clouds and utilizing equipment that can resist explosion pressures.

   Explosion isolation aims to avoid the spreading of an explosion from one process equipment to another via ducts and pipes, to reduce the accelerating combustion that occurs in ducts due to

turbulence, and limit the extent of the incident (e.g., fast acting valves or venting in strategic points).

Suppression systems is intended to add a suppressive substance that quenches the deflagration at an early stage.

Venting is intended to reduce the pressures within a system. The explosion can be led in a chosen direction, utilizing vent covers, light walls, or explosion panels.

Mitigation strategies usually rely on dust explosion indices such as K_{St} and P_{max}. As such, mitigation measures such as explosion venting, suppression, isolation, and process design depend on the K_{St} value of the dust in question.

2.1.5 Particle size distribution

When handling dust in bulk, particles commonly segregate by size when the sample is disturbed. Smaller particles accumulate at the bottom, while larger particles stay on top. Thus, a representative particle size distribution is only as accurate as the sampling. Whenever possible, Terence Allen's (1997) golden rules of sampling should be followed; samples should always be taken when the powder is in motion, and take many small samples of the whole cross-section, instead of one large sample.

Various parameters can express measurements of the particle sizes in a dust sample:

- *The arithmetic mean, D[1,0],* is the number mean—the average size of the particles based on the number of particles.
- *Sauter mean diameter, D[3,2]*, is calculated as the ratio of the particle's average volume to the average surface area of the particles. It tells us the average particle size that would, as a total, give the same volume-to-surface area as all the particles in the sample.
- *Volume mean diameter, D[4,3],* is the mean diameter based on the volume of the bulk of the particles. It tells us the average particle size that would collectively exhibit a volume equal to that of the bulk of the particles.
- *Mass mean diameter, D50,* is the smallest particle size, of which 50% of the total weighted sample is below.

2.1.6 Speed of sound

The speed of sound is at the velocity that a soundwave can travel through a medium. It is affected by the given medium's temperature, pressure, and density; as such, it is different for solids, fluids, and gases. Mach numbers give the ratio of the flow's speed to the speed of sound of the medium. Thus, Mach 1 equals the speed of sound for the given medium. When Mach < 1, the flow is subsonic, and for Mach > 1, the flow is supersonic.

In an ideal gas, the speed of sound equation is governed by the adiabatic index γ, the gas constant R, the temperature T, and the molar mass M (Young et al., 2004, p. 535).

$$a = \sqrt{\frac{\gamma * R * T}{M}} \tag{1-7}$$

The adiabatic index γ = 1.4, the gas constant R = 8.314 $J \cdot K^{-1} \cdot mol^{-1}$, and the molar mass of air M = 0.0296 kg/mol.

For a multiphase flow, like gas-particle flow, we distinguish between two conditions; the frozen speed of sound (a_f), usually higher than the ideal speed of sound, is when the particles do not interact with the gas.

The equilibrium speed of sound (a_e) represents the condition when particles in the flow are in a state of equilibrium with the surrounding gas (Rudinger, 1980). According to Eckhoff (2003), in an explosible dust cloud where the volume fraction of particles is negligible, the frozen speed of sound is assumed to be equivalent to the sound speed in an ideal gas.

Utilizing Eq. (1-7) and the assumption that the largest temperature of the burned dust cloud will heat up the burnt gases to the maximum pyrometric flame temperature of silicon, as specified in Table 2-1, the speed of sound in the burnt combustion gases can be determined.

$$a = \sqrt{\frac{1.4 * 8.314\ J/(K \cdot mol) * 2400\ K}{0.0296\ kg/mol}} \approx 970\ m/s \tag{1-8}$$

Using the temperature of 2400 K ultimately assumes that the gas surrounding the burning particles does not become hotter than this temperature. One could take precautions and use the adiabatic flame temperature, 3240 K, and get a speed of sound at ~1130 m/s in the burnt gases.

2.1.7 Compression waves and shock waves

Compression waves are formed and propagate in both flow directions whenever there is a change in the flame velocity or heat release. During flame acceleration in a pipe, the compression waves eventually increase their speed and become shock waves (Chu, 1953).

A *shockwave* is a mechanical wave or a pressure front that moves faster than the speed of sound. When a fluid crosses a shock wave, the velocity decreases while temperature, density, and pressure rise (El-Sayed, 2016).

Nonstationary shock waves originate from the explosion itself (e.g., compression wave, detonation wave, and retonation wave), while stationary shock waves are motionless and can form behind nozzles as standing shocks. Shockwaves interact with each other and reflect from impacts with solid walls, and have been shown to inhibit superposition properties (Krehl, 2008). Reflections in conical contractions

are shown to significantly increase the intensity of the shock waves due to the increased gain in shock strength at each reflection. The reduced cross-section allows more reflections to occur. Increasing the cross-section of a duct or a pipe leads to a reduction in strength (Ben-Dor et al., 2001, p. 295).

Normal shocks are shockwaves that form normal to the flow, where the velocity of a flow changes from supersonic to subsonic velocity. Occasionally they are formed behind converging nozzles, abruptly reducing the velocity of passing flow and increasing pressures.

When a supersonic flow interacts with an inclined geometry, such as a nozzle, a shock wave oriented to an angle of the flow direction may form from the corner of the geometry. The shock wave is called an oblique shock wave.

2.1.8 Expanders and reducers

In the field of thermodynamics, expanders and reducers are commonly known as diffusers and nozzles. A nozzle is used to increase the velocity of a flow while reducing the pressure. The diffuser does the opposite, reducing velocity while increasing the pressure. The nozzle and diffuser's ability to adjust the flow characteristics are highly dependent on the initial velocity of the flow, as illustrated in Figure 2-1.

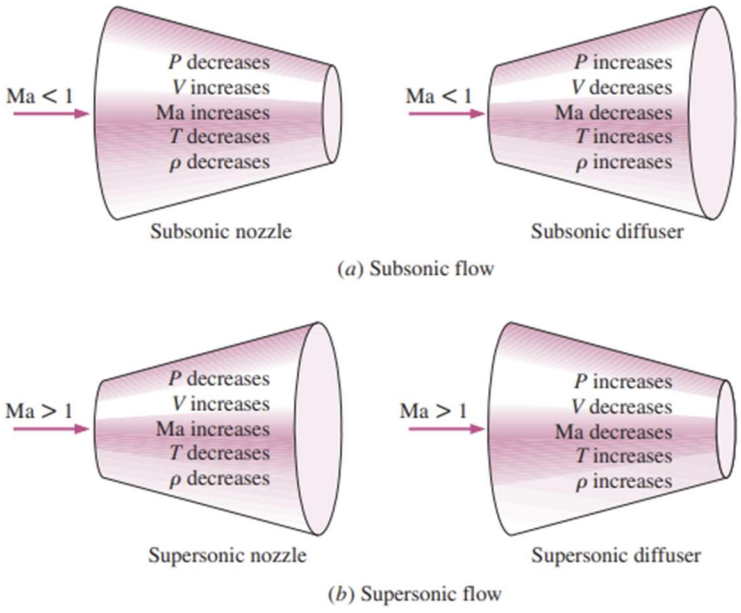

Figure 2-1: How the flow characteristics changes with varying initial velocities in nozzles and diffusers. From Cengel & Boles (2006)

A nozzle's length determines the velocity increase that can be achieved. When the flow velocity at the nozzle throat reaches Mach 1, the flow becomes choked and can't accelerate further.

2.2.1 Previous work

Due to dust clouds' inherent irregularity, experimental tests often show poor reproducibility (Eckhoff, 2003). Even identical experiments can give rise to vastly different results.

In an experimental investigation of dust and gas explosion in a 3.6-m FAT conducted by Skjold et al. (2014), considerable variations in the results were observed, despite modest differences in the initial conditions. Significant variations in the results make it harder to obtain consistent and reliable data and draw conclusive findings.

2.2.1 Layered dust explosions in ducts and pipes

Pre-layered dust explosions differ from pre-suspended dust explosions in that the initial explosion must be intense enough to suspend the layered dust particles, mixing them with air.

Investigations of pre-layered dust explosions, propagating in large length-to-diameter (L/D) geometries, became a target of interest due to coal mine explosions. One of the pioneering studies in this field was conducted by Hall, performing coal dust experiments in about 1890 (Cybulski, 1975, as cited in Eckhoff, 2003). Since Hall's work, numerous studies and experiments have been carried out in this area, some of which are mentioned below.

Greenwald and Wheeler (1925, as cited in Eckhoff, 2003) conducted experiments in a tube with a length of 230 meters and a diameter of 2.3 meters, resulting in an L/D ratio of 100. Their objective was to examine the impact of vent size and location on dust explosion propagation in a large-scale environment. They spread the coal dust on the gallery floor at approximately 1500 g per meter of gallery length from 60m to 230m, corresponding to a nominal dust concentration of 360 g/m^3 when fully dispersed. They then varied the degree of the opening and kept the other end completely closed. The results showed maximum flame velocities of about 800 m/s when the gallery was closed in one end and completely open in the other end. The velocities reduced with the degree of opening in the closed end.

Bartknecht (1981) conducted experiments with pre-dispersed and layered dust. The pre-dispersed experiments were well-defined but not representative of real-life explosion incidents in mines or industry. The layered dust was spread along the floor of the tube, with a nominal concentration of 250 g/m^3. A methane/oxygen explosion was used as an ignition source. The layered dust experiments resulted in lower flame velocities than experiments conducted with pre-dispersed dust, but higher flame velocities were recorded when the primary explosions were sufficiently violent. His work

indicated that dust could detonate in pipes of sufficient diameter, given that the dust is sufficiently reactive (K_{St} > 200 bar · m/s).

Pineau and Ronchail (1982, cited in Eckhoff, 2003) conducted experiments in straight pipes with diameters ranging from 250 mm to 700 mm and lengths from 12 m to 42 m to study the effects of the degree of opening in the ends. The results indicated that smaller diameter pipes gave rise to higher maximum flame speeds, and partially closed pipes increased the maximum explosion pressures. Results indicated that flame propagations were more successful in pipes of larger diameters. They also conducted experiments in pipes with diameters ranging from 25 mm to 100 mm with lengths from 10 m to 40 m connected to vessels of varying volumes. Their experiments show that the propagation of explosion relates well to the reactivity of the fuel, the pipe diameter, and the initiating vessel volume. Additionally, powders having K_{St} higher than 200 bar·m/s could generate detonations in these tubes, thus producing pressures above 20 bar(g) and flame speeds of about 2000 m/s.

Tamanini (1983, sited in Eckhoff, 2003) conducted experiments in a gallery to study the minimum amount of dust spread as a layer on the floor that could propagate a dust explosion. He also investigated if venting a primary explosion could prevent the development of secondary explosions. The results indicated that explosions could propagate with dust layers considerably smaller than that corresponding to the LEL. This was because the dust was only dispersed in the lower part of the gallery, resulting in high concentrations without filling the complete volume of the gallery.

Kauffman et al. (1984a, cited in Eckhoff, 2003) conducted experiments on the propagation of dust explosions in a horizontal tube that was 36,6 m long and had a diameter of 0,30 m, resulting in an L/D of 122. The objectives of the experiment were identical to that of Tamanini; the minimum amount of dust as a layer on the internal surface of the tube that could propagate an explosion. The tested dusts included maize starch, mixed natural organic dust, wheat grain, and oil shale dust. The results indicated that a unified layer on the inside surface of the pipe resulted in the most violent explosions and that the strength of the secondary explosion generally increased with the strength of the primary explosion.

Li et al. (1995) investigated the role that dust layers and moisture content plays in severe dust explosions in a 70 m-long Flame Acceleration Tube (FAT) with a diameter of 30 cm. They distributed the same amount of dust in two different layers, one wide and one narrow. The widest layer gave rise to the strongest combustion because more dust particles would get exposed to the dispersing flow. The dry dust spread in a wide layer produced the fastest pressure development, while moist dust spread in a wide layer produced higher pressure than dry dust in a thin layer. This indicates that the layer thickness has a more considerable impact on explosion severity than moisture content. They also

implied that the K_{St} might not be a sufficient parameter to evaluate the explosibility or detonability in layered dust explosions.

A study of deflagration to detonation of aluminum dust in a 28 m pipe of 199 mm in diameter was performed by Liu et al. (Liu et al., 2009). Using pressure transducers, they measured the velocities and propagation distance of the pressure waves during the DDT process. They found that transition distance varied with ignition time delay and that aluminum dust-air mixture readily can transition to a self-sustained detonation wave. The Aluminum cell size in the current configuration was decided to be about 0.495 m.

Jinzhang and Xiuyuan (2022) did a comprehensive study of shock wave propagation in a network of diagonal pipelines. The explosive mixture was a mixture of methane and coal dust, the coal dust was evenly layered in the pipeline. The evolution of secondary explosions due to the ignition of suspended coal dust gave rise to the highest overpressures, with reverse shock waves resulting in pressure development at earlier monitor locations.

As an exception, Radandt's (1989) experiments will be mentioned. Though not experiments that investigate phenomenas associated with layered dust explosions, he conducted several dust explosions in a feeder-cyclone loop, as illustrated in Figure 2-2.

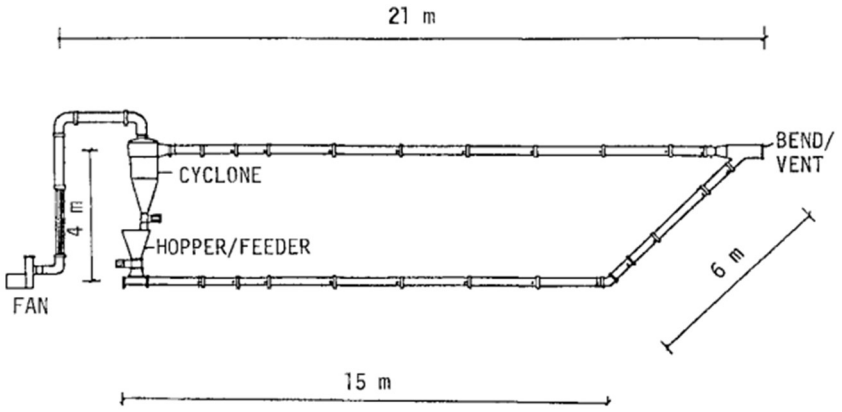

Figure 2-2: Loop for dust explosion experiments. (Radandt, 1989, sited in Eckhoff, 2003)

In most of the experiments, the maximum explosion pressures were sufficiently reduced due to the vent at the sharp end. When the dust was ignited close to the feeder, the maximum pressure and flame speed became higher with venting, than without. Due to explosion propagation the vent would open at a given pressure. As soon as the vent is opened, the flow velocity in the pipes increases. This induced more turbulence and an increase in the combustion rate. The increase in combustion rate can choke the flow out of the vent, which can give rise to very high explosion pressures. Although it is not an experiment that investigates pre-layered dust explosions, Radandt's experiments highlight the necessity for CFD to understand and interpret phenomena encountered in complex situations.

The studies mentioned above have provided valuable insights into parameters that influence dust layer explosions. Conducting experiments during controlled conditions give researchers the ability to consider and determine the effect of various factors, a summary of the results obtained is listed below.

i. Vent size – closed ended pipes gave highest overpressures, whilst open ended pipes gave higher flame speeds. Flame acceleration only occurs when igniting the opposite end of the opening.
ii. Particle size – as with a general dust explosion, the lower the particle size, the more powerful the explosion becomes.
iii. Layer geometry – wider layers of dust expose more dust to the dispersing flow above the dust, thus more dust will be dispersed and able to react, giving rise to stronger explosions.
iv. Moisture content – increasing moisture content leads to decreased flame velocities and pressures.
v. *Pipe diameter* – reducing pipe diameter leads to increased flame velocities and pressures, too small of a diameter can quench the flame.
vi. *Pipe length* – increasing pipe length, leads to increased flame velocities and pressures.
vii. *Deflagration to Detonations* – layered dust explosions can transition from deflagration to detonation given a reactive dust, optimum diameter, and sufficiently long pipes.
viii. *Pre-compression* - of the unburned mixture can give rise to very large pressures.

2.2.2 Silicon dust explosions

Silicon exhibits a heat of combustion of 830 kJ/mole O_2, almost as high as the heat of combustion of aluminium. The high flame temperature of silicon poses a significant danger to personnel and equipment in the vicinity of an explosion. This means that the consequences can be severe and potentially catastrophic if an incident occurs.

Experimental research on silicon dust explosions is limited, and the literature available is challenging to compare due to differences in experimental conditions and methods. Despite these limitations, a summary of relevant literature is provided below.

Eckhoff et al. (1986) conducted an analysis of experimental data of eight batches of silicon dust with different chemical compositions and particle sizes. The experimental data were obtained over a period of 6-7 years as part of standard testing at the Christian Mikkelsen Institute (CMI). Open Hartmann tubes were used to measure the minimum ignition energy, while the Hartmann bomb was used to measure P_{max} and $(dP/dt)_{max}$. Table 2-2 presents the data obtained from these tests.

Table 2-4: Data of silicon explosion experiments from CMI. (Eckhoff, 1986)

Sample number	**D50** [µm]	**S** [m^2/g]	**E_{min}** [mJ]	**P_{max}** [barg]	**$(dP/dt)_{max}$** [bar/s]
a	6.5	1.9	32	6.8	1000
b	7.5	1.8	32	7.3	1100
c	3.6	5.7	55	6.7	1650
d	5.3	2.1	70	6	820
e	3.6	3.8	4.5	6.6	1350
f	13.5	1.3	70	7.8	170
g	5.5	3.7	10	7	1060
h	18	0.5	>2.9 J	No ignition in Hartman bomb	

The results indicated a systematic increase in sensitivity to electric spark ignition and combustion rate as the particle size of silicon dust was reduced. Figure 2-3 demonstrates how the maximum pressure rise is dependent on the particle size, as smaller particle sizes give higher pressure rises. The two outliers marked in orange, labelled as *"a"* and *"b,"* were suspected of having been tested under different procedures because CMI changed some of their test procedures after these batches were tested.

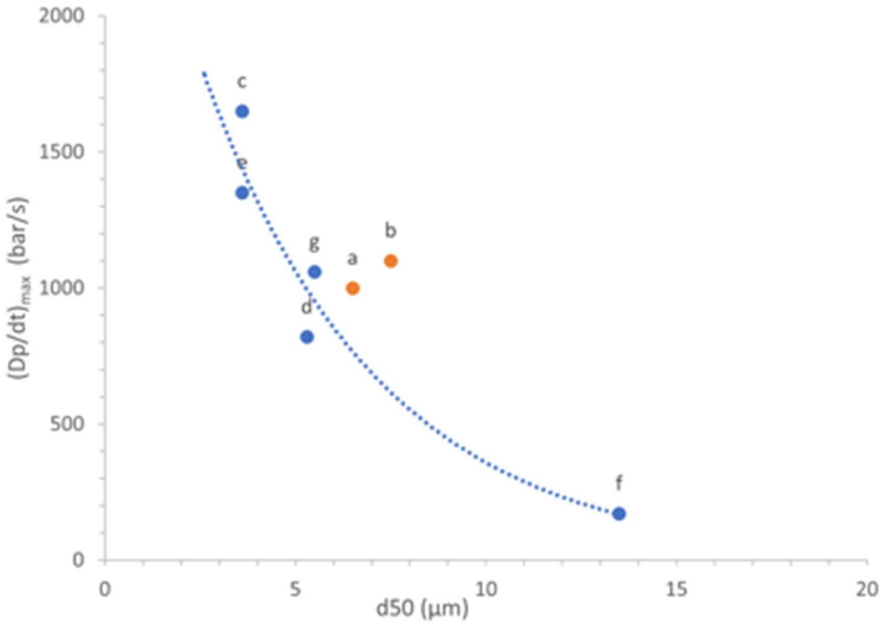

Figure 2-3: Results from silicon tests. Maximum rate of pressure rise increases with decreasing particle sizes. Reproduced from Eckhoff et al.(1986)

An interesting observation was made by Eckhoff et al.(Eckhoff et al., 1988) while investigating venting during explosion propagation in a bag filter, using three different organic dusts and silicon dust. When the silicon dust cloud was ignited by a silicon dust-flame jet, it gave rise to overpressures vastly greater than any of the other tests. This might be the result of the thermal radiation contribution in the flame propagation process, or the fact that silicon had a large amount of fine dust with more than 15 % of the dust being below 10 µm (though the median particle size was 50 µm).

A study of the effects of particle size, concentration, pore size, and chemical composition on the explosibility of dust, was conducted by van der Wel et al.(1991). The experiments were conducted in a standard Siwek - chamber of 20 litres. Their experiments on silicon showed that the solid oxide layer that forms during combustion restricts further reaction. Thus, maximum values of the explosion index are found at concentrations well above the stoichiometric ratio. In their experiments, only a quarter of the particles' masses reacted before the oxide layer ended the reaction. Nevertheless, the experiments confirmed how the maximum rate of pressure rise increased with decreasing particle sizes.

Matsuda et al. (2001) presented a study that explored the use of different test methods and apparatuses based on the properties of the dust. They conducted experiments on several different dusts, including silicon dust of decreasing particle sizes and varying concentrations. In their silicon experiments, the dust was tested in a 30-l spherical vessel because the 20-l vessel tends to be too small to handle fluffy dust at high concentrations. The results further support the theory that decreasing particle size increases explosion severity, although the maximum explosion pressure approaches a constant value.

As part of his master thesis, Skjold (2003) extensively studied turbulent flow and combustion in two different explosion vessels, a 19.97-l cubical vessel, and a 20.50-l modified USBM vessel. Among the dusts he examined was silicon, specifically Silgrain from Elkem, which is also used in this thesis. Nine different batches of silicon were tested in the cubical vessel, with an electric arc discharge of about 6 Joules as the ignition source. Some tests were also initiated by two five kJ chemical igniters.

The results presented in Figure 2-4 shows that the explosion pressures of silicon were almost independent of the type of ignition source, whilst the rate of pressure rise is considerably higher with chemical igniters than with electrical discharge. As the ignition delay time was increased for each batch, the explosion pressure decreased. When sufficiently increasing the delay time, the pressure became unsteady, and it was no longer possible to ignite the mixture.

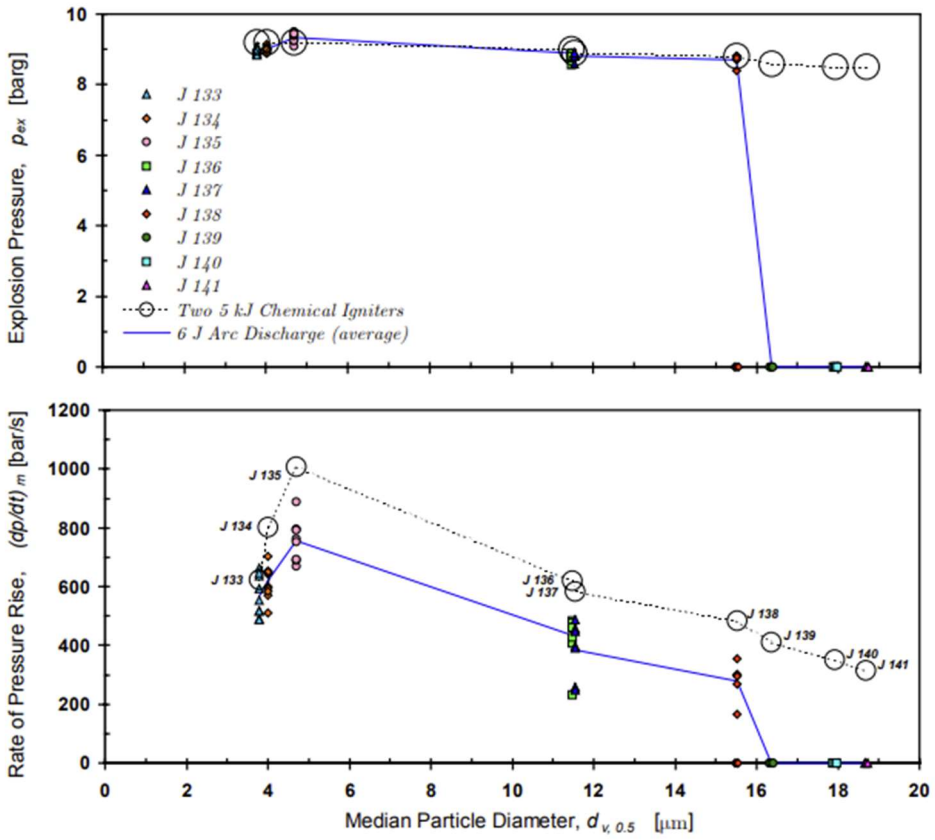

Figure 2-4: Explosion pressure and rate of pressure rise for different batches of silicon. (Skjold, 2003)

Due to silicon's high flame temperature, it has been suggested that thermal radiation affects the propagation mechanism of the flame. Experiments performed by Eckhoff et al. (1988), further increase this assumption. They performed experiments in a bag filter of 5.8 m^3 connected to a 2 m^3 process equipment by a 22 m long duct. The experiments involved four organic dusts and silicon dust. Even though the silicon dust did not have the largest K_{St} value (145 bar·m·s^{-1}), it still gave rise to the highest pressures in the bag filter and the connecting duct. Indicating that thermal radiation indeed contributes to increased combustion mechanisms.

Vast amounts of silicon explosion tests were performed by Tore Østgård (2022) in the 20-litre modified USBM sphere. His findings indicated a correlation between the explosion indices P_{max} and $(dP/dt)_{max}$ and the particle size distributions D[3,2] and D10. And a correlation between LEL and D[3,2].

3. Materials and Methods

This chapter presents the experimental setups and procedures used in the experiments. The chapter is divided into two sections, the first describing experiments in the 20-litre apparatus. The second section introduces the layered dust experiments. The dusts involved in the testing are presented in Appendix B.

Due to the amount of work needed to carry out large-scale experiments, two researchers collaborated on the experiments. All the tests were done with three different dusts, one individual dust each and one reference dust, Si-1, in which the results were shared.

3.1 Dust samples

The dust used in the experiments is silicon dust of different particle size distributions supplied by Elkem. They will, throughout this thesis, be referred to as Si-1 and Si-2. The main difference between the two dusts is their particle sizes, and Si-2 has a D50 almost 20 times larger than Si-1. The respective particle size distributions of the two dusts are listed in Table 3-1. The composition of the dust is highly similar, with Si-1 consisting of over 99.6 % silicon and Si-2 containing over 92 % silicon. Due to their high silicon content, it is assumed that the dust would behave similarly during combustion. Any differences in combustion can probably be directly attributed to the variations in particle sizes.

Si-1 is a commercial product whose particle size regularly gets measured as part of production quality assurance. Si-2 is present in the dust-extraction cyclone filter as a by-product of production. Elkem Kristiansand tested the samples in a Malvern particle-size analyser. Elkem took a reference sample of Si-2 before shipping the dust to UiB, where new tests were taken from the batch and sent for analysis in Kristiansand.

Table 3-1: Particle size distributions for the dusts.

Dust samples	**D50** [µm]	**D10** [µm]	**D90** [µm]	**D[3,2]** [µm]	**D[4,3]** [µm]	**Surface area** [$m^3 \cdot kg^{-1}$]
Si-1	2.65	0.756	4.91	1.74	2.81	1479
Si-2 ref.	53.1	5.81	191	12.5	79.7	206.7
Si-2 UiB	50.3	5.55	195	11.7	78.7	219.6

3.1 Experiments in the 20 – l apparatus

Preliminary tests were conducted to determine the explosion indices of two selected dust using a modified USBM sphere with a volume 20.50 ± 0.02 litres. The apparatus was constructed by Skjold(2003) to use in his master's thesis, and is located at the dust explosion lab at the University of Bergen (UiB). All tests were conducted with the default ignition time delay of 60 milliseconds. The tests aimed to measure the maximum rate of pressure rise $(dp/dt)_{max}$, maximum explosion pressure (P_{max}), K_{St}, and the lower explosive limit *(LEL)*, for each dust.

3.1.2 Control system and data acquisition

The control system is identical to the control system of the Siwek 20-l apparatus, a system for measuring and controlling the valves and ignition source (KSEP 332), a gas control system (KSEP 310), and software for acquisition and analysis (KSEP 7.1).

The KSEP 332 controls the ignition source and the valves while simultaneously measuring pressure over time through two piezoelectric pressure sensors, specifically the Kistler 701A. The KSEP 332 unit is connected to a computer that initiates the test sequence. The amount of dust is manually entered into the software, along with ignition energy and delay time, before initiating the test sequence. The software analyses the collected data and reports the calculated P_{max}, $(dp/dt)_{max}$, and K_{St} for every test. It also presents curves illustrating the relationship between the explosion indices and the dust concentration.

3.1.3 Procedure

The tests were conducted according to the following checklist.

1. Two chemical igniters of either 1 kJ or 5 kJ (depending on the test's purpose) are mounted in the middle of the apparatus, facing in opposite directions.
2. The correct amount of dust is weighed and inserted into the dust reservoir.
3. Close the apparatus lid and tighten the bolts extensively.
4. Check that all the valves are closed.
5. Depressurize the chamber to 0.600 +/- 0.05 bar with the vacuum pump.
6. Pressurize the reservoir to 20 barg.
7. Initiate the test with the KSEP software.
8. After the test, open the exhaust valve, pressurize the reservoir to a couple of bars, and depressurize, repeat 2-3 times. This prevents the build-up of heat and simplifies the cleaning.

Between tests, the apparatus was thoroughly cleaned using an industrial vacuum, a brush, and pressurized air. Before initiating a new test, the temperature on the inside of the apparatus is controlled by the palm of a hand. If the temperature feels lukewarm, wait for the chamber to cool down.

3.1.4 Calculation of maximum pressure

P_{max} is given by the mean value of the maximum results based on three series of tests. Each of these maximums cannot deviate more than 10% of P_{max}, or the series must be repeated. Cesana & Siwek(2020).

$$P_{max} = \frac{P_{\max,\ [\text{series 1}]} + P_{\max,\ [\text{series 2}]} + P_{\max,\ [\text{series 3}]}}{3} \tag{3.1}$$

The ratio between volume and surface area is much larger in the Siwek sphere due to its smaller volume (compared to the 1 m^3cubic tank, which is standard for explosion testing). This leads to an increased cooling effect that results in lower P_{max} and $(dp/dt)_{max}$. To compensate for the cooling effect, the following correction factor is used when $P_{max} \geq 5{,}5$ bar:

$$P_{max} = 0{,}775 \cdot P_{max}^{1{,}15} \tag{3.2}$$

When the apparatus measure pressures below 5.5 bar, the chemical igniters can give sufficiently high pressures to corrupt the measurements (two 5 kJ igniters can give a pressure of 1.6 bar). Correction of pressure when $P_{max} \leq 5{,}5$ bar:

$$P_{max} = \frac{5{,}5*(P_{max}-P_{ci})}{(5{,}5-P_{ci})} \tag{3.2}$$

Here P_{ci} represents the pressure generated by the chemical igniters in bar, and E_i represents the ignition energy in joules.

$$P_{ci} = \frac{1{,}6*E_i}{10000} \tag{3.3}$$

3.1.5 Calculation of maximum rate of pressure rise and K_{St}

The maximum rate of pressure rise is given by the mean value of the maximum results based on three series of tests.

$$(dP/dt)_{max} = \frac{(dP/dt)_{ex,\ [series\ 1],} + (dP/dt)_{ex,\ [series\ 2],} + (dP/dt)_{ex,\ [series\ 3]}}{3} \tag{3.4}$$

Its value is dependent on the volume of the test apparatus and is lower for larger volumes. The K_{St} value is volume independent. As such, the K_{St} value is given in the 20-l sphere by the following equation:

$$K_{St} = 0.02^{\frac{1}{3}} \cdot \left(\frac{dP}{dt}\right)_{max} \tag{3.5}$$

3.2 Experiments in pipes

The primary objective of these experiments was to learn more about silicon dust explosion propagation in pipes. To achieve this, a vast number of experiments were conducted in different experimental configurations, including variations in pipe diameters, nozzles and diffusers, pipe lengths, concentrations, and particle sizes.

3.2.1 Ignition chamber

Figure 3-1 illustrates the ignition chamber. The chamber consists of a concentric transition with a flange welded in both ends, and a vertically hinged cap. The total volume is 32 litres. During the experiments, cap is shut with 16x24mm bolts in the closed end. The chamber can easily be opened for cleaning and installation of ignitors and adapted to fit different dimensions of pipes. Every test sequence was ignited by a single 5 kJ chemical igniter mounted in the middle of the inside of the lid. The chamber was assembled at the workshop at UiB, and the assembly is depicted in Figure 3-2. The dust container, high-speed valve, pneumatic pipes, and dispersion nozzle are all borrowed from an older experimental setup (Enstad, 2009; Kalvatn, 2009; Skjold et al., 2009).

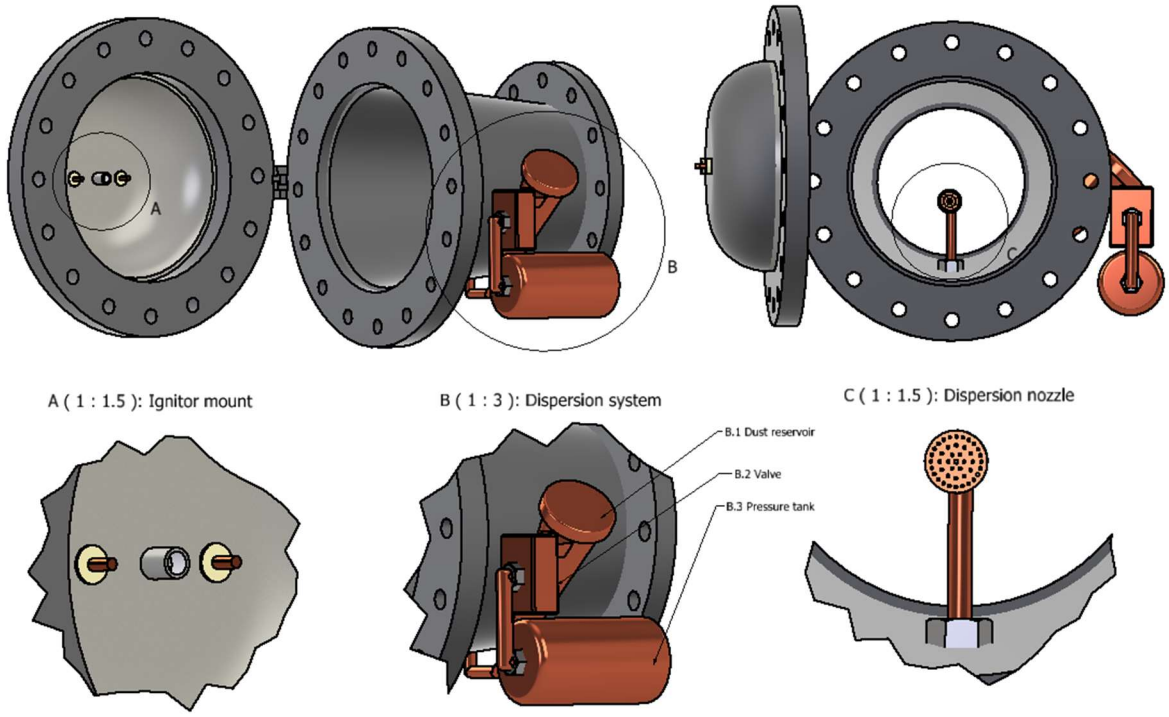

Figure 3-1: Ignition chamber illustration. Detail A illustrates the ignition mounting position, B the dispersion system, hereby a pressure tank, a high-speed valve, and a dust reservoir, and at the end the dispersion nozzle.

Figure 3-2: Ignition chamber assembled at the UiB workshop. The objects in stainless-steel, are part of the dispersion system, a pressure tank, a valve, and a dust reservoir (as illustrated in Figure 3.1, detail B). The cables to the left in the picture are connected to the chemical igniter. Dispersion nozzle and chemical igniter mounting to the right.

3.2.2 Pipes, reducers, and expanders

The pipes utilized in the present experiment are certified to withstand pressures of at least 670 bar. Four pipes were used in the experiments; the specifications of the pipes are listed in Table 3-1. The pipes are machined with threaded holes at intervals ranging from 0.5 to 5.5 meters to accommodate thermocouples with a set distance of one meter between them. Additionally, they were outfitted with mounting points for pressure transducers at intervals of 1, 3, and 5 meters along pipes DN250 and DN160. It should be noted that DN60 was equipped with holes for thermocouples at the same intervals as the larger pipes but has only one mounting point for pressure transducers middle of the pipe. The location for mounting points is illustrated in Figure 3-3.

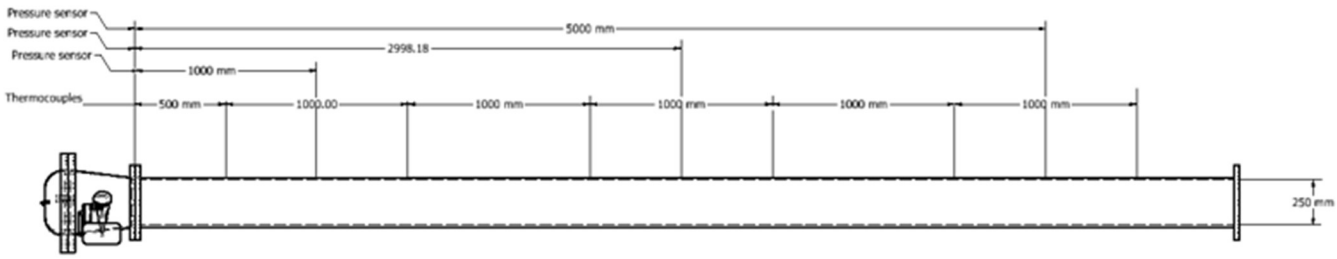

Figure 3-3: Locations of pressure sensors and thermocouples on configuration 1 (DN250). The locations are identical on DN160.

Table 3-2: Dimensions of pipes, and the amount of dust corresponding to concentrations.

Dimensions					**Amount of dust in pipes, given concentrations**					
Pipe length [mm]	Number of pipes	Outer diameter [mm]	Inner diameter [mm]	Pipe designation	250 [g/m^3]	500 [g/m^3]	750 [g/m^3]	1000 [g/m^3]	1500 [g/m^3]	2000 [g/m^3]
6000	1	273	245	DN250	70.72 [g]	141.43 [g]	212.15 [g]	282.86 [g]	424.29 [g]	565.72 [g]
6000	1	178	157	DN160	29.04 [g]	58.08 [g]	87.12 [g]	116.16 [g]	174.23 [g]	232.31 [g]
6000	2	73	62	DN60	4.53 [g]	9.06 [g]	13.59 [g]	18.11 [g]	27.17 [g]	36.23 [g]

The reducers and expanders used to connect the pipes of different configurations consists of a concentric transition with a flange welded in both ends, which can be observed in Figure 3-4.

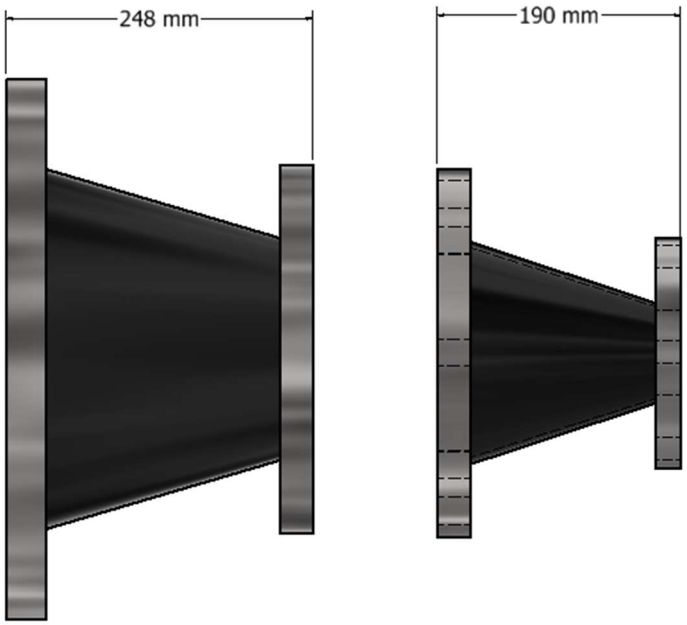

Figure 3-4: The crossovers used to connect the different pipes to each other.

3.2.3 Control system and data acquisition

The pressure transducers were connected to a Kistler SCP amplifier, which converts the signals from the transducers to a standardized voltage of ± 10 V. Signal is then sent to a data acquisition module of the type NI USB-6259 with a sampling frequency of 50 kHz. The acquisition module was connected to a personal computer controlling the trigger sequence and data acquisition through LabVIEW software created by Matthijs van Wingerden.

All the videos from the experiments are captured with a Go Pro Hero 11 at a frame rate of 240 frames per second. Unfortunately, this frame rate is not sufficiently large to give an accurate measurement based on the frames. At 240 frames per second, there is a time delay of 4.167 milliseconds between every frame, which leads to significant uncertainties when calculating flame velocities.

Large amounts of interference in the form of 50 Hz noise gravely impaired the signals, both the piezoelectric pressure transducers and the thermocouples. Due to the 50 Hz frequency, the assumption was that the disturbances originated from the 240V equipment used in the setup. Attempts were made to get rid of the noise without any success. As such, the data was processed in a program named Analyze, developed internally at Gexcon by Matthijs van Wingerden. The smoothing function used was the Savitzky-Golay filter. Figure 3-5 illustrates the difference between raw and filtered data.

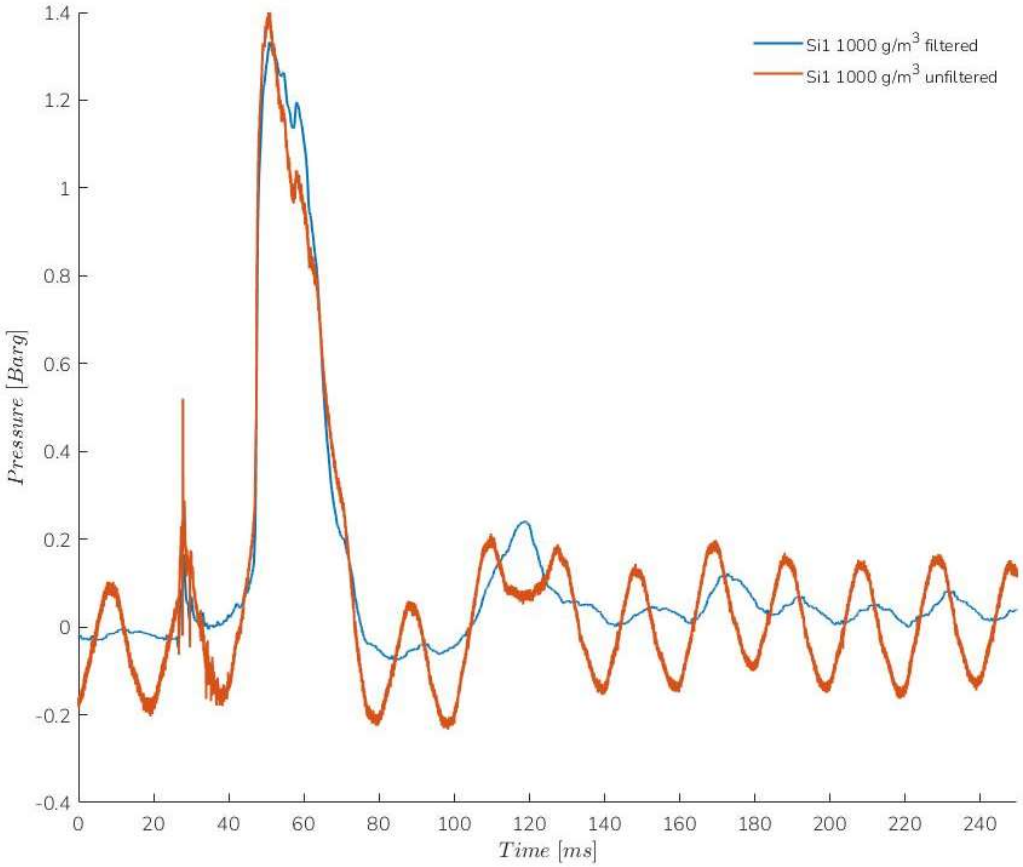

Figure 3-5: Example of data noise from experiments, in this case a test with 1000 g/m³ Si1 inside DN250 . The red curve illustrates the data before filtration, the blue after filtration.

3.2.4 Pressure transducers

Piezoelectric pressure transducers of the type Kistler 701A are installed in threaded holes in both the ignition chamber and the pipes. The placement of theses sensor varies depending on the accompanied configuration and is illustrated in Figure 3-7.

3.2.5 Thermocouples

Two types of thermocouples were used in the DN250 configuration: a “homemade” type and a more robust type with a stainless-steel sheath provided by Gexcon. The homemade thermocouples were fabricated based on the design of Skjold, Kalvatn and Enstad (2009; 2009; 2009). The thermocouples were produced by machining several probes capable of reaching the centre of every pipe, welding together thermoelement type K cable with a diameter of 0.315 mm and mounting these together. The three different sized thermocouples are illustrated in Figure 3-6. Thermocouples inherent a slight delay since the burning gas must heat the thermocouple wire. This delay is assumed to be equal for all thermocouples, thus, the measured velocity equals the flame velocity.

An AD597 setpoint controller is used to amplify the thermocouple signals. The temperature range is given to be from –200 °C to +1250 °C, from thermocouple type K inputs (Analog Devices, 1998). Due to the high temperature of silicon, the thermocouples are intended to measure the arrival of the flame front, not the temperature of the flame.

Figure 3-6: The different sizes of thermocouples, to reach the centre of the pipes.

3.2.6 Configurations

The experiments were conducted in five distinct configurations, as Figure 3-7 illustrates. The specific configuration and sensory location are described in the subsequent results section. In configurations 1 and 2, two complete series of Si-1 and Si-2 were conducted. It should be mentioned that the configurations were also tested utilizing a "reference explosion," with dust only present in the ignition chamber. The dust was distributed along the whole length of the tube. The nominal concentrations and amounts of dust are listed in Table 3-2.

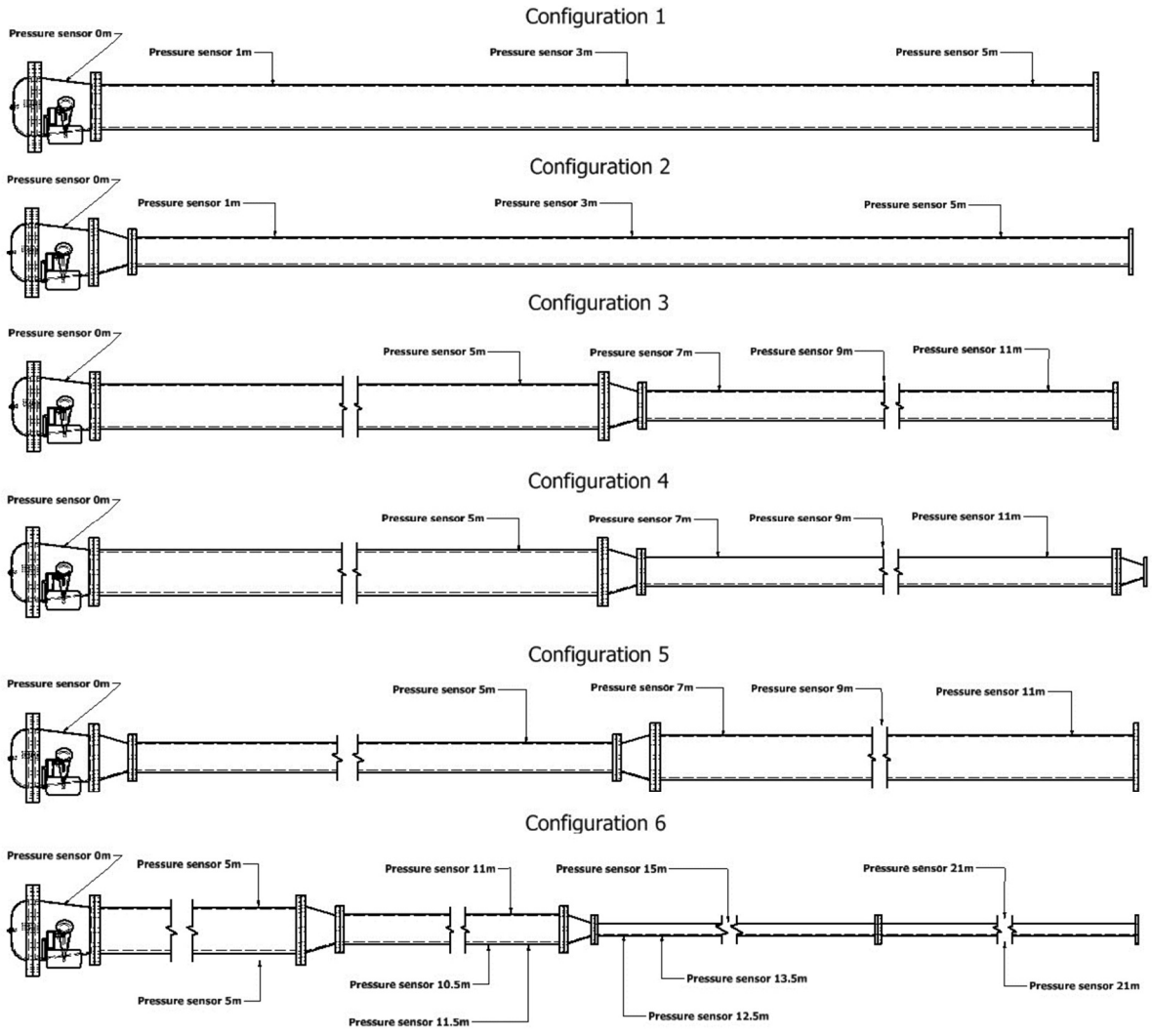

Figure 3-7: Complete overview of the configurations tested during the experiments. Pressure sensor locations are marked on every assembly.

Tests in configurations 3 and 5 were performed with a reduced series of dust concentrations, hereby 750, 1000, and 1500 g/m^3. The dust was initially distributed solely in the pipe furthest from the ignition chamber to dampen the initial explosion. Additionally, one experiment with Si-1 of 1000 g/m^3 distributed in both pipes was conducted. Configuration 4 was only tested once, with a

nominal concentration of 1000 g/m^3. Five tests of Si-1 were conducted in configuration 6, with a nominal concentration of 1000 g/m^3, distributed along all the connected pipes.

3.2.7 Preliminary tests

Preliminary tests were conducted to adjust various parameters, such as reservoir pressure, dust concentration, and ignition time delay, to achieve an initial explosion of sufficient power to suspend the layered dust. The dust cloud was adjusted through visual observations, determining a seemingly well-dispersed and dense cloud. The ignition time delay and the dust concentration were determined based on the flame length produced by an explosion in the open ignition chamber, as illustrated in Figure 3-8. Based on the preliminary tests, standard conditions for all subsequent experiments were established: a reservoir pressure of 21 barg, an ignition time delay of 200 ms, and a dust concentration of 750 g/m^3, corresponding to 24 grams of dust.

Figure 3-8: Ignition chamber test with 750 g/m Si-1 ^{3}, corresponding to an amount of 24 grams.

3.2.8 Procedure

1. Preparing the pipes

The pipes shall be thoroughly cleaned between every test, using a 7m long flexible brush attached to a drill, pressurized air, and an industrial vacuum cleaner. Whenever the configurations extend beyond six meters, the pipes must be split at the transition point and cleaned individually. (In experiments involving thermocouples, the thermocouples must be disassembled prior to cleaning the pipes to clean and repair them).

2. Preparing the dust

Dust samples are measured up according to the amounts observed in Table 3-2. The test sample is distributed evenly in one of two angled irons of lengths 6 m, as illustrated to the left in Figure 3-9. The angled iron is then inserted into the pipe, turned upside down/and distributed on the lower part of the pipe's inner surface.

Figure 3-9: To the left; dust corresponding to a concentration of 250 g/m^3 distributed in the largest angled iron, about to be inserted into DN160. To the right, DN160 with dust distributed on the inner surface.

3. Preparing the ignition chamber

A 5-kJ chemical igniter is inserted into the igniter mounting bracket, shown in Figure 3-1. The ignitor cables are inserted into small holes on each side, and the nuts are tightened to hold them in place. The hinged lid of the ignition chamber is closed, a steel-armed rubber gasket is placed between the lid and the flange, and the 16 bolts are tightened. A weighted sample of 32 grams of Si-1 is inserted into the dust reservoir, and the air reservoir is pressurized to 21 barg.

4. Preparing the data acquisition system

Manual registration of dust type configuration and dust concentration must be typed into the logging program. The acquisition settings must be selected for every experiment. Make sure that these are correct and that the trigger sequence is accurate.

5. Execution of test

Make sure that no unauthorized personnel are in the vicinity. Use an air horn to notify personnel in the area that an explosion is about to be triggered. Then initiate the trigger sequence of the logging program.

4. Results and discussion

This chapter is split into seven subsections. The first section presents the results from the 20-litre experiments, followed by a discussion of the results. The second summarises the flame velocity measurements in DN250, and the rest presents the key findings from all pipe configurations. Malvern reports of the dusts, as well as KSEP reports can be found in Appendix B.

4.1 Experiments in the 20-l apparatus

Silicon dust consisting of two different particle sizes was tested in the 20-liter apparatus; Si-1 with a D50 of 2.65 µm and Si-2 with a D50 of 50.3 µm. Tests aimed to discover the dust explosion indices, P_{max}, $(dP/dt)_{max}$, K_{St}, and LEL, for both dusts. Three different series of tests were conducted for each dust type. The results for Si-1 can be observed in Figures 4-1 and 4-2, plotted against Silgrain results from Skjold (2003) and Østgård (2022). The results for Si-2 are shown in Figures 4-3 and 4-4. The main results are presented in Table 4-1.

Table 4-1: Experimentally measured explosion indices for Si-1 and Si-2, complete reports created by the KSEP software can be found in Appendix C.

Dust sample	**D50 [µm]**	**LEL [g/m³]**	**P_{max} [bar]**	**$(dP/dt)_{max}$ [bar/s]**	**K_{st} [m·bar/s]**
Si-1	2.65	100 ± 10%	9.5 ± 10%	716 ± 12%	194 ± 12 %
Si-2	53.10	180 ± 10%	7.9 ± 10%	299 ± 20%	81 ± 20 %

Throughout the testing in the 20-litre explosion chamber, the results were in good agreement with theory. The maximum explosion pressure, maximum rate of pressure rises, and K_{St}, clearly increased when decreasing particle size, including the lower explosion limit (LEL), which decreased with decreasing particle sizes.

Three different lots from Skjold (2003) were used to compare the results of Si-1, hereby J133, J134 and J135. The average particle size, represented by the D50 value are 3.78, 4.01, and 4.69 µm successively. In addition, nine tests conducted by Østgård (2022), were included to compare the results of Si-1. These dusts had a D50 of 2.77 µm.

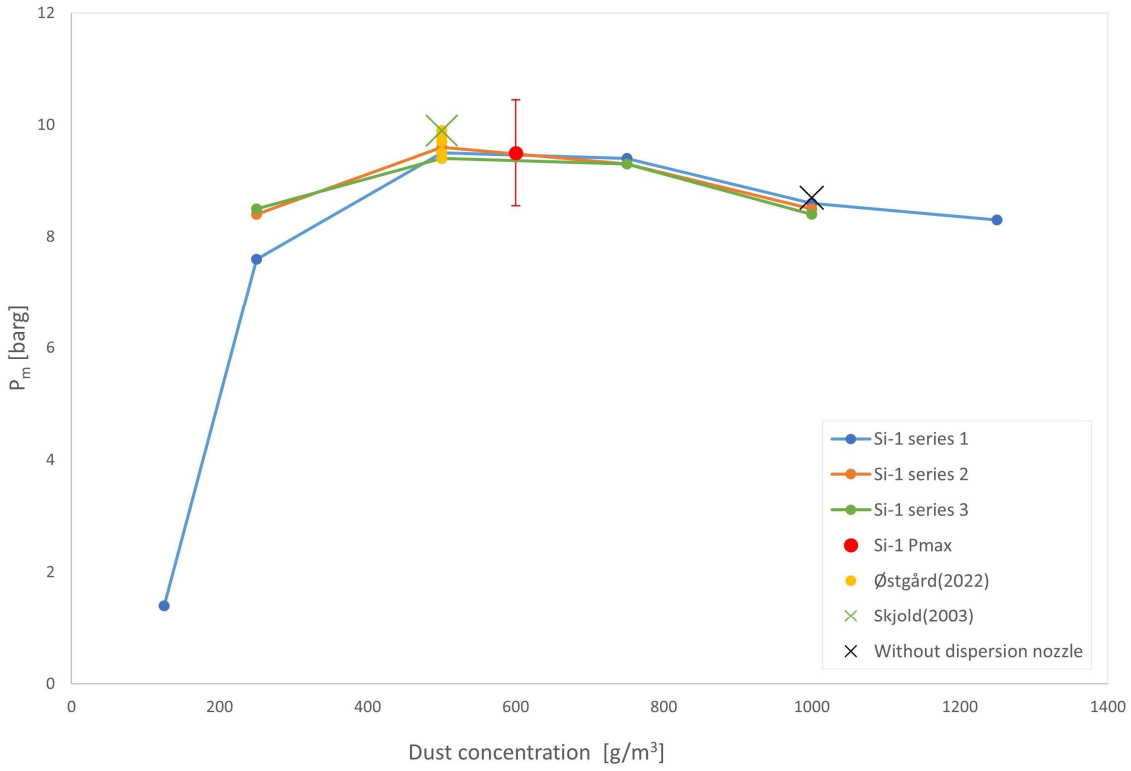

Figure 4-1: Maximum pressure vs concentration for Si-1. Including results from Skjold (2003) and Østgård (2022).

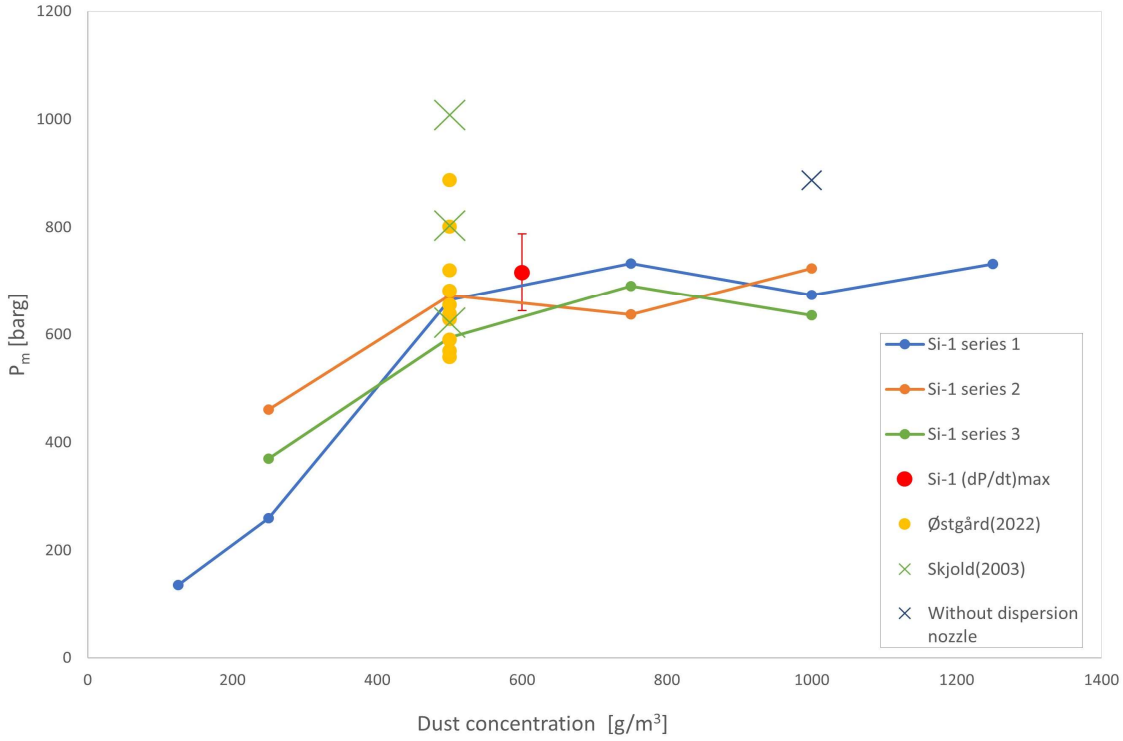

Figure 4-2: Maximum rate of pressure rise vs concentration for Si-1. Including results from Skjold (2003) and Østgård (2022).

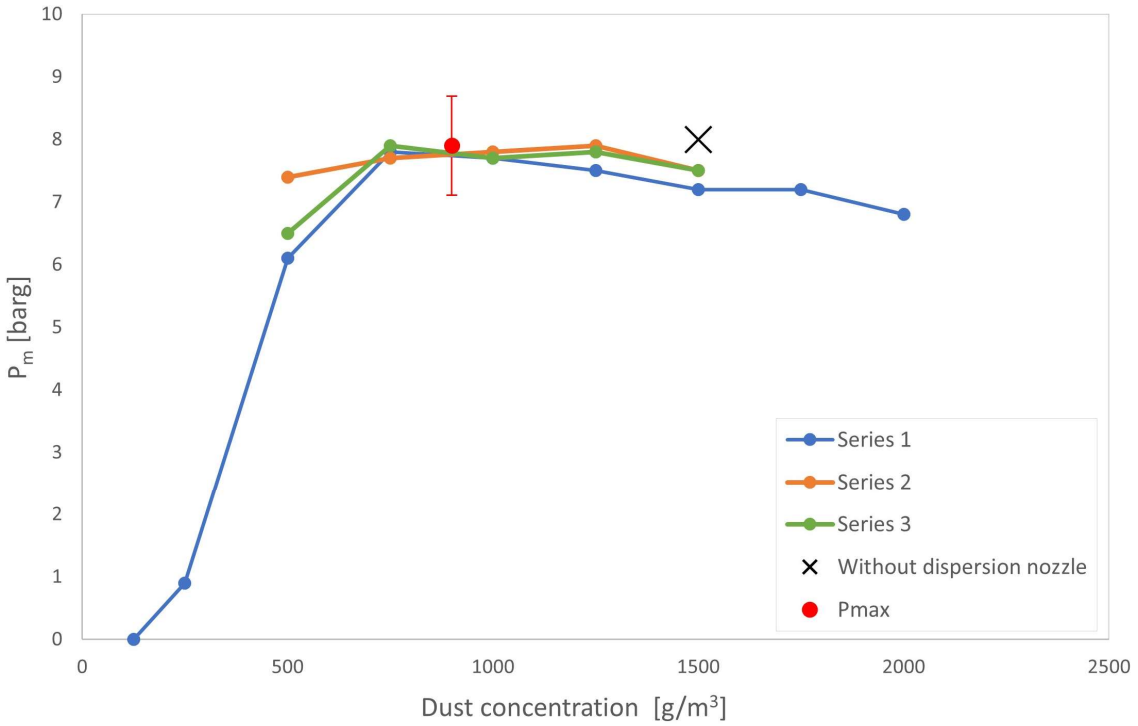

Figure 4-3:Maximum pressure for Si-2. The error of the third series is another incident of igniting the mixture without a dispersion nozzle present in the apparatus. What's interesting is that this misfire led to the highest recorded pressure for this dust, 8.0 barg.

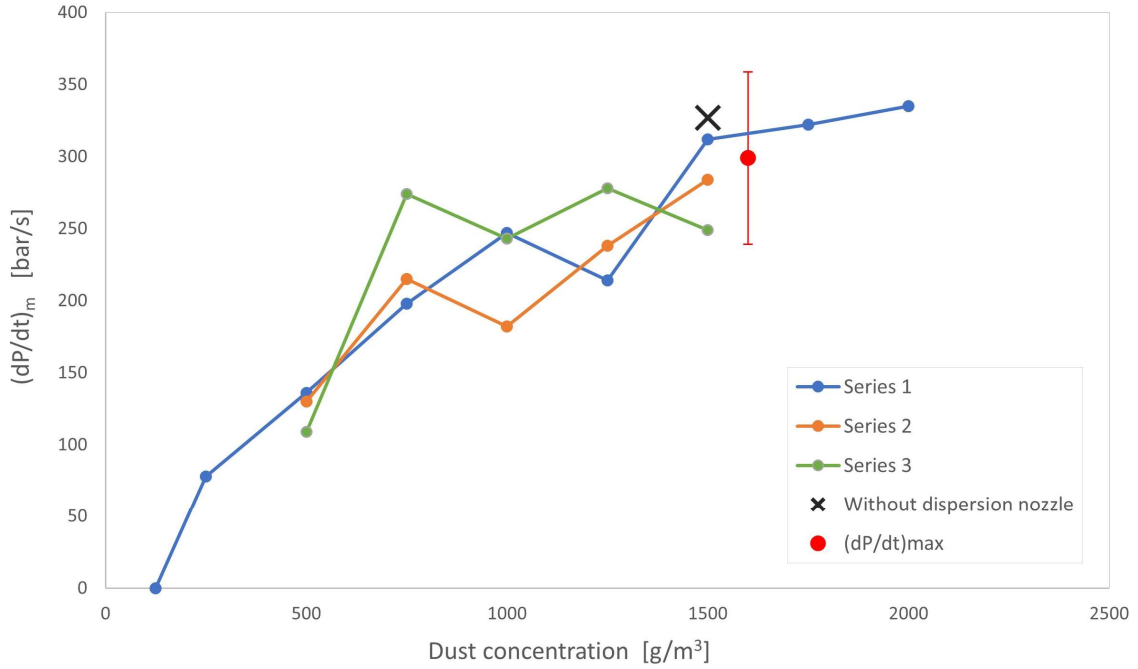

Figure 4-4: Maximum rate of pressure rise for Si-2. Series one indicates that the maximum value of $(dP/dt)_{max}$ has yet to be found.

4.1.1 Discussion

With a K_{St} of 194 ± 12%, Si-1 is on the limit of being classified as strong explosible dust, St2, but is classified as a weak explosible dust, St1. Si-2 is less reactive and classified as a weak explosible dust, St1. This is attributable to the substantially larger particle size distribution of Si-2. The maximum pressures for both dusts were found at concentrations of more than twice the stoichiometric, a phenomenon following leading theories (Nagy and Verakis, 1983, sited in Ogle, 2017, p. 13). The explosion indices of Si-1 are reasonably consistent with the findings of Skjold and Østgård (2022).

One of the upsides of cooperating with experiments is the opportunity of double-checking the work. This might lead to heightened accuracy and reliability of the experiments. Some sources of error are still unavoidable and could impact the results. Some of them are mentioned below.

- Temperature of the chamber. When the chamber has a temperature below 25 degrees C°, the resulting pressure will be higher. Given temperatures higher than 25 degrees C°, the pressure will be lower. There was no way of measuring the surface temperature of the chamber except from physical skin contact. As this is not an ideal scientific solution, there might be some minor discrepancies in the results. Nevertheless, the results seem to be consistent with previous work.
- Test samples. The samples had to be extracted from containers ranging from 20 to 50 litres and might be subjected to segregation. The containers were rotated and mixed according to best practices, and samples were collected by scooping from the top of the containers (Allen, 1997). There is no way of knowing if the test samples represented the bulk of the dust, but the sampling was done as accurately as possible.
- In most of the tests, what seemed to be unburned dust was observed under the dispersion nozzle and in the reservoir pipe. The amount seemed to be increasing with higher dust concentration. This observation might be the result of the initial dispersion pressure, not being able to empty the dust reservoir when more dust is present completely. Some unburnt material will always be in the chamber, especially where dust is trapped. The dust in the reservoir pipe was deemed too minor to impact the results significantly.
- The mass of the dust samples was measured with a digital weight with an error of ± 0.01 g. This error is considered negligible as it is so tiny that it would not impact the precision of the results obtained in the tests.

4.2 Flame velocity measurements

4.2.1 Results

This section presents the data obtained from thermocouples during tests in configuration 1.

The data provided in Figure 4-5 illustrate selected values of disturbance and saturated thermocouple signals. The manual selection of data points proved to be a challenging task to do with high accuracy. Despite this, the first amplitudes at a minimum of ± 0.5 V were selected as an indicator of flow disturbance, whilst the saturated signal at 2.32 V would be a positive flame detection. The manually selected data points and calculated velocities can be found in Appendix C.

Three red lines can be observed in Figure 4-5, the one at ±0.5 V mark the first signal the thermocouples receive, while the red line at 2.32 V indicate the point of which the thermocouples is assumed to be saturated. Velocities illustrated in Figure 4-7 is calculated from selected datapoints at ±0.5 V.

A camera with an FPS of 240 m/s were employed to measure the flame velocity. By taking the number of frames from ignition to visual flame at the end of the tube, a velocity of 180 ±70 m/s is found.

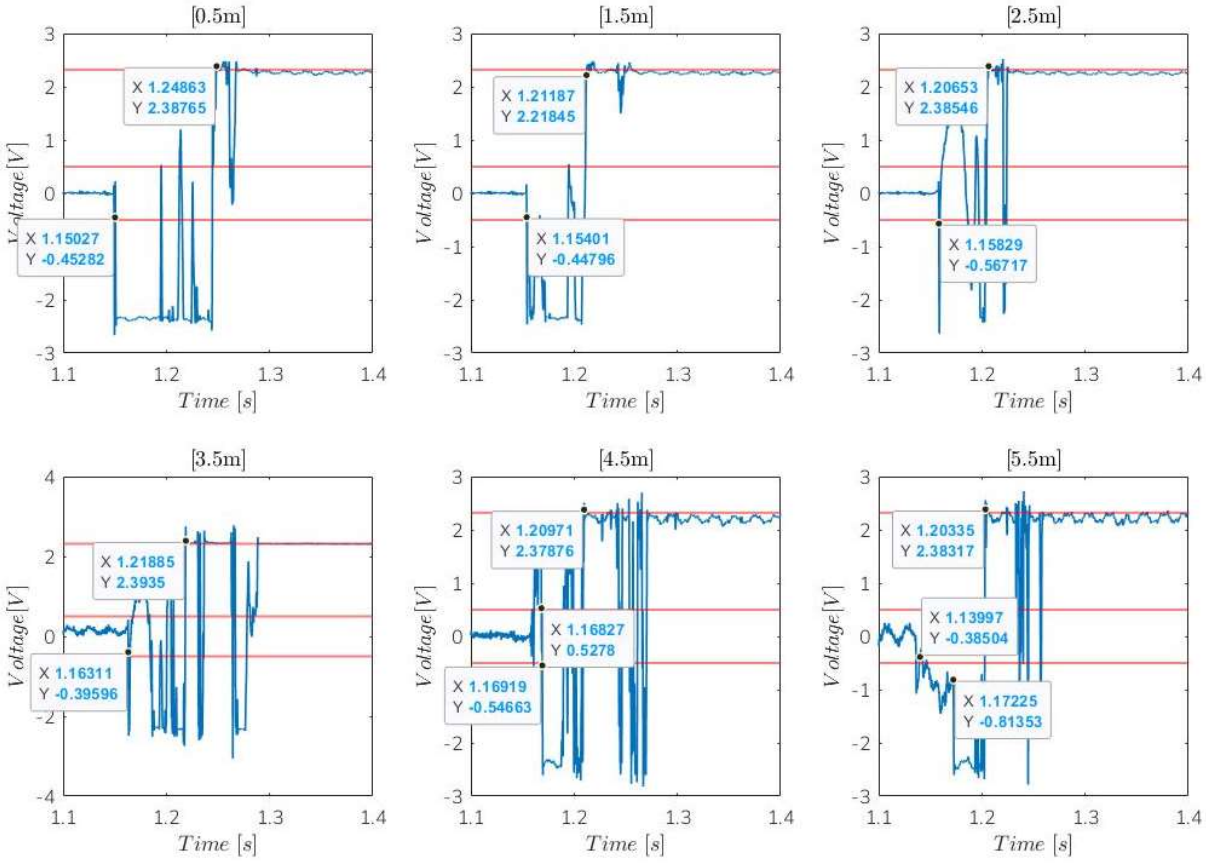

Figure 4-5: Signal from thermocouples during DN250 – Si-1 250 g/m^3 test. The data is filtered, and the datapoints are selected manually.

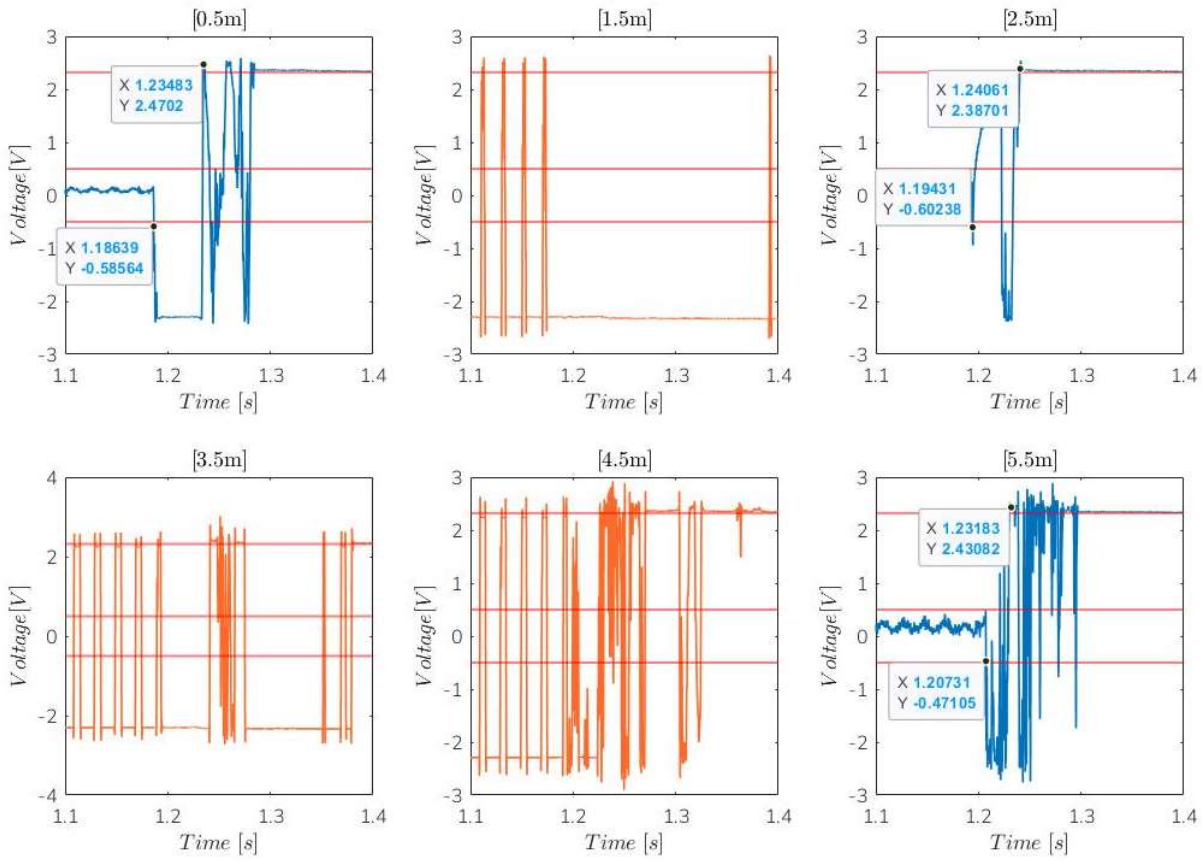

Figure 4-6: Signal from thermocouples during DN250 – Si-1 1000 g/m³ test. The data is filtered, and the datapoints are selected manually. The orange plots show the result from defect thermocouples, which either melted during the previous test, or broke during cleaning between the tests. The signal is no longer usable.

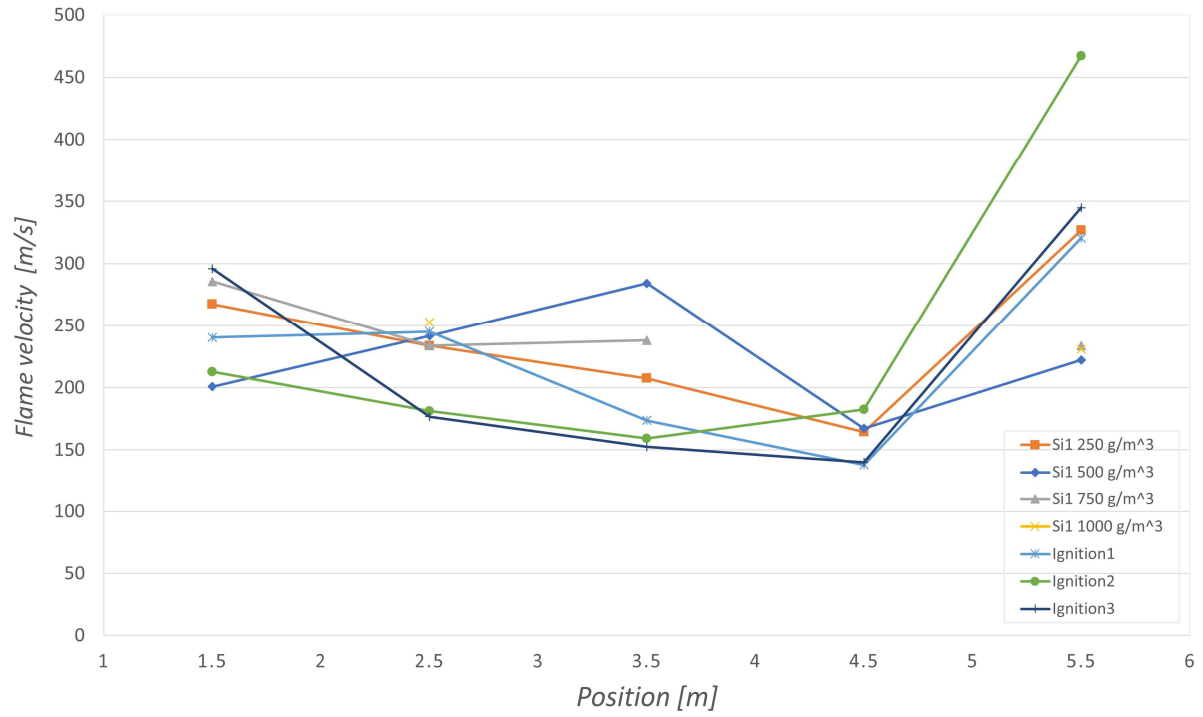

Figure 4-7: Velocities calculated from thermocouple signals.

4.2.2 Discussion

Unfortunately, heat generated during the combustion of silicon resulted in the melting of thermocouple wires during the experiments; thus, only semi-usable datasets were obtained from the first four concentrations, as well as three experiments with dust purely present in the ignition chamber. Subsequently, the thermocouples were replaced with the sheathed thermocouples, and the whole Si-1 series was repeated. The new thermocouples proved to react too slowly to the temperature increase of the flame to generate any valuable data.

Defining the criteria for positive flame detection using thermocouples poses a challenge. It is unclear whether the exact moment the sensor sends any signal should be considered positive flame detection or if the criteria should be a given value where there is no doubt that the sensor has reacted to changes in temperature. Unfortunately, there is a variation in the time it takes for the thermocouples to reach saturation, indicating an individual delay between the thermocouples. This, including the amount of noise in the datasets, make it impossible to use the saturated signal as a positive flame detector, as the signals are not successive, leading to velocities between -100 to 1100 m/s. Using the first amplitude of ± 0.5V show a correlation between the measured tests, but due to the thermocouples not being saturated, one do not know if it is the measurement of a flame or just the disturbance from the initial explosion.

It is essential to point out the uncertainties present in the flame velocity calculations. Captured video from identical DN250 experiments shows complete flame propagation through the pipe after eight frames for all concentrations. At 240 frames per second, this corresponds to an average flame speed of 180 ±70 m/s. Which is a very large uncertainty.

Although measuring flame velocities with thermocouples has been proven successful for gases and organic dusts (Enstad, 2009; Skjold et al., 2009), it does not work silicon dust explosions. Due to silicon's high combustion temperature, the thermocouple wire will likely burn up during the reaction. Using cameras with a higher frame capture rate would also be ideal if the goal is to have reliable flame velocity measurements.

4.3 Experiments in configuration 1

4.3.1 Result

Two complete series of Si-1 and Si-2 were tested, with concentrations ranging from 250 to 2000 g/m^3, and a reference test with only dust in the ignition chamber. The location of the pressure transducers is illustrated in Figure 4-8.

Pressure histories of all concentrations of Si-1 are presented in Figure 4-9, while the results of Si-2 are presented in Figure 4-10. The fireballs depictured in Figure 4-11 represent the most significant fireballs from each experiment of Si-1, while Figure 4-12 is the largest ones found for each experiment of Si-2.

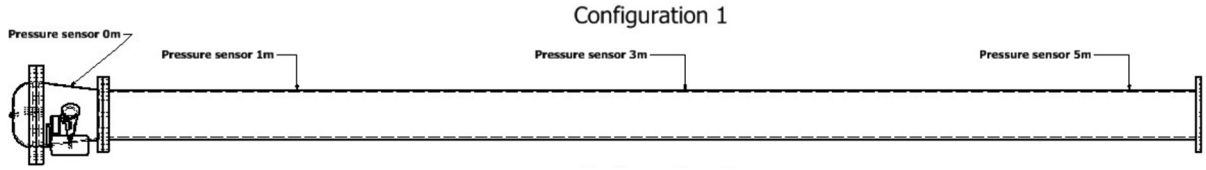

Figure 4-8: Illustration of ignition chamber connected to DN250, with the locations of the pressure transducers.

The pressures presented in Figures 4-9 and 4-10 do not seem to depend on the amount of dust in the pipe. Neither the Si-1 nor Si-2 pressure series stand out. The highest pressures are not located around the concentration that led to the highest pressures in the 20-litre experiments, nor do there seem to be outliers or distinct trends in the results, at least not for the Si-1 series.

Si-2 series create identical pressure curves almost independent of concentrations, though a minimal increase in pressure is present with concentrations of 250 and 500 g/m^3. This increase is deemed so small that it could be a coincidence due to the lack of repeatability of dust explosions. Table 4-2 lists the measured lengths of all the fireballs observed. Fireballs from Si-1 increased in length with increasing nominal concentration. Si-2 did not.

Table 4-2: Length of fireballs vs the nominal dust concentration in configuration 1.

Concentration [g/m^3]	**Fireball Length Si-1** [m]	**Fireball Length Si-2** [m]
0	1.5	1.5
250	4	3
500	4	3
750	4.5	1.5
1000	4	2
1500	5	3
2000	5	2.5

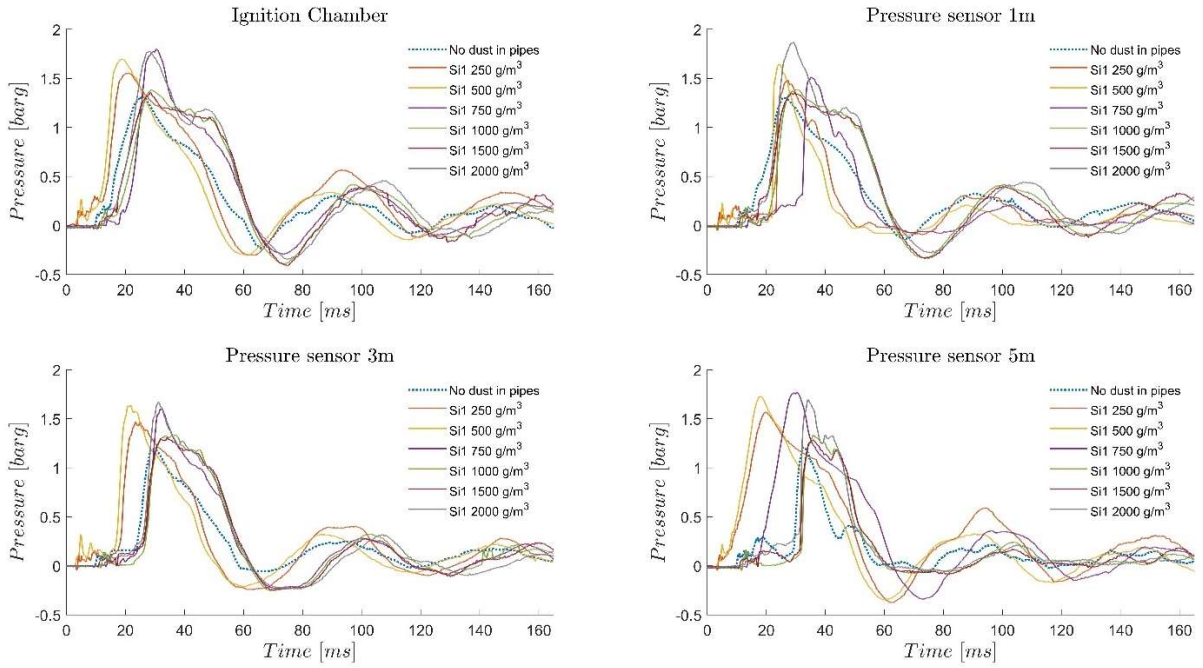

Figure 4-9: Pressure history for all concentrations of Si-1 in DN250 configuration.

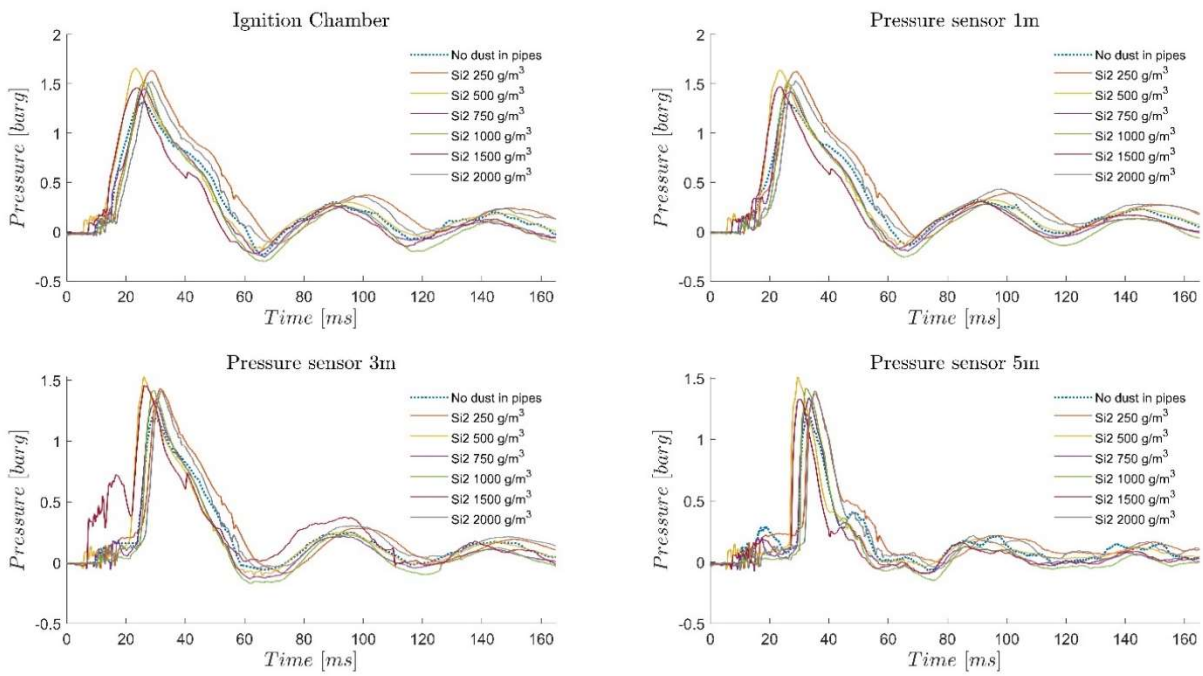

Figure 4-10: Pressure history for all concentrations of Si-2 in DN250 configuration.

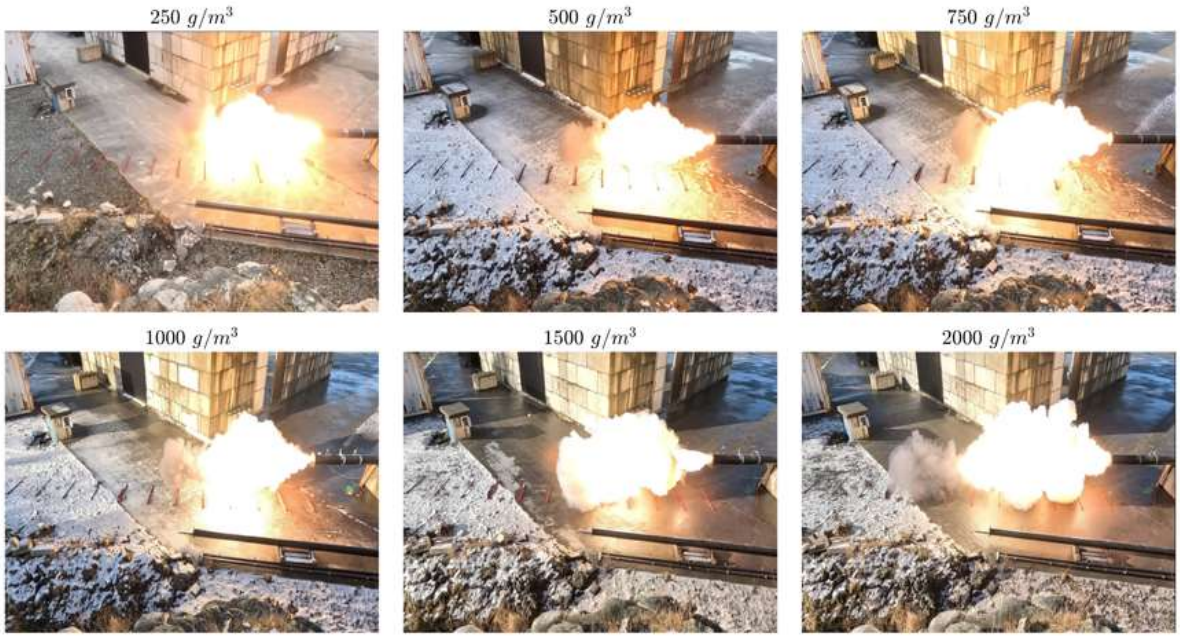

Figure 4-11: Fireball from every experiment of Si-1 in DN250. It can clearly be observed that higher concentration of dust leads to a larger fireball.

Figure 4-12: Fireballs from every experiment of Si-2 in DN250.

4.3.2 Discussion

Due to its significantly smaller particle size distribution, the Si-1 series was expected to produce notable higher pressures than the Si-2 series. Si-1 pressures observed in Figure 4-9 show a slightly elevated pressure development, though the difference is close to negligible. The leading assumption is that the initial explosion is of such intensity that most of the layered dust gets suspended and pushed out of the pipe before reacting on the outside. The recordings of the experiments back up this assumption to some degree. A comparison of the pressures at the 5-metre transducers for Si-1 and Si-2 is presented in Figure 4-13. No clear correlations is observed between the maximum pressures and the nominal concentration.

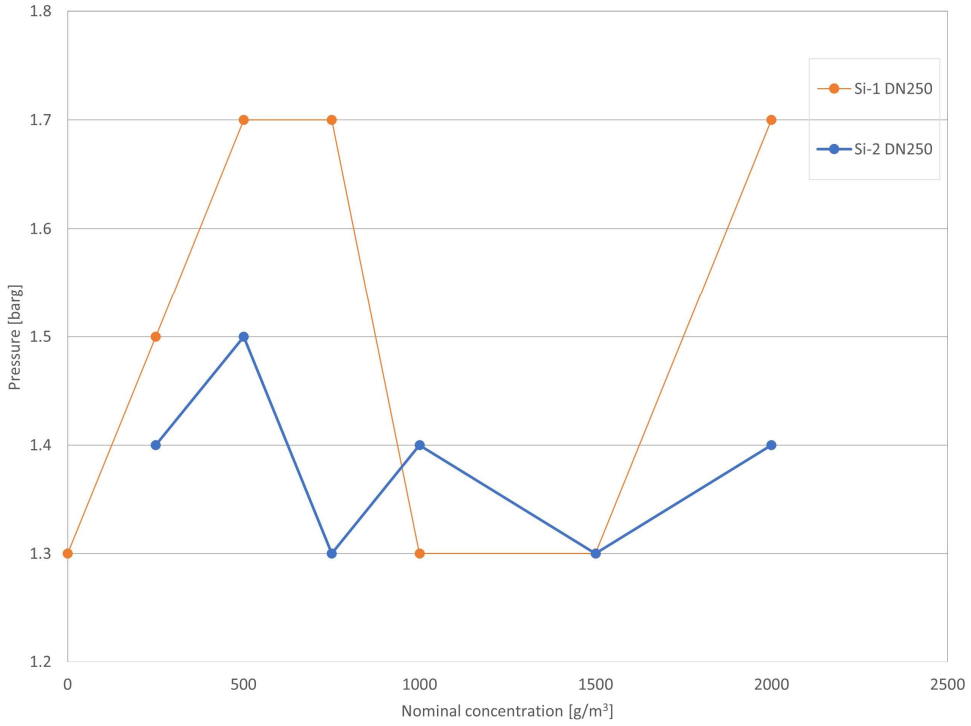

Figure 4-13: Pressure vs nominal concentration.

There is a steady increase in the size of the fireball from the Si-1 series. Interestingly, the fireballs from Si-2 do not increase in size when the nominal dust concentration increases. However, it is possible to observe more significant amounts of dust ejected from the pipe. Presumably, this is due to the large particle size of Si-2 being more challenging to suspend and ignite. Thus, a smaller amount of the present dust will react. A comparison of the length of the fireballs between Si-1 and Si-2 is presented in Figure 4-14.

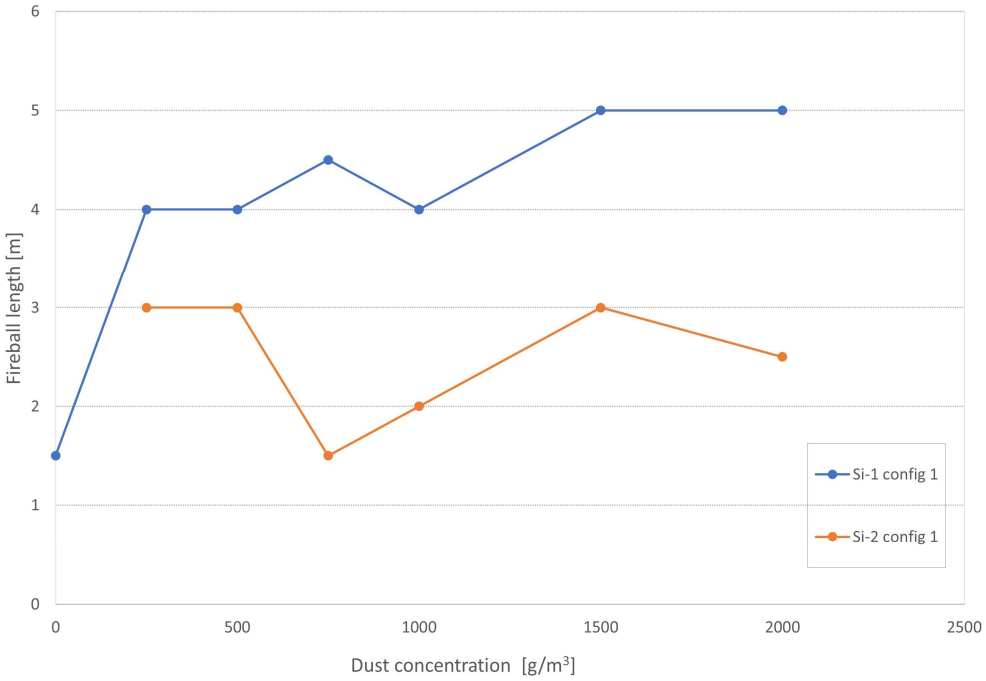

Figure 4-14: Fireball length vs nominal dust concentration.

A phenomenon of interest can be observed in the slow-motion video of the fireballs. The explosion within the pipe appears to happen in three stages. After the initial explosion which entrains and push dust out of the pipe, the flame in the opening becomes smaller before suddenly flaring up again. This effect occurs at least three times for every test concentration, though the flame grows smaller with each iteration. A potential explanation for this phenomenon might be that when the initial combustion wave leaves the pipe, fresh oxidizer can enter the pipe, and thus more of the dust in the pipe can react. Alternatively, the convective flow from the initial explosion did not suspend all the dust in the pipe, leaving dust to be entrained by the deflagration wave. The observations might then be the re-ignition of previously dispersed dust that did not react in the first combustion wave.

4.4 Experiments in configuration 2

4.4.1 Results

The results from experiments in the DN160 pipe are presented. Two complete series of Si-1 and Si-2 were tested, with concentrations ranging from 250 to 2000 g/m^3, and a reference test with no dust in the pipe. The location of the pressure transducers was identical to the DN250 configuration and can be observed in Figure 4-15.

Figures 4-16 and 4-17 show the pressure histories of the different dusts. Figures 4-18 and 4-19 depict collages of the most significant fireballs observed in the experiments.

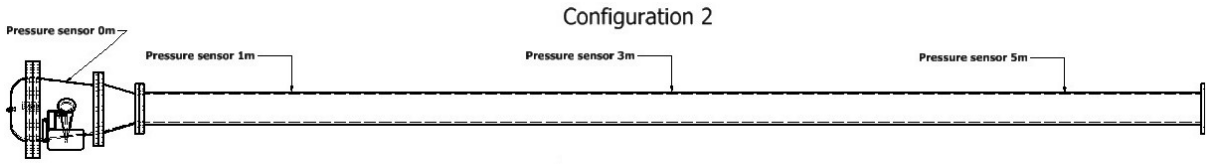

Figure 4-15: Illustration of ignition chamber connected to DN160 pipe.

As suspected and in accordance with the theory mentioned in section 2, the maximum pressures increased when the pipe diameter was reduced. The Si-1 reference explosion gave rise to pressures about twice the size of those in the DN250 pipe. In contrast to the DN250 configuration and Si-2 in DN160, all the concentrations of layered Si-1 proved to give substantially larger pressures within the DN160 pipe, which seem to increase along with the length of the pipe. Table 4-3 lists the measured lengths of all the fireballs observed during tests in configuration 2.

Table 4-3: Length of fireballs vs the nominal dust concentration in configuration 2.

Concentration [g/m^3]	**Fireball Length Si-1 [m]**	**Fireball Length Si-2 [m]**
0	2	2
250	4	3
500	4	3.5
750	4.5	4
1000	5	4
1500	5.5	4.5
2000	6	4.5

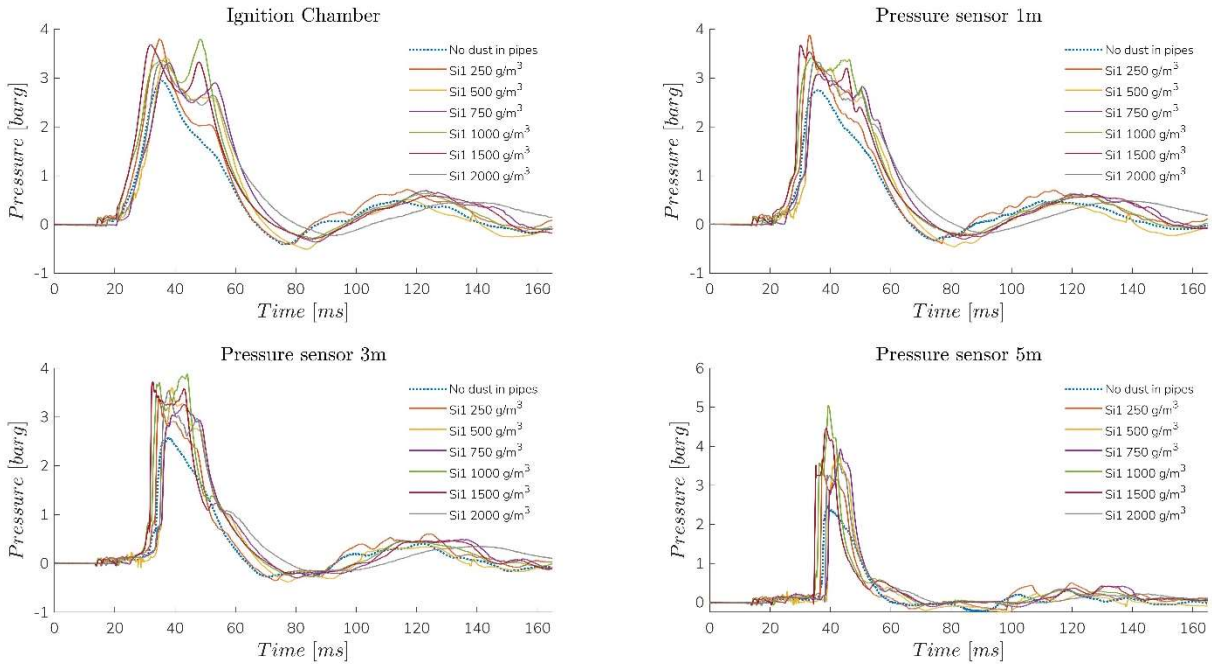

Figure 4-16: Pressure time histories at all transducer locations for Si-1 series in DN160 configuration.

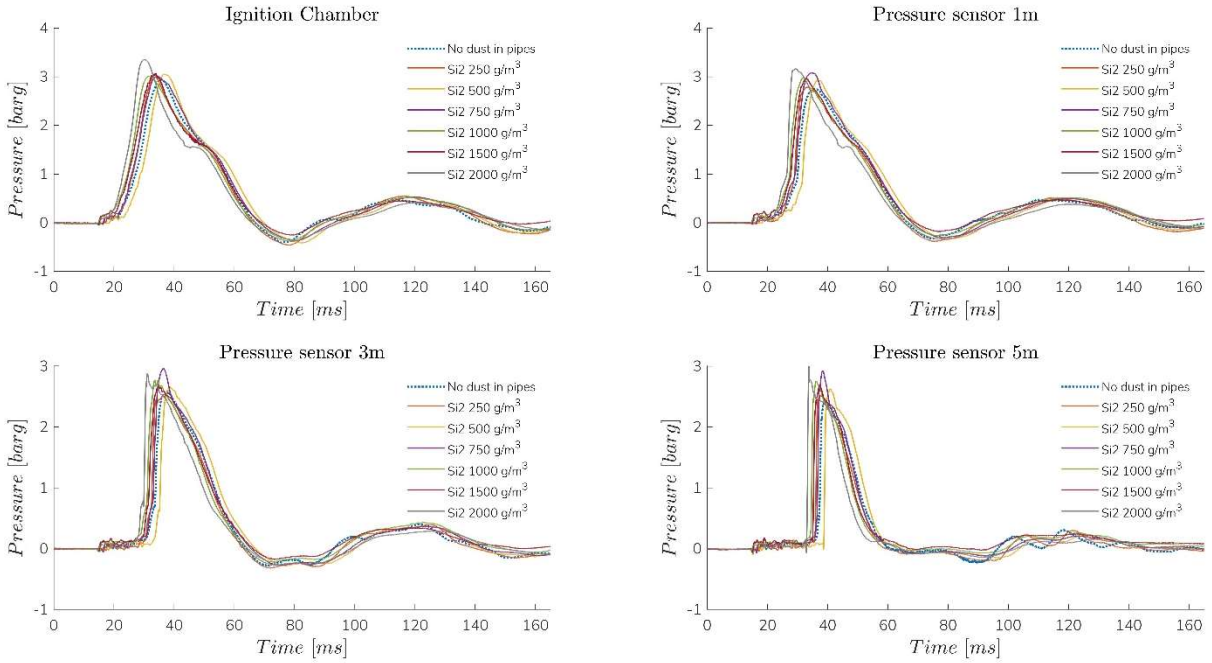

Figure 4-17: Si-2 series in DN160 for all transducer locations. Show very little differences between the reference explosion and the varying concentrations.

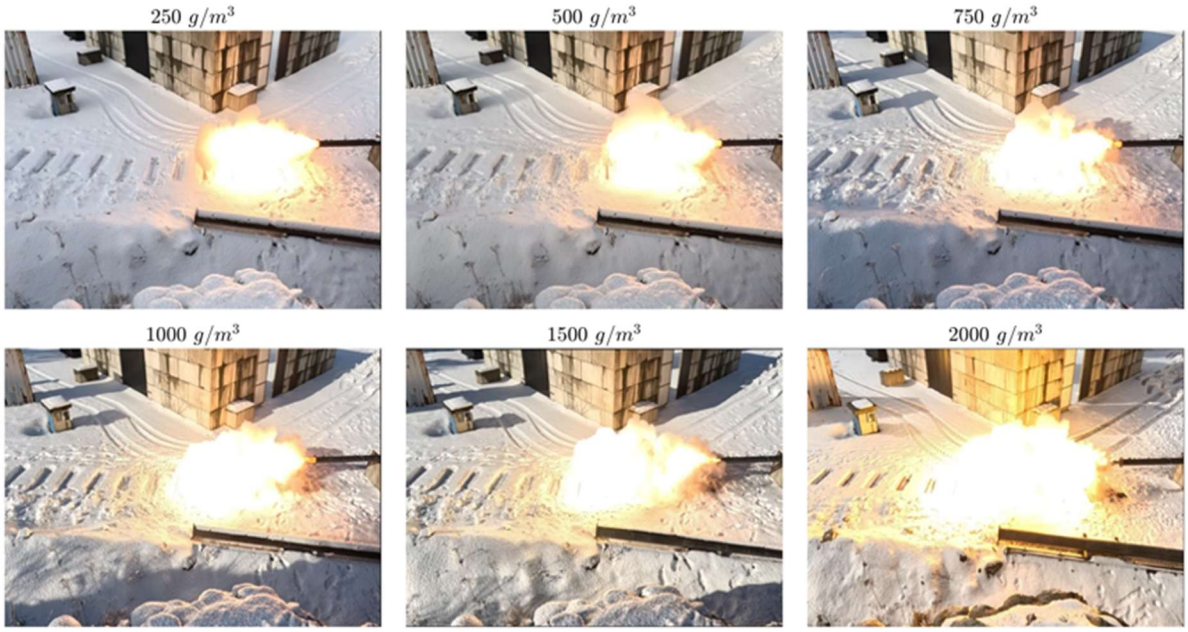

Figure 4-18: Fireballs from every experiment of Si-1 in DN160. Higher concentrations yield larger fireballs.

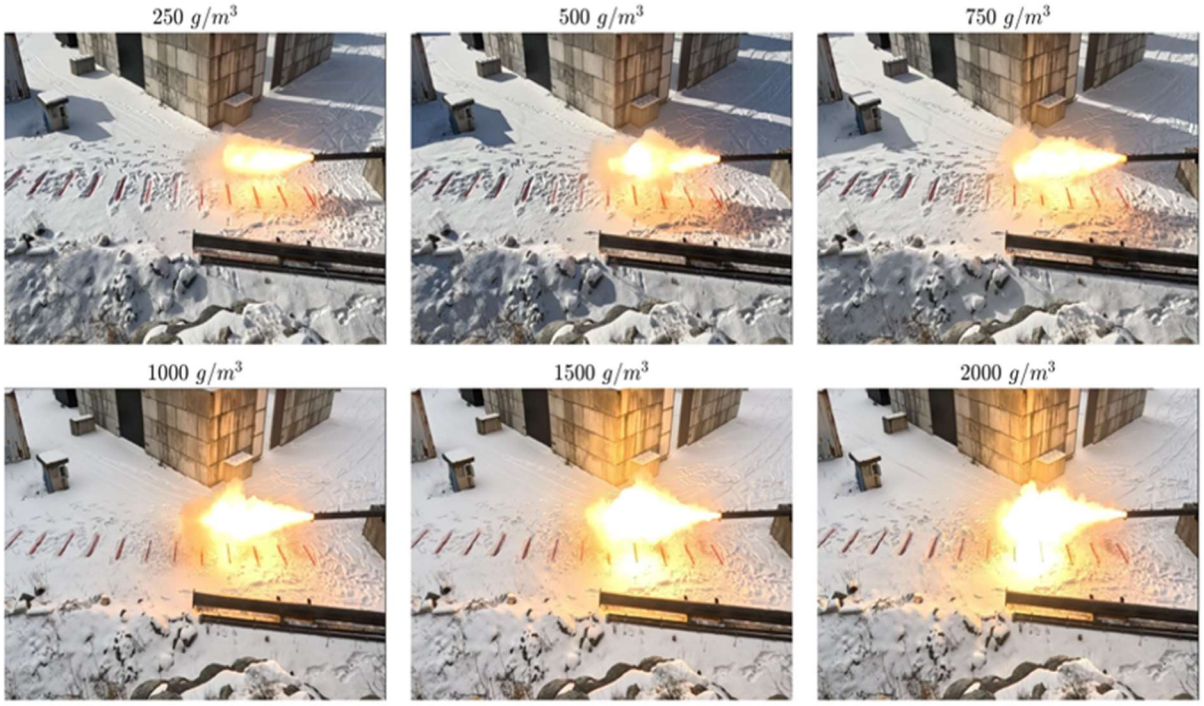

Figure 4-19: Fireball from every experiment of Si-2 in DN160. Higher concentrations of dust seem to give rise to larger fireballs.

4.4.2 Discussion

Given the smaller diameter of the pipe, the initiating explosion will give rise to a higher pressure, as have been demonstrated by previous research. The increased pressure leads to a more powerful convective flow, that manages to suspend more of the layered dust, then the deflagration wave ignites it. As the flame propagates further along the pipe, more dust can react, thus the combustion wave accelerates, increasing in speed and pressure, which leads to higher pressures the further away from the ignition that the combustion travels. The highest pressures are recorded at the 5-metre pressure transducer at a concentration of about 1000 g/m^3, as illustrated in Figure 4-20. Though the higher pressures might indicate flame acceleration, there is no clear correlation between the concentration and observed pressures.

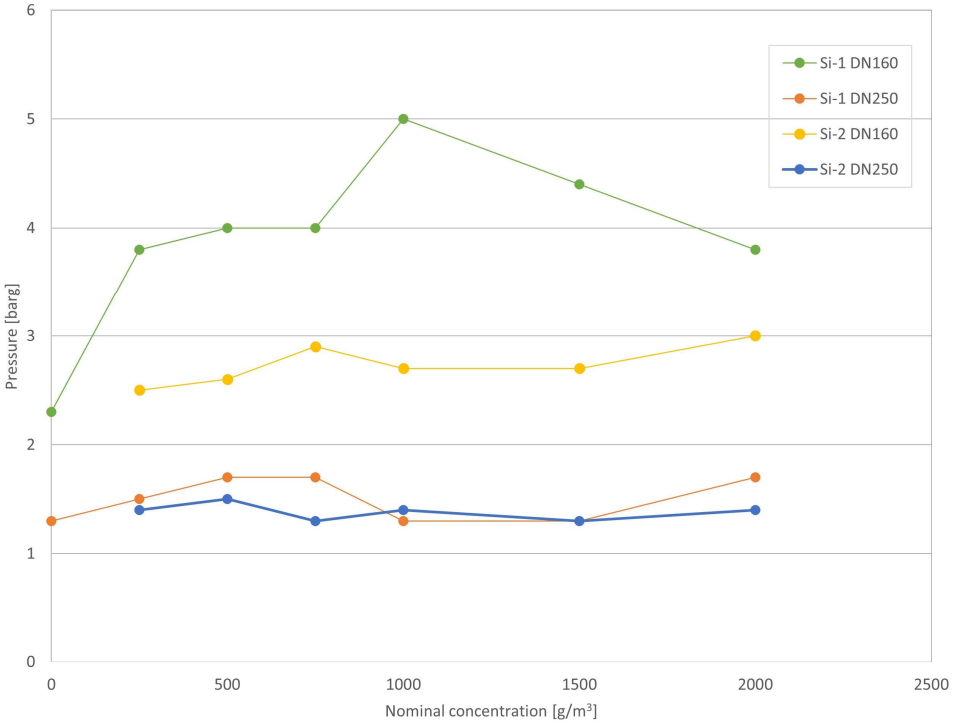

Figure 4-20: Pressure vs nominal dust concentration, at the 5-metre transducer in configuration 1 and 2.

An elevation of pressures can be observed at approximately 45 ms at the 5-metre pressure transducer. The elevated pressures can be seen in consecutive order at all the other sensory locations. This might indicate the generation of a pressure wave from an increase in flame acceleration between the three-metre and 5-metre transducers.

Figure 4-21 show the length of the fireballs for all concentrations of Si-1 and Si-2 in configuration 1 and 2. The size of the fireballs of Si-1 increase when increasing the nominal concentration of dust, in both configurations. Fireballs from Si-2 did not increase during configuration 1, but they do increase in length with increasing concentration in configuration 2.

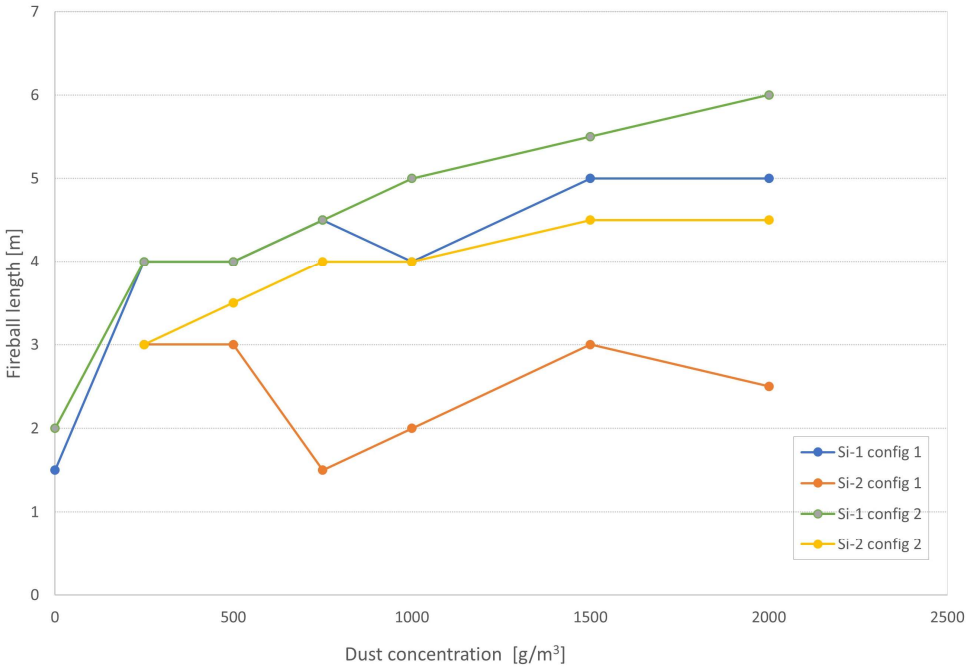

Figure 4-21: Length of fireballs vs nominal concentration for configurations 1 and 2.

No substantial increase in pressure was recorded during the Si-2 tests. Even though the initial explosion was equal to that of Si-1, it does not seem that a further reaction with Si-2 occurred inside the pipe. The size of the fireball increases with an increasing amount of dust in the pipe, suggesting that the increased power of the initial explosion allowed more Si-2 to be entrained by the flow, then ignited on the outside of the pipe.

4.5 Experiments in configuration 3 and 4

4.5.1 Results

The reduced series of Si-1 distributed in DN160, with concentrations of 500, 1000, and 1500 g/m^3, is presented in Figure 4-23, along with a representative test without dust present in the pipes. Figure 4-24 presents Si-1 in both pipes, including plots of Si-1 and Si-2 in DN160. Figure 4-26 present the differences in pressures between configurations 3 and 4.

An illustration of the configurations and the location of pressure transducers can be observed in Figure 4-22. Figure 4-25 depicts the flames and dust clouds ejected from the configuration.

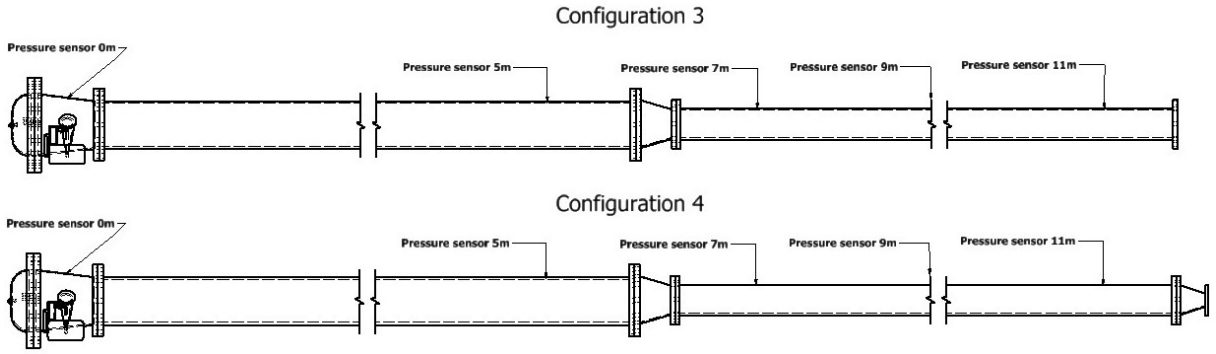

Figure 4-22: Illustration of configurations 3 and 4.

The tests in configuration 1 showed little to none sign of dust lifting and flame acceleration inside the pipe, probably due to the powerful initial explosion. To compensate for the initial explosion, a series of tests was done with dust solely distributed in DN160 whilst connected to DN250 (with the intention that DN250 would dampen the initial explosion). Subsequently, one test was done with dust present in both pipes.

The Si-1 series from Figure 4-23 demonstrated no indications of flame acceleration inside DN160. The pressure histories are consistent with the reference explosion for all concentrations.

Neither of the dusts generated elevated pressures when distributed in DN160. However, a slight increase for all pressures could be noted at the 5-metre mark before the nozzle. This indicates a weak pre-compression induced by the flow before being ignited by the deflagration wave. When Si-1 was present in DN160 and DN250, pressures of 10.4 bar could be observed at the 11-metre transducer, as illustrated in Figure 4-24, higher than any of the maximum pressures found in the 20-litre apparatus. Interestingly, neither the Si-2 nor the 1000 and 1500 g/m^3 Si-1 could propagate a flame throughout the pipes.

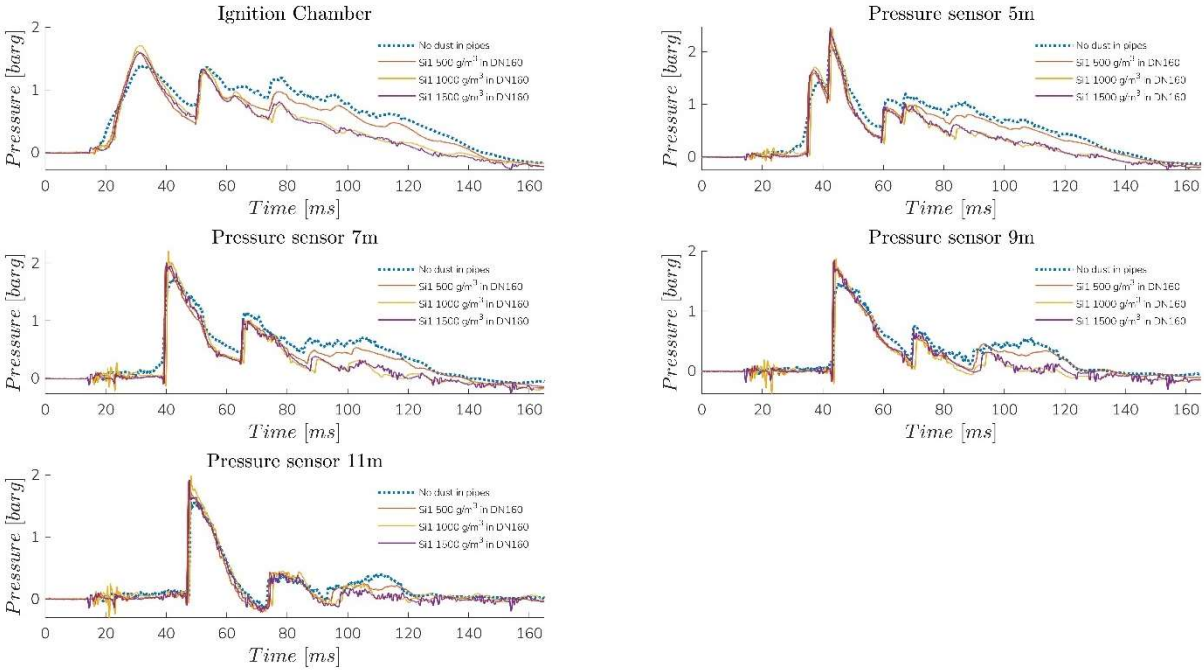

Figure 4-23: The reduced Si-1 series distributed in DN160.

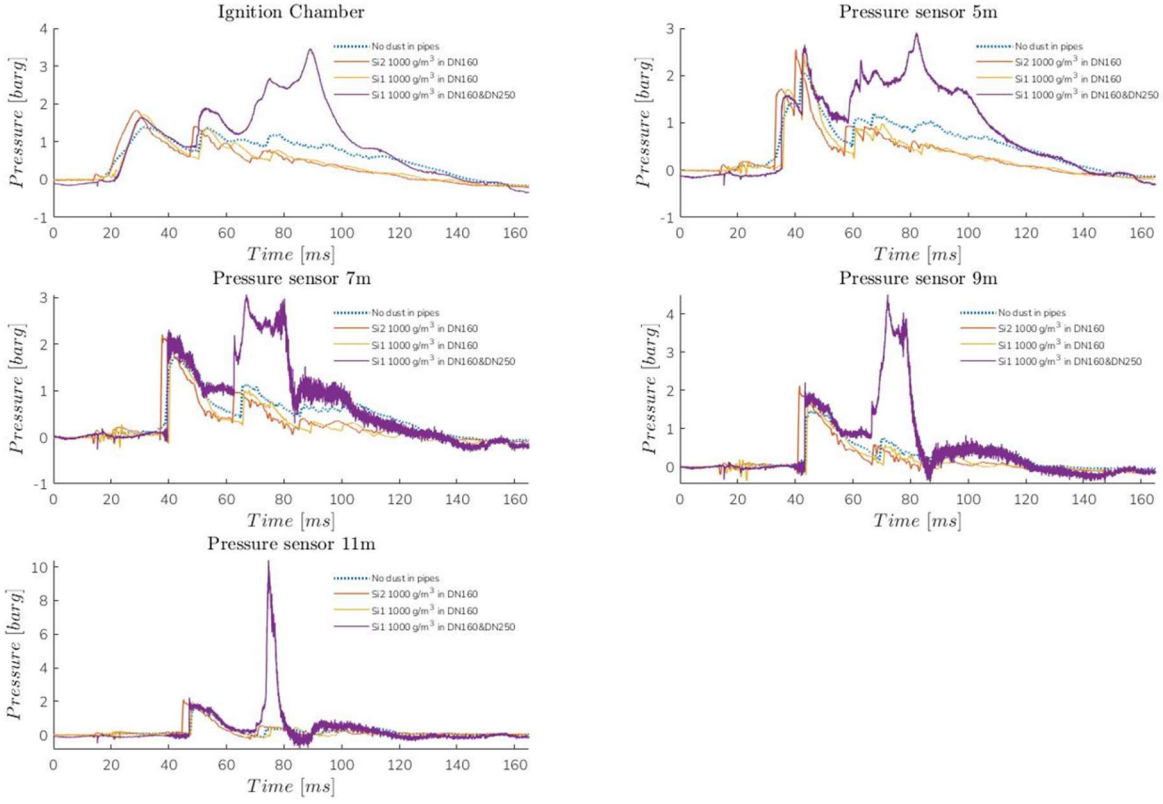

Figure 4-24: Si-2 distributed in DN160, 1000 g/m^3 Si-1 distributed in DN160 and 1000 g/m^3 Si-1 distributed in both pipes. Observe how the maximum pressure of Si-1 increases with the length of the pipes. The purple pressure history's data is unfiltered.

Figure 4-25: Ejected dust clouds and flames from the DN250/DN160 configuration. Notice the colors of the ejected dust clouds, the dark clouds indicate large amounts of unburnt dust.

4.5.2 Discussion

Every pressure history from Figure 4-23 shows a gradual decrease in pressure following the initial explosion. At the 5-metre transducer location, an abrupt increase in pressure can be observed at approximately 35 ms, indicating the leading shock. The leading shock can also be observed at the seven-metre transducer at 40 ms, with a clearly higher amplitude. This could be explained by the leading shock's interaction with the converging nozzle, which is known to amplify pressure waves (Ben-Dor et al., 2001).

A subsequent increase in pressure can be observed at the 5-metre transducer at 45 ms, followed by an extended period of decreasing pressure. This might be the deflagration wave interacting with the nozzle. The expanding burnt gases push the unburnt gases ahead of itself like a piston; when approaching the nozzle, a normal subsonic flow would decrease pressure while increasing speed (Cengel & Boles, 2006). The expanding gases will try to push the unburnt gas through the nozzle, leading to a weak form of compression of the flow approaching a smaller diameter. At some point, the nozzle's contribution to the flow will be larger than the contribution of the expanding gases, resulting in a decrease in pressure and an increase in velocity.

The pressure histories of Figure 4-24 are of particular interest, especially the situation of dust distributed in both pipes. All the transducers show a gradual pressure drop from 40 ms to 60 ms. This might be according to fluid flow theories, with the subsonic deflagration wave approaching the converging nozzle, resulting in the pressure of the flow decreasing while the velocity increases (Cengel

& Boles, 2006), but given no flame velocity data, it remains uncertain. At 60 ms, a new increase in pressure occurs at the seven-meter transducer, indicating an accelerating flame that increases in speed and pressure until a maximum of 10.42 barg at 11 meters, at about 75 ms. Reverse shock waves can be seen in successive order at the other transducer locations. The increased acceleration of the flame and subsequent maximum pressures is believed to be caused by turbulence generated by the flow intersection with the nozzle and the tube walls, which stretches the flame and increases the reaction's burning rate.

Comparing the configuration with and without a nozzle in Figure 4-26 clearly shows the impact of the nozzle at 12 metres. The steep pre-compression at the 11-metre transducer due to the nozzle is evident and results in a faster maximum pressure when the deflagration wave ignites the pre-compressed mixture, as can be observed at 43 ms at the 7 and 9-metre transducers. For some reason, the maximum pressures are more considerable without a nozzle than with a nozzle.

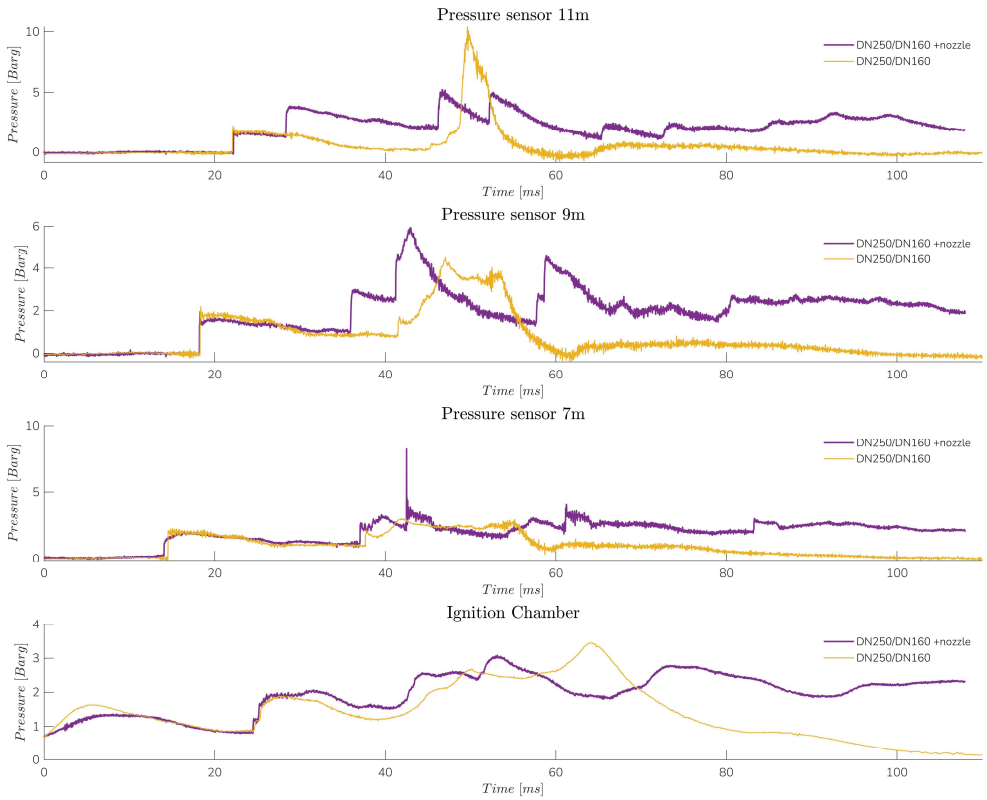

Figure 4-26: Comparison of pressures in configurations 3 and 4.

The lack of complete flame propagation for Si concentrations above 500 g/m^3 remains a mystery. The nozzle might choke the flow to the extent of limiting flame propagation, but that does not explain the complete flame propagation for the reference and 500 g/m^3 tests. Introducing a nozzle in the pipes produced more complex pressure wave interactions and pressure-time histories.

4.6 Experiments in configuration 5

4.6.1 Results

The configuration was tested with a reduced series of Si-1 layered in DN250, one experiment of Si-2 layered in DN250, and one experiment with Si-1 distributed in both pipes. The reduced series consisted of concentrations ranging from 500 to 1500 g/m^3 distributed in DN250. Si-2 was tested at a concentration of 1000 g/m^3. The experiment with dust in both pipes was at a concentration of 1000 g/m^3. All the pressure histories can be observed in Figures 4-28 and 4-29. Figure 4-30 is a collage of flames and dust ejected from the configuration during flame propagation. The location of pressure transducers can be seen in Figure 4-27.

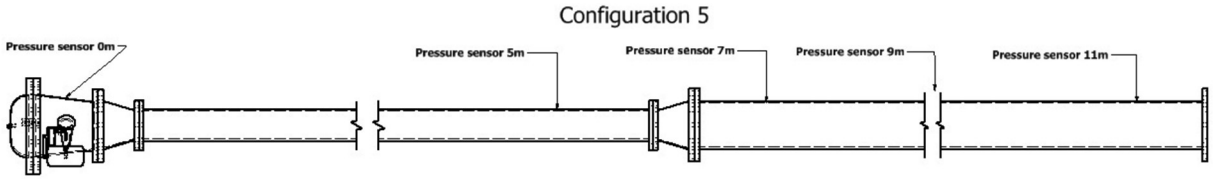

Figure 4-27: Illustration of the DN160/DN250 configuration, along with locations of pressure transducers.

Like previous configurations, the pressure resulting from Si-1 combustion increases with the length of the pipes if there is dust in the pipe. This can be observed by the yellow line in Figure 4-29, representing Si-1 1000 g/m^3. The purple line represents pressure history based on raw data of Si-1 distributed in DN160 and DN250. The most significant pressures were observed when dust was distributed in both pipes, a maximum pressure of 5.4 barg.

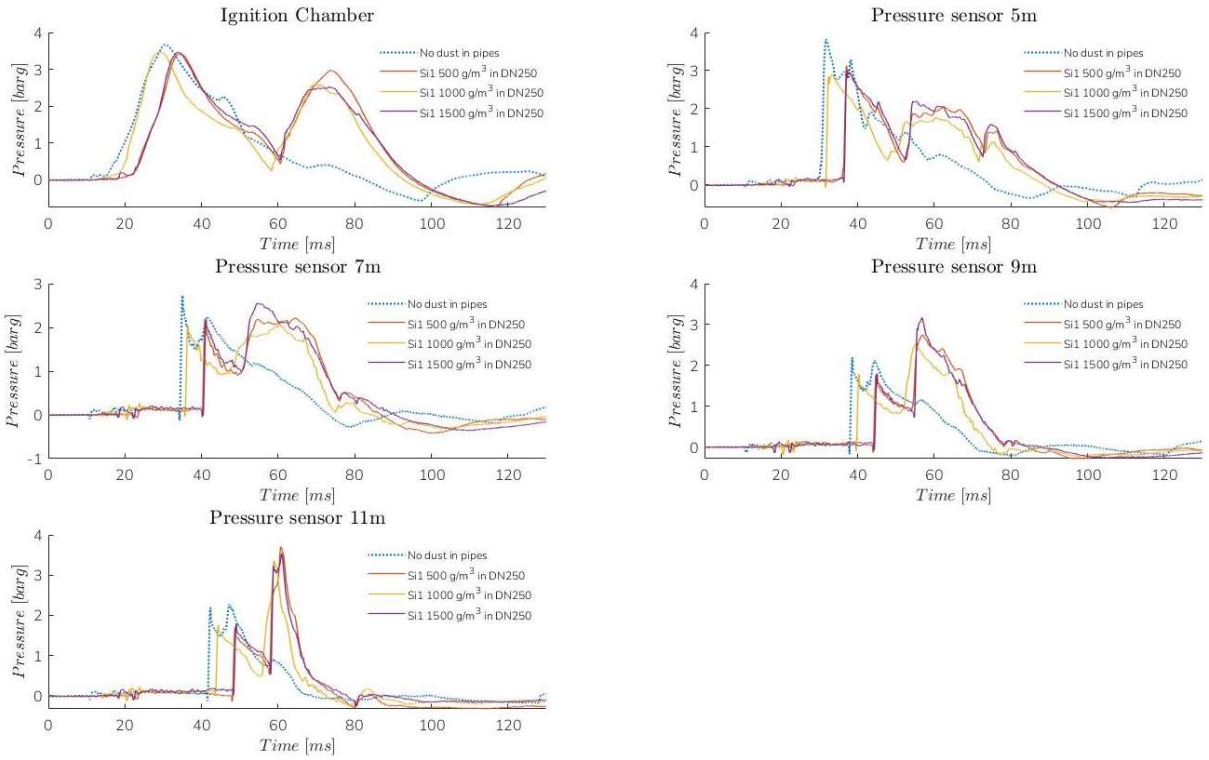

Figure 4-28: Tests in DN160/250 configuration with dust distributed solely in DN250.

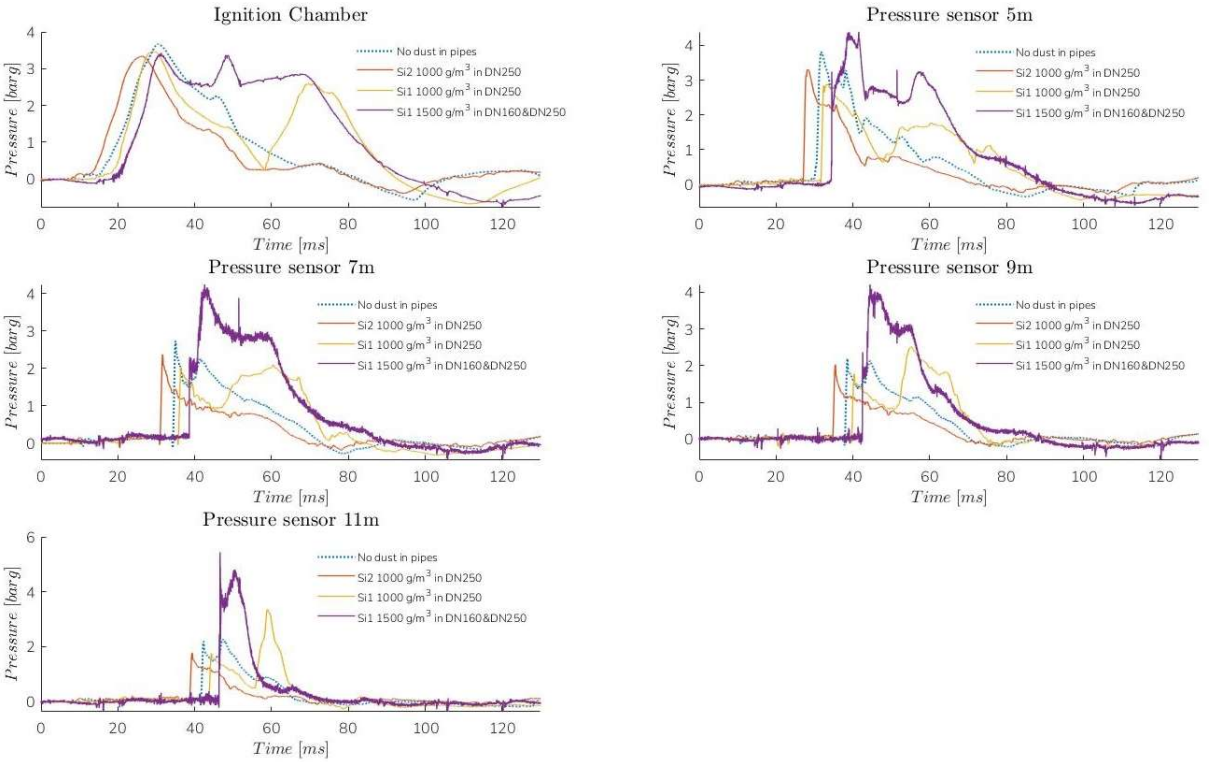

Figure 4-29: 1000 g/m³ Si-2 distributed in DN250, 1000 g/m³Si-1 distributed in DN250 and 1000 g/m³ Si-1 distributed in both pipes.

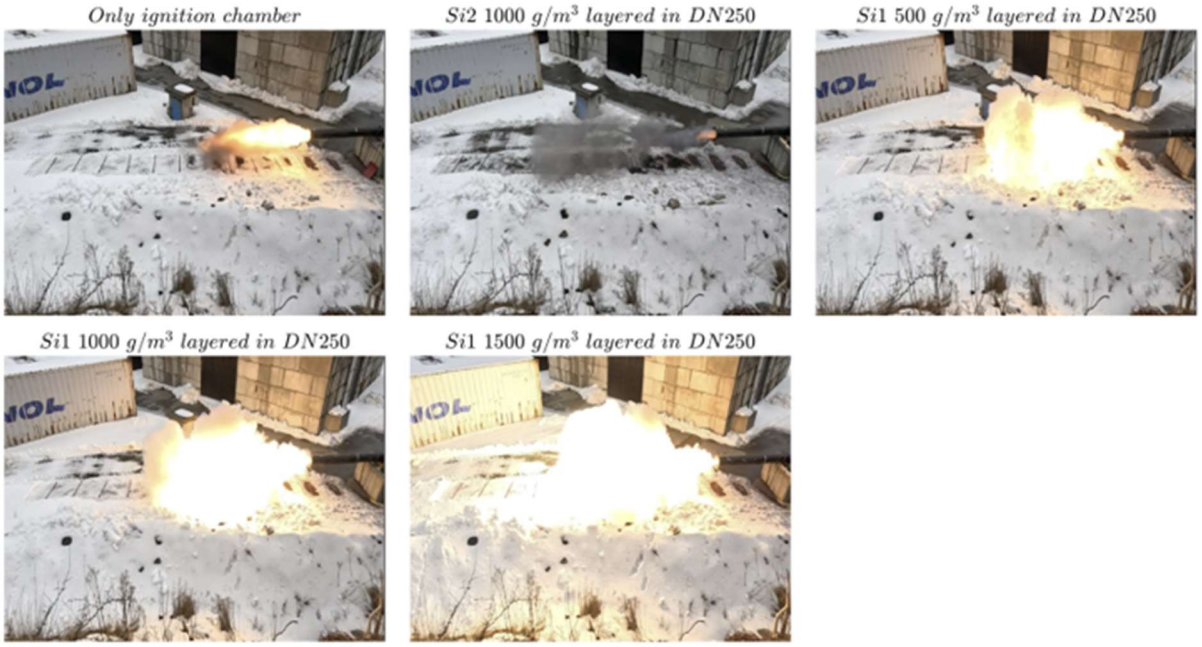

Figure 4-30: Flames ejected from the DN160/DN250 configuration.

4.6.2 Discussion

As with the tests executed in DN160, the initial explosion in DN160/DN250 shows about twice the initial explosion pressures of DN250/160. All concentrations of Si-1 appear to give successful dust lifting and flame propagation at about 50ms, shortly after the deflagration wave has passed the diffuser as can be observed by the increased pressure in Figure 4-28. After this, the pressure increases with the length of the pipe, indicating flame acceleration.

The pressure histories of Figure 4-29 are of particular interest, specifically the purple plot, indicating dust present in both pipes. Pressures from the initial explosion are nearly identical for all concentrations; when the explosion propagates to the 5-metre pressure transducer, the purple pressure increases compared to the other concentrations. This might indicate dust lifting and flame acceleration between the ignition chamber and the 5-metre transducer A slight increase in the ignition chamber at about 50 ms supports this assumption.

Another explanation might be that the diffuser slows down the speed of the deflagration wave, thus increasing the pressure of the flow. Even the reference explosion, with no layered dust in the pipe, shows a slight increase in pressure before the diffuser, which further support the assumption of pressure increase due to the presence of a diffuser.

After passing the diffuser, the turbulent combustion increases with the length of the pipe, accelerating and increasing in pressure, leading to the maximum pressure measured at 11 metres.

4.7 Experiments in configuration 6

4.7.1 Results

A total of five tests were conducted in the complete assembly. Test 1 to 4 was carried out with a concentration of 1000 g/m^3 of Si-1, distributed along the entire length of the connected pipes as depicted in Figure 4-31. Test number 5 had a higher concentration of 5000 g/m^3. Unlike most of the previous configurations, these results are presented as raw data.

The location of pressure transducers for the first two tests is shown above the pipe configuration in Figure 4-31. Figures 4-32 and 4-33 show the pressure-time histories for both tests. All the transducers were adjusted with sensitivity to ± 20 barg for the first test. Ahead of test number 2, all transducers were adjusted to ± 50 barg, to compensate for the high pressures seen in test number 1.

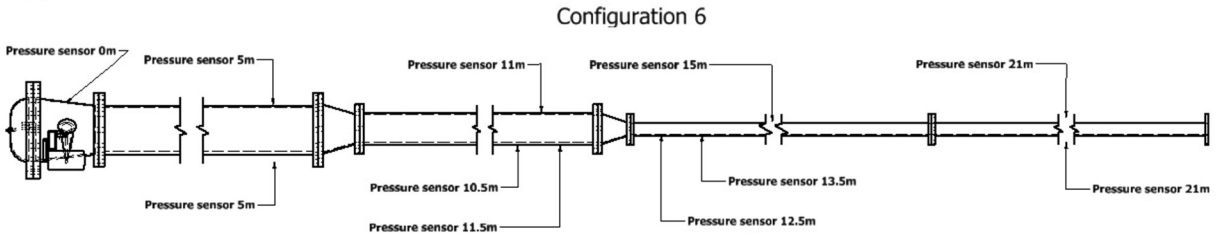

Figure 4-31: Location of pressure transducers for test number 1 and 2.

During the last three tests the transducers sensitivity were adjusted to ± 250 barg, to account for the high pressures observed during test number 2. The locations of the transducers are illustrated below the configuration in Figure 4-31. The pressure-time histories for these tests are presented in Figures 4-36, 4-37 and 4-38.

Test number 1 resulted in pressures above 21.10 barg, saturating the pressure transducers at 11, 15 and 21 metres, as shown in Figure 4-32. This occurred because the sensitivity of the transducers was set to ± 20 barg, which might indicate that the actual pressures would be significantly higher. During test number two, the pressure transducer at 11 metres reached its maximum capacity at 52.80 barg.

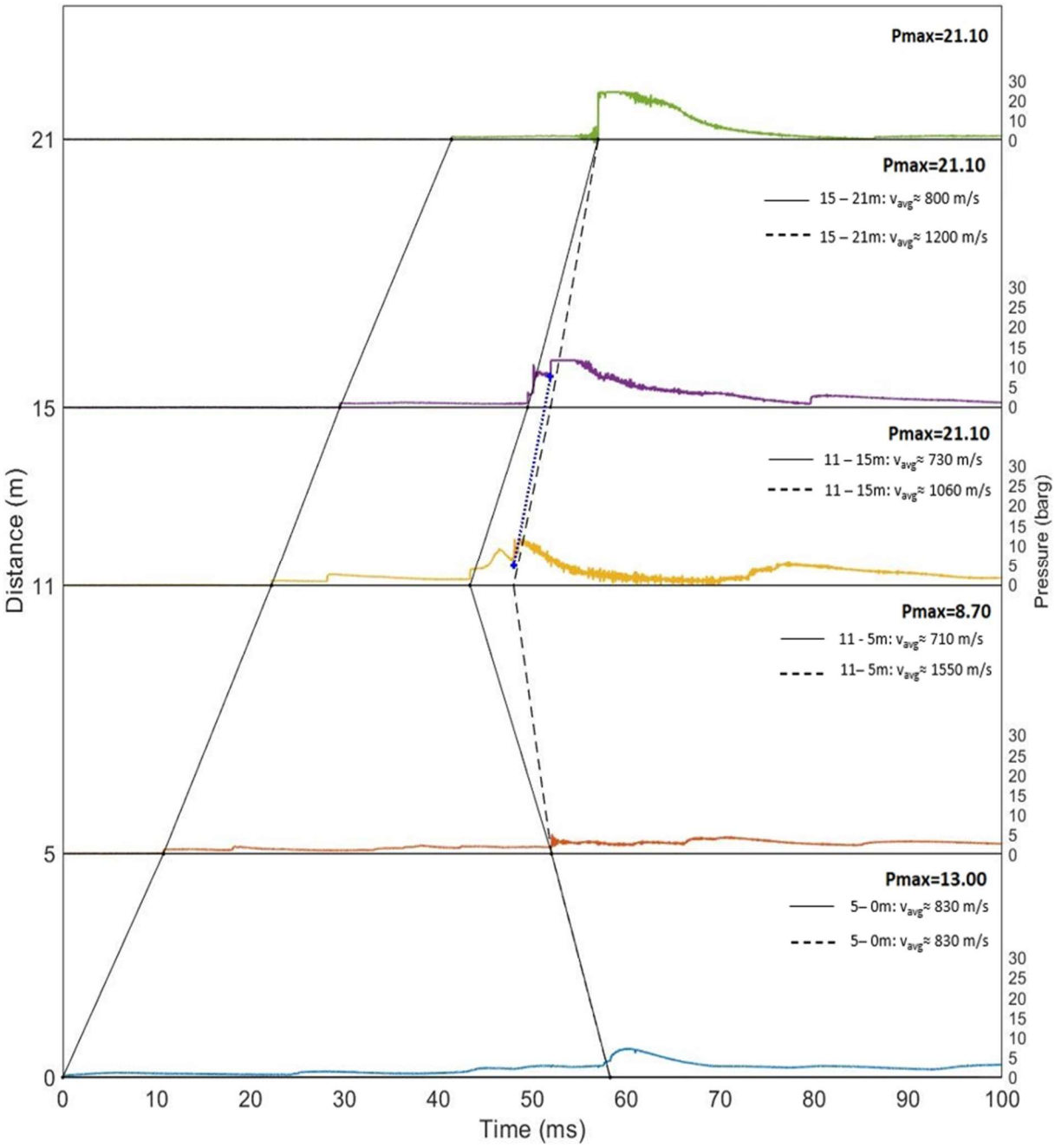

Figure 4-32: Distance scaled pressure plot of test number 1.

The solid line to the left in Figures 4-32 and 4-33 indicates what is believed to be the leading shock wave after ignition. The blue dotted line in the middle is a point of interest and is shown in detail in Figure 4-34. The V-shaped solid line in the middle is presumably the route of the largest shock wave and the returning shock, while the dashed line might be another explanation to the route of the largest shock.

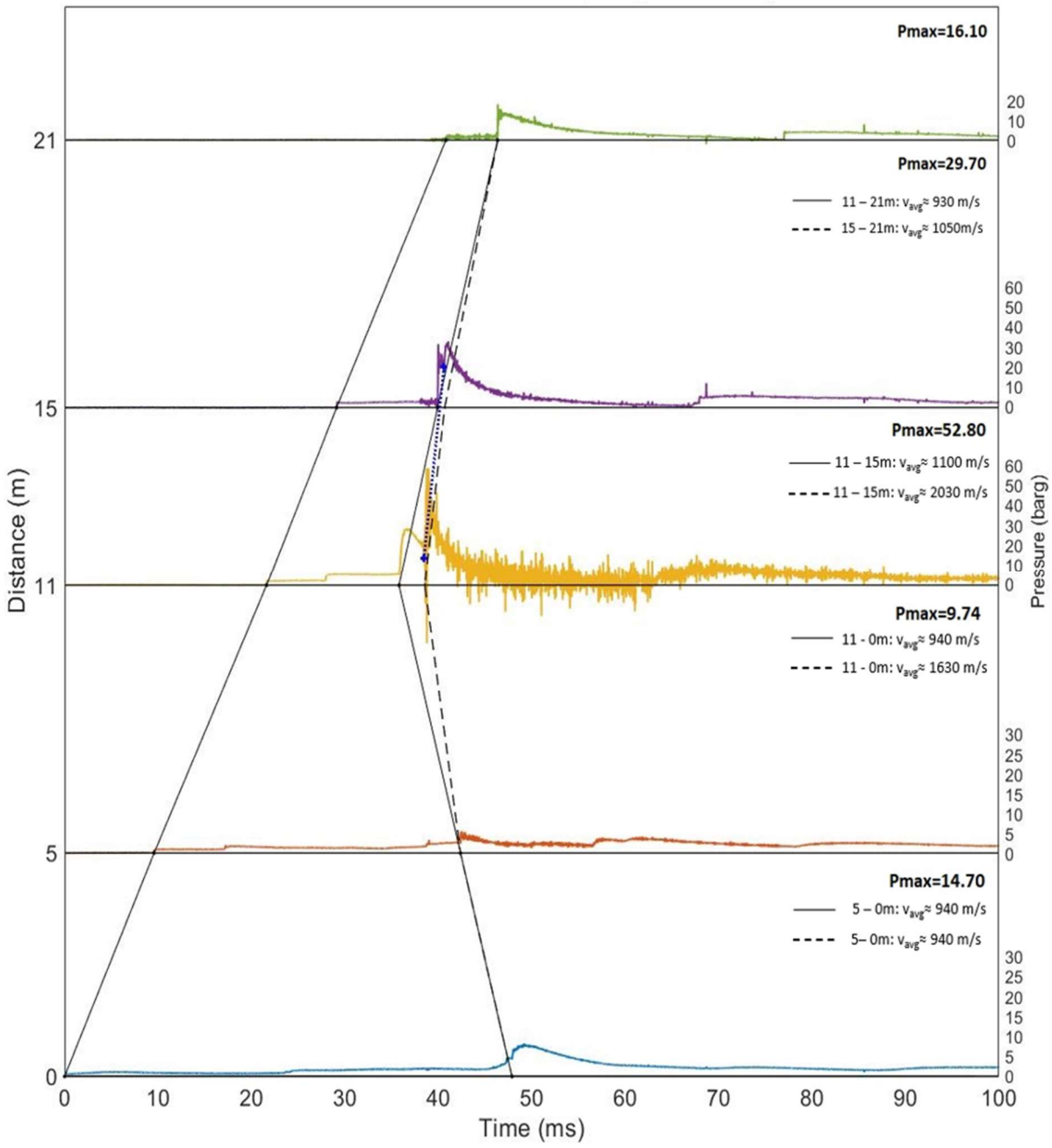

Figure 4-33: Distance scaled pressure plot of test number 2.

Of particular interest is the line indicated in Figure 4-34, where the pressure drops significantly before abruptly rising again. The yellow plot indicates the pressure transducer located at 11 metres, one metre away from a converging crossover. While the purple plot is the transducer located at 15 metres (three metres away from the crossover). The pressure difference between the two points is 23.1 bar, and the average speed of the shock wave between them is above 2000 m/s.

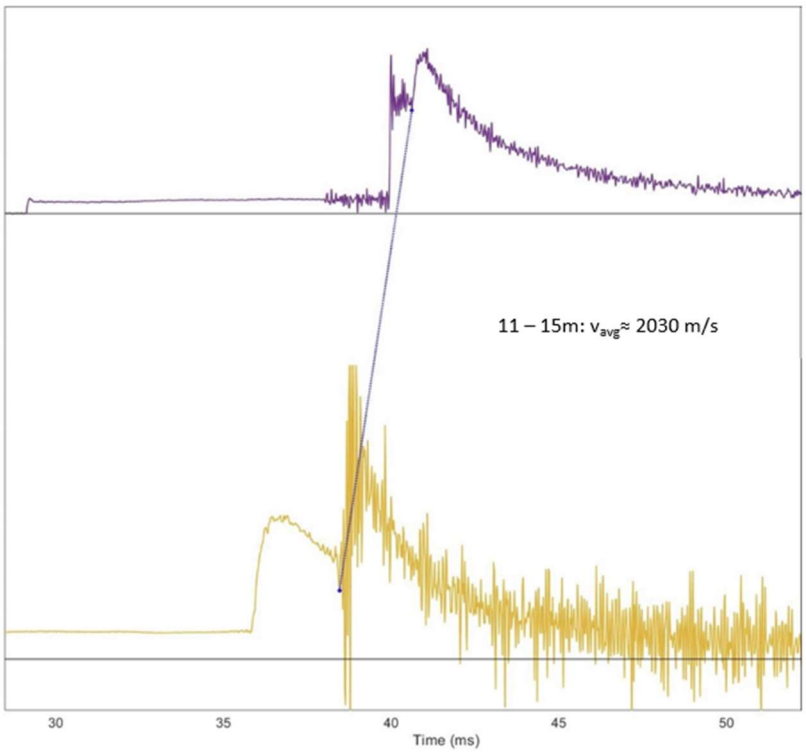

Figure 4-34: A detailed illustration of the blue dotted line from Figure 4-30

The recorded explosion pressures from both tests are vastly larger than the maximum explosion pressure measured in the 20-liter explosion chamber. The calculated velocities of the pressure waves, together with the high pressures indicate that the explosions might be within the detonation regime+.

Figure 4-35 illustrate the effects of the interaction between the leading shock and geometry, with and without a nozzle. The purple, red and yellow plot show that the leading shock compress the unburnt when approaching the nozzles at 6 and 12 metres. As opposed to the blue plot which only show pre-compression at the 5-metre transducer. It seems like the 12-metre nozzle shortens the distance needed for the flame to accelerate, since the last pressure peak can be observed to occur earlier in configurations with a nozzle at 12 metres.

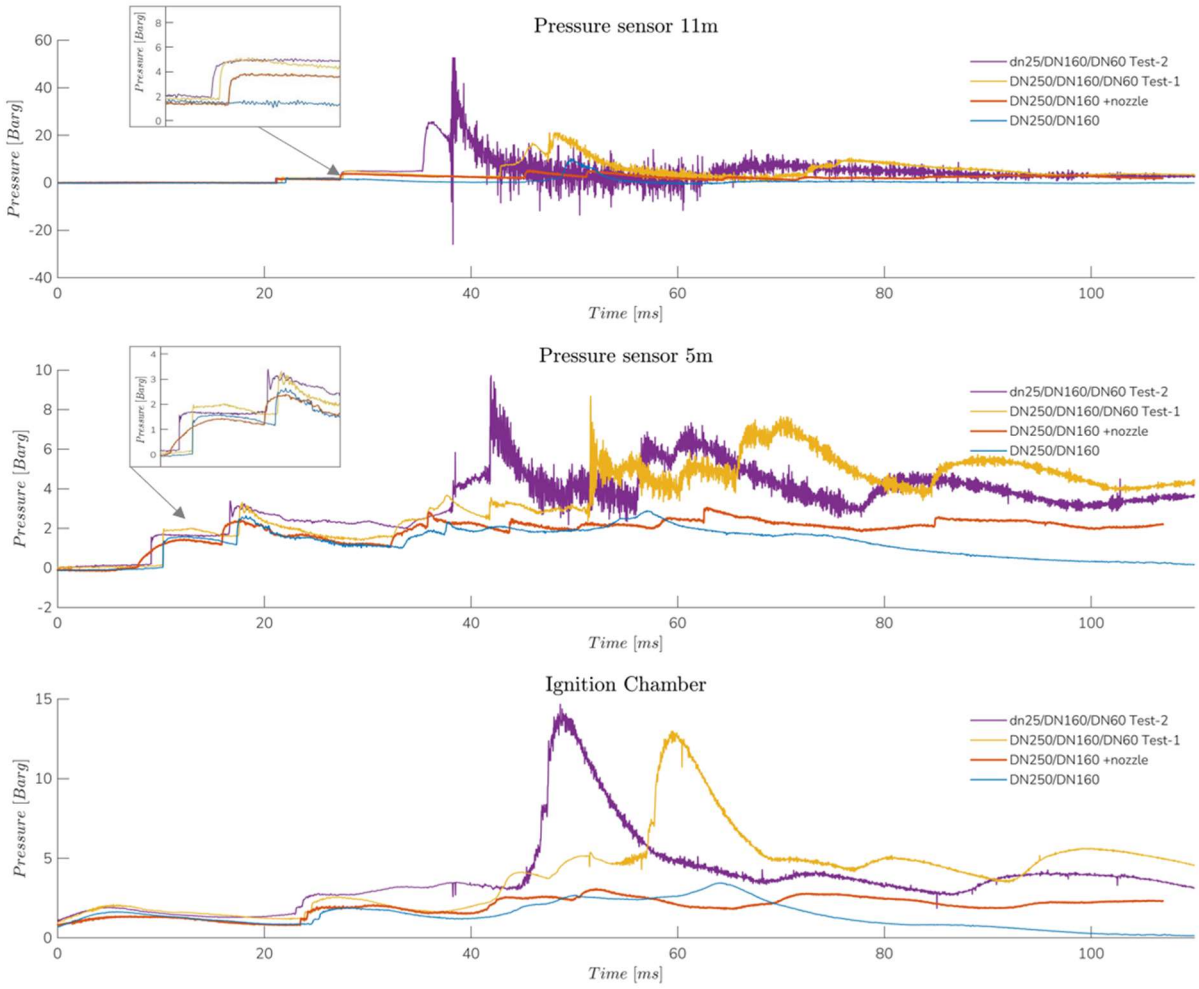

Figure 4-35: Comparison of DN250/DN160 with and without nozzle, and DN250/160/60 1 and 2. All experiments conducted with 1000 g/m^3 Si-1, distributed in all pipes.

Figure 4-36 illustrate the results for test number 3. All transducers registered oscillating pressures until a pressure spike propagated from the 11-metre transducer at ~210 ms, increasing in strength until a maximum pressure of 47.4 barg was registered at 21 metres. The result is very different from tests 1 and 2, which showed signs of a gradual pressure build-up before the abrupt pressure spikes appeared. Test 3 also shows a vastly longer run-up time for the maximum explosion pressure to occur. The blue line shows the location of oscillations in the transducers, appearing slightly before the pressure spike at 21 metres. The most significant pressure wave velocities registered are located between 13.5 to 21 metres and 10 to 5 metres.

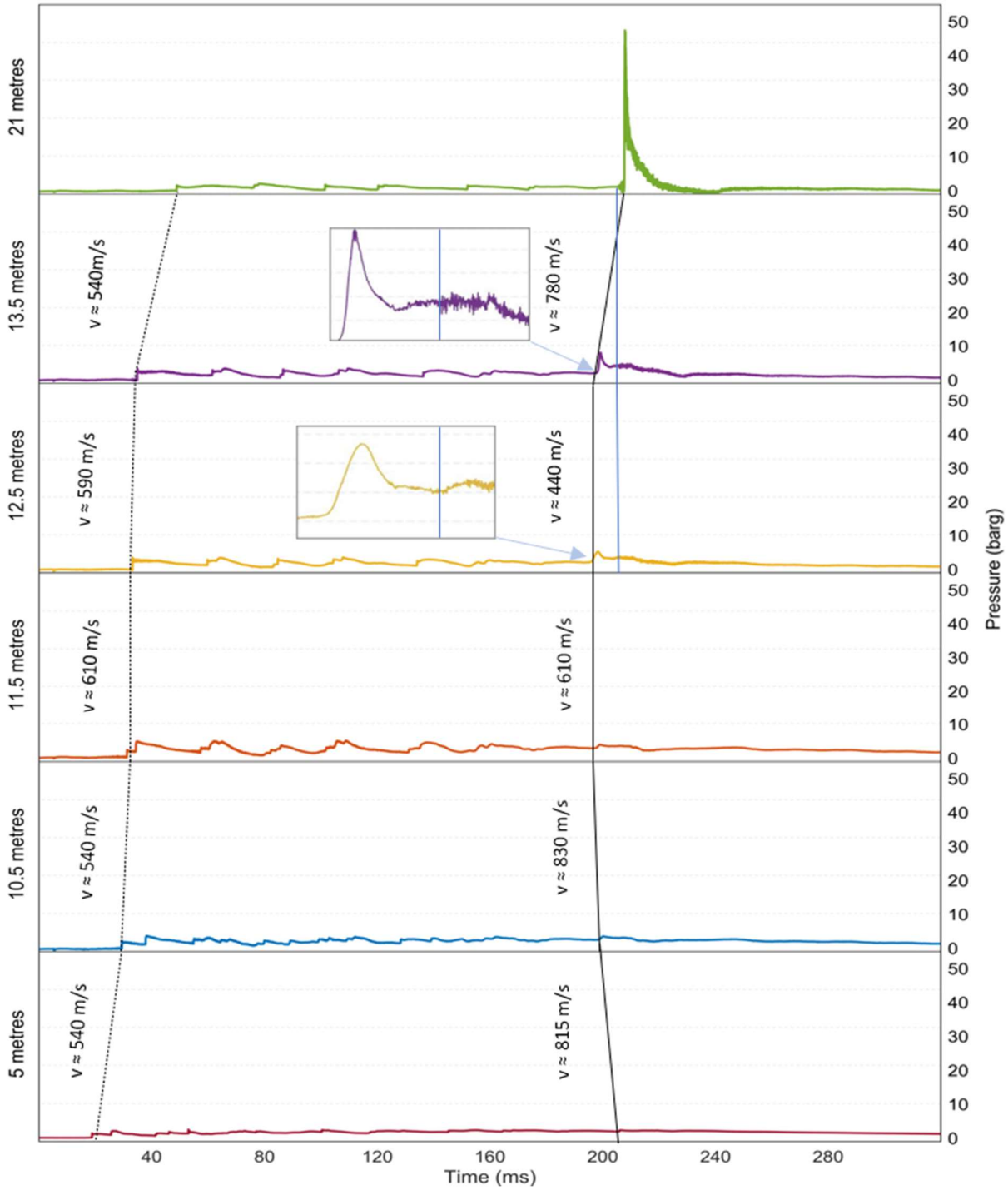

Figure 4-36: Pressure-time history of test number 3. The distance between the plots is not scaled.

Figure 4-37 summarize the results for test number 4. The transducers at 10.5, 11.5, 12.5 and 13.5 metres all show signs of pre-compression between 50 and 60 ms, first induced by the initial explosion, then amplified by the interaction of compression waves and nozzles. The first and most significant pressure spike of 26 barg at 59.83 ms is located at the 11.5-metre transducer. The fastest pressure waves lie between 13.5 and 21 metres and 11.5 to 5 metres with velocities of nearly 1200 m/s. Following a minor indication of pre-compression, a violent increase in pressure is observed at the 21-metre transducer, from 10 barg to 104 barg.

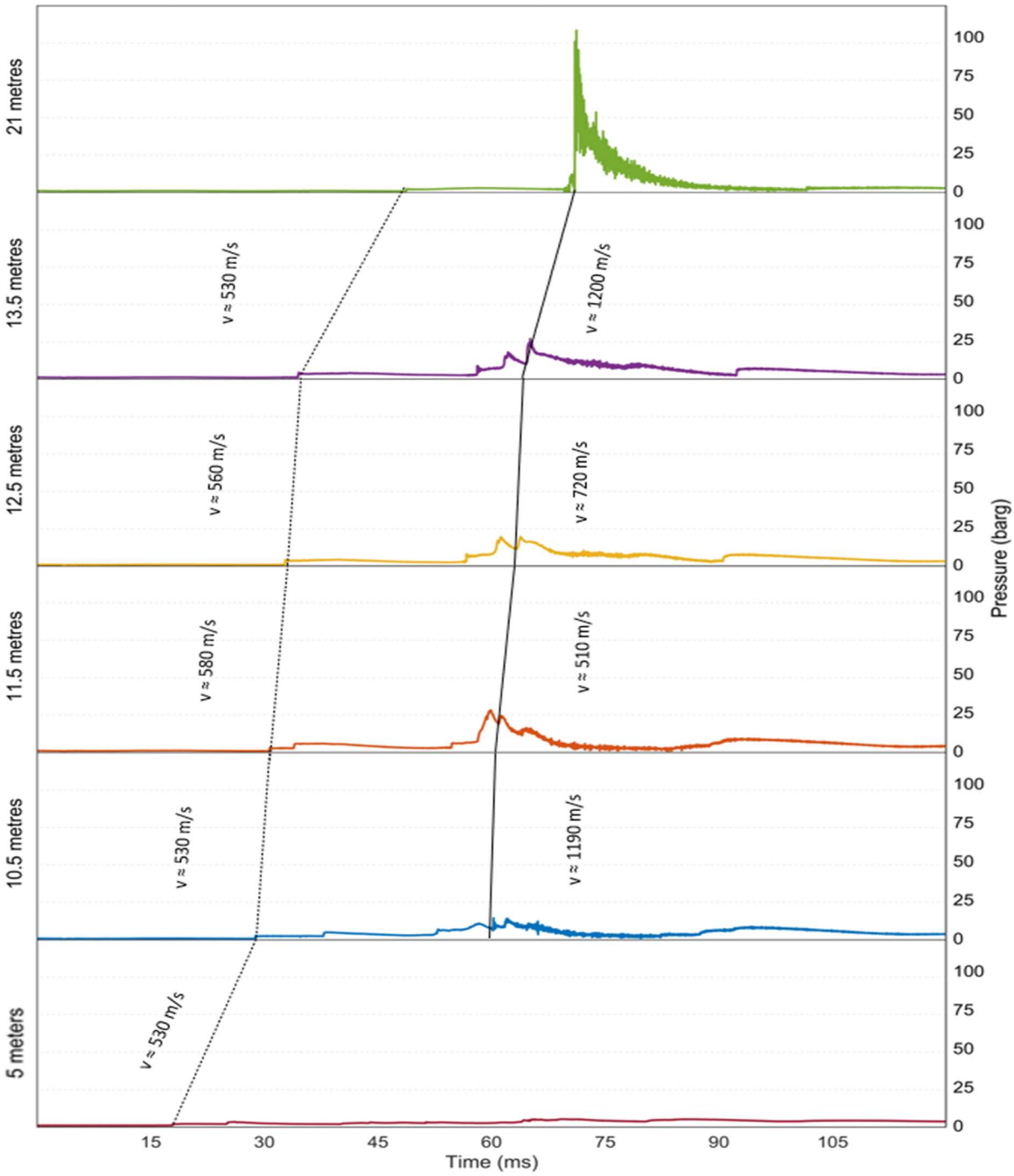

Figure 4-37: Pressure-time history of test number 4. The distance between the plots is not scaled, resulting in the angle of the lines not being representative to their velocity.

Figure 4-38 present the results for test number 5. As with test numbers 4, 2, and 1, several transducers show signs of pre-compression before sharp pressure increases. The most significant pressure is located at the 13.5-metre transducer with a pressure of 55.6 barg. The pressure wave velocity between 13.5 and 12.5 metres is about 1670 m/s. A secondary pressure peak is registered at 10.5, 11.5, 12.5, and 13.5 metres at 37.4 ms. The velocity between the peaks at 10.5 and 12.5 metres is above 10 000 m/s.

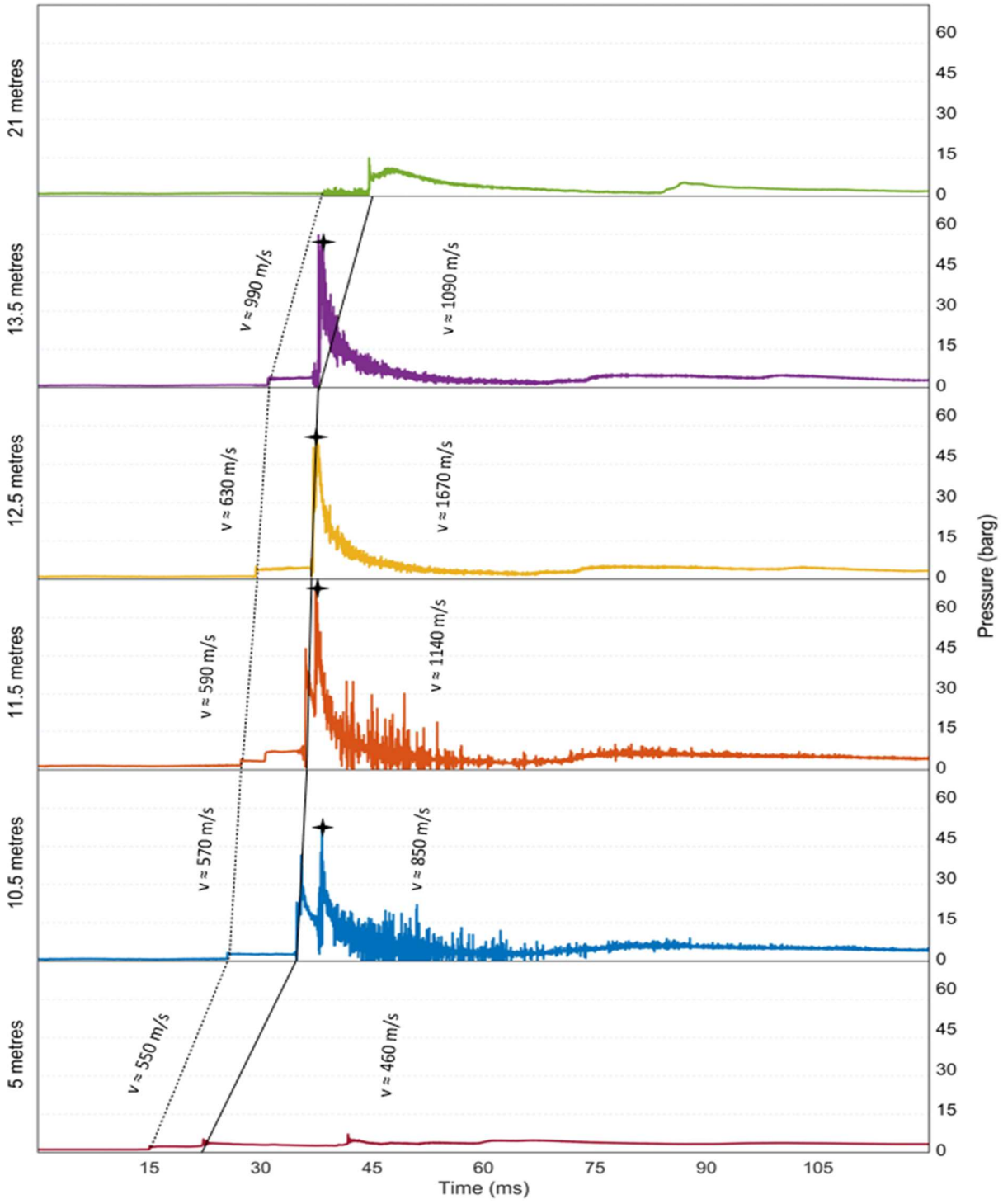

Figure 4-38: Pressure-time history of test number 5. The distance between the plots is not scaled.

Figures 4-39 and 4-40 show the flame and dust clouds that escape the configurations of test 1 and 2. Test number 1 developed a fireball of small dimension, which was followed by large amounts of burnt dust. It seems like test number two didn't propagate the flame all the way through the pipes, but some indications of flame exiting the pipe was distinguishable on the video, including sparks that can be seen thrown out. At first it blew out a cloud that resembles unburnt dust, which was followed by a vast amount of burnt dust.

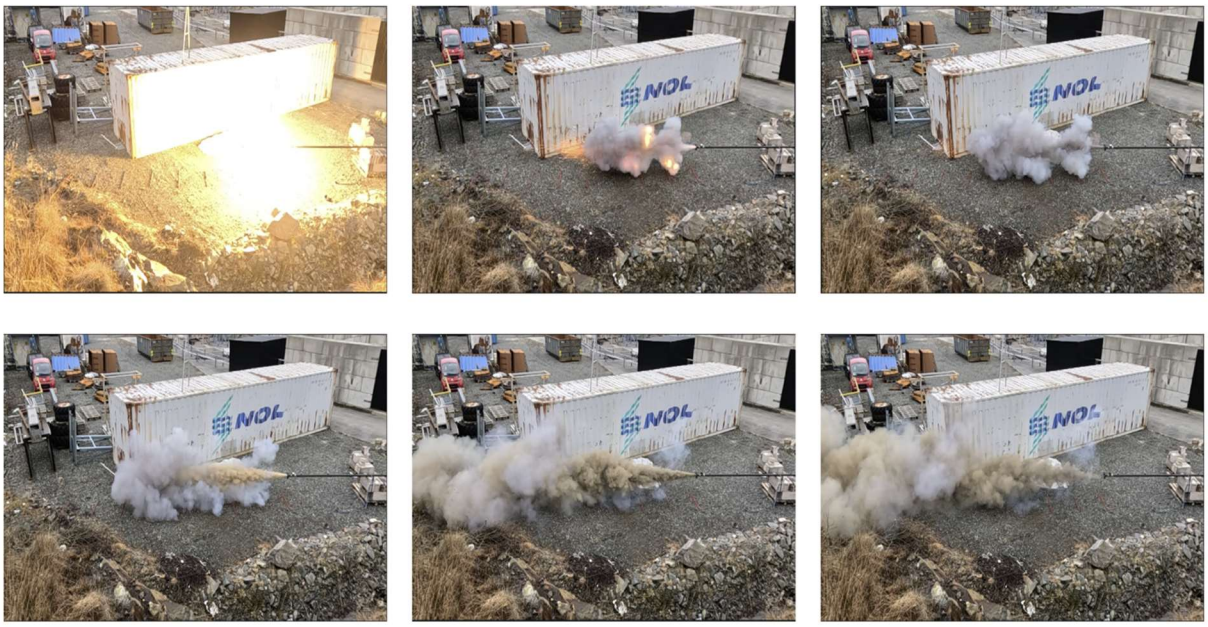

Figure 4-39: Collage of the flame and dust that escape the complete configuration during test number one.

Figure 4-40: Collage of the dust that escape the complete configuration during test number two, it is difficult to percept the fire from the pictures, but some indications of flame exiting the pipe was distinguishable on the video.

Figure 4-41 presents the ratio between the final and pre-compressed initial pressures, for every test except test number 3. The ratios are significantly scattered, with no correlation between the tests, though test number 4 and 5 exhibit individual ratios more closely spaced.

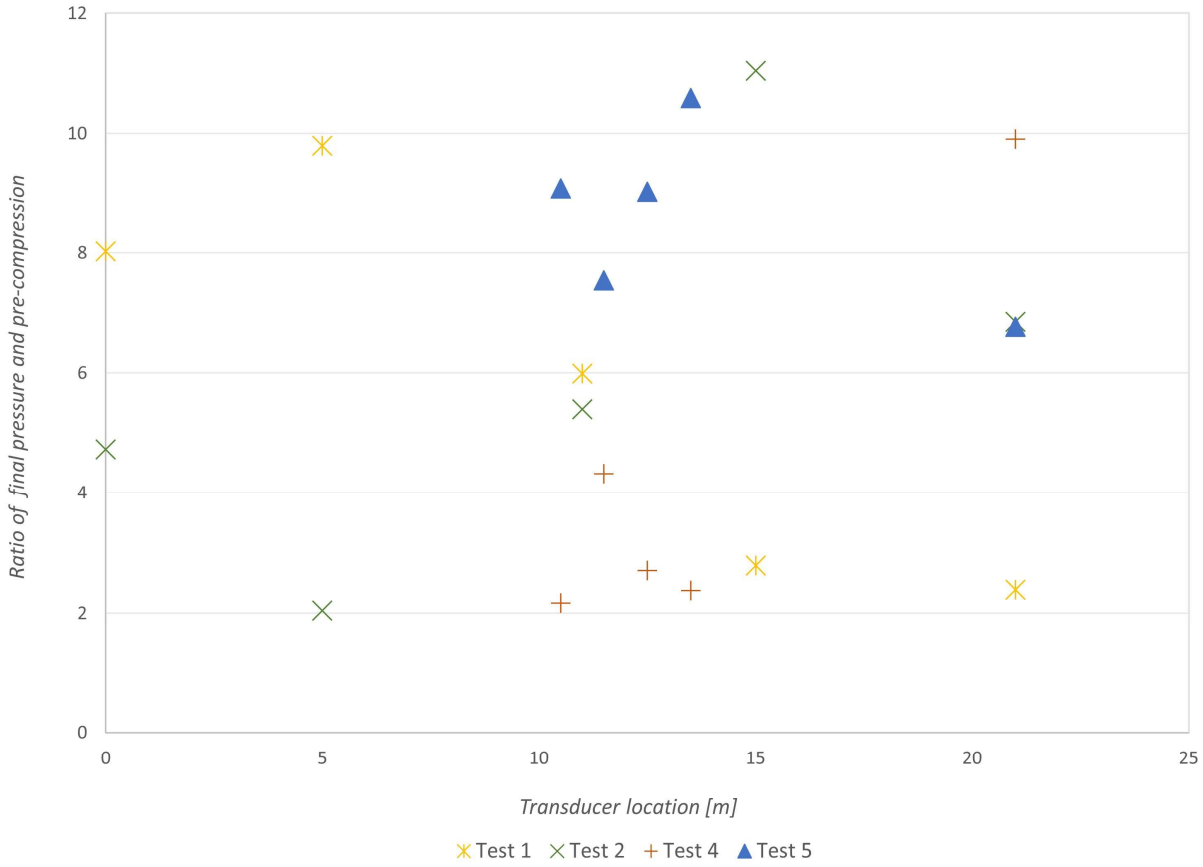

Figure 4-41: The ratio of the final pressure and pre-compressed pressure registered at each transducer.

4.7.2 Discussion

The limited instrumentation used during the experiments, make it problematic to come to specific conclusions of the phenomena that affect flame propagation in the pipe configuration. Nevertheless, some potential explanations are suggested for the observations made in test 1 to 5.

Test 1

Liu et al.(2009) shows that the onset of detonation create a retonation wave that propagate in the opposite direction at the same speed as the detonation wave. In Figure 4-32, the initial solid V-shaped line signifies a possible pressure wave path caused by an "explosion within the explosion" near the pressure transducer of 11-m. The average velocity of the compression wave and the returning pressure wave ranges from 710 m/s to 830 m/s and propagate at relatively constant speeds. Assuming a maximum calorimetric flame temperature of 2400 K (Cashdollar & Zlochower, 2007), the speed of sound in the burnt gases is believed to be about 970 m/s, as shown in section two. As a result, the compression waves are considered subsonic, which could indicate that the combustion is not occurring in the detonation regime.

The reasoning above might have been a good explanation if the pipe consisted of constant diameter, without any nozzles or diffusers. The transitional changes in diameters lead to complex flow and shock interactions. Given the sonic flow of the deflagration wave, it might reduce in pressure but increase in speed when interacting with the nozzle (El-Sayed, 2016). However, the expanding gases pre-compresses the unburnt mixture in front of the nozzle, increasing in pressure the closer to the nozzle It comes. This led to a pressure piling effect. For all tests except number 3, an increase in initial pressure can be observed before the nozzle. When the deflagration wave ignites this pre-compressed mixture, a violent increase in pressure can be observed.

The converging section of the nozzles will increase the strength of compression waves (Ben-Dor et al., 2001) which can lead to a more significant effect of stretching the flame front, which in turn might increase flame acceleration prior to passing the nozzle.

Following Figure 4-32, the pressure suddenly jumped to about eight barg at 43 ms near the 11m transducer. Then it increased to above 20 barg within 47 ms. Subsequently, the pressure dropped to 10 barg before rapidly increasing again, maxing out the transducer’s recording at 21.20 barg. This violent increase in pressure created vibrations in the piping that can be observed in the plots as an oscillating “noise.” From this, the alternate route of the dashed line has been drawn between the sharpest pressure inclines for every transducer location. This led to vastly higher-pressure wave velocities; 1530 m/s between 11 and 5 meters.

Based on the violent pressures and large shock velocities, the propagation mechanism could be placed in the detonation regime, like similar results in aluminium dust explosions (Liu et al., 2011; Liu et al., 2009). Their experiments of aluminium dust measured the detonation cell size of the reaction to be larger than 0.4 m. This is further supported by the work of Zhang et al.,(2001), which showed that minimal pipe diameters for self-sustained detonation increased with decreasing K_{St}. Aluminium with a K_{St} of 359 bar·m/s had a critical tube diameter (d_c) of 0.12 m. The inner diameter of DN60 is 0.062 m, significantly smaller than the d_c of aluminium. Detonation cell sizes have been shown to be directly affected by the material's reactivity (Hussaini et al., 1992), which would imply that silicon dust has a larger detonation cell size than aluminium. Thus, the diameter of the final pipes would be insufficient to accommodate a self-sustaining detonation of silicon dust.

Comparing the configuration and pressures obtained in Figure 4-35, it becomes clear that the nozzle located at 11 metres strongly influences the obtained pressures and shock velocities. First, the leading shock for every configuration that inhabits a nozzle shows signs of interaction with the nozzle, increasing the pre-compression of the mixture ahead. Subsequently, the resulting maximum pressure appeared earlier in configurations with a nozzle, suggesting that the nozzle interaction amplified flame acceleration.

Test 2

Some similarities can be found in tests 1 and 2. The leading shock from the initial explosion gives nearly identical average propagation velocities for the pressure wave created, 530 m/s, indicated by a solid line, starting from 0 ms.

After roughly 35 ms, an abrupt pressure increase is evident at the 11-metre transducer, which might signify that the deflagration wave catches up with the pre-compressed mixture. The pressure registered at this location was approximately 25 barg. It produced powerful pressure waves propagating in both directions, with a constant average velocity of ~ 940 m/s.

The steep incline at about 48 ms sends vibrations in both directions, affecting all the transducers. The pressure abruptly increases from 14 barg to over 50 barg, maxing out the transducer. This point can be better observed in Figure 4-34. Tracing the pressure waves generated by the “explosion within the explosion,” the average pressure wave velocities become vastly higher. The average velocity between 11-15 metres is about 1910 m/2, while the velocity between 11 and 5 metres is 1600 m/s. The location and source of the large increase in pressure cannot be known with certainty, thus the average velocity between 5 and 15 metres is closer to 1750 m/s.

The vastly increased pressures at 15 and 21 metres, coupled with the shock velocities might indicate that a change in the reaction mechanism is occurring at 48ms, indicating that the combustion wave

might have transitioned to a quasi-detonation state. Though it is difficult to determine with no information of the flame velocities.

As formerly seen by Li et al.(1995) and Zhang et al.(2001), dust explosions in pipes can accelerate to a speed at which it resembles a quasi-detonation, even though the detonation cell size of the material in question may not support self-sustained detonations in the given pipe diameters.

Another explanation for the large shock velocities and the significant pressures can be unstable fast deflagration. Large flame propagation velocities and considerable pressures are similar for quasi-detonations and fast deflagrations, making distinguishing between them difficult (Chan & Greig, 1989). Large overpressures have also been reported in the past in situations of vented explosion in ducts; vents can induce a choked flow that leads to compression of the unburnt gases prior to the vent (Eckhoff, 2003).

Notably, the pressure registered at the transducer at 21 metres during test number 1 was maxed out, as opposed to 15.10 bar registered at test number 2. Moreover, test number 1 had complete flame propagation throughout the length of the configuration, as opposed to test number 2, which did not. Such vast discrepancies in the results of nearly identical tests illustrate the inherent challenges in achieving repeatability of dust explosion experiments, a challenge that has been reported by various researchers (Eckhoff, 2003; Skjold et al., 2014).

Test 3

As with the other tests, a clear pre-compression is visible at all transducer locations due to the leading shock's interaction with the nozzles. However, a vast difference from the other tests is that the pressures are significantly lower. The pressure spike appears significantly later than in other tests, which might indicate a substantially slower flame acceleration. Nevertheless, the pressure spike at 12.5 metres can be seen again at 13.5 metres, increasing in strength, which might indicate an accelerating deflagration. The distance between 13.5 and 21-metre transducers might explain the significant pressure increase, but the lack of pre-compression heightens the likelihood of error in the measurement.

The blue line in Figure 4-36 shows an onset of oscillations in the transducers, occurring slightly before the maximum pressure at 21 metres. The oscillation occurs simultaneously at the 21, 13.5 and 12.5-metre transducers, which indicate vibrations from the pipe—further supporting inaccurate measurement at 21 metres.

Test 4

As with the other tests, test number 4 showed signs of pre-compression for most transducers. The first pressure spike is observed ahead of the 12-metre nozzle, first a pre-compression to 6.1 barg due to the shock induced flow, then ignition of the pre-compressed mixture with a maximum pressure of 25.8 barg. Following the same transducer, the pressure drops slightly before increasing again. The transducers at 11.5, 12.5 and 13.5 metres show similar pressure development, with pre-compression followed by ignition. The pressure and compression wave velocity increase from 12.5 to 13.5 metres, possibly due to flame acceleration. From 13.5 to 21 metres, the pressure increases from 26 barg to 104 barg, after a short pressure increase of 10.7 barg, which could be a fast pre-compression. It should be noted that test number 1 showed that the pressure measured at 21 metres had the most prolonged state of saturation, which might indicate that it also inhabited the largest maximum pressure. This could indicate that maximum pressures in 3 out of 5 tests were located at the 21-metre transducer.

Similar oscillations as observed in Figure 4-34 can be observed occurring simultaneously at all transducer locations, which might indicate vibrations and faulty measurements. It is hard to imagine that silicon dust with a K_{St} of 194 m·bar·s-1 can reach maximum pressures of 104 barg in a pipe with an inner diameter of 62 mm. The steadily increasing pressure at 12.5 and 13.5 metres could indicate a flame acceleration that could lead to larger pressures.

Test 5

Prior to test number 5, the 21-metre transducer was exchanged with the 13.5-metre transducer due to the considerable pressures observed at the location during previous tests. This test was conducted with a concentration of 5000 g/m^3. In hindsight, swapping transducers while changing the nominal dust concentration was probably not the best solution.

Test number 5 exhibits signs of pre-compression before being ignited by the deflagration wave, which gives rise to vastly larger pressures. The first significant increase in pressure occurs at the 11.5-metre transducer. The 10.5, 11.5, 12.5 and 13.5-metre transducers showed maximum pressures of 38.3, 44.2, 37.10 and 37.10 barg successively. However, they all exhibit a secondary peak with even higher pressures, up to 66.4 barg at 11.5 metres. These peaks are marked with a black star in Figure 4-38. The pressure spikes gave rise to large oscillations simultaneously at every transducer, and the maximum speed between 11,5 and 13.5 metres is above 10 000 m/s, more than twice the speed of sound in steel. These velocities indicate that the results cannot be trusted and are most likely induced by deceptive signals and errors in the transducers caused by vibrations in the pipes.

The increased amount of dust show signs of increasing the pressure several transducers compared to test number 4. This might be a result of more dust suspended which during the convective flow and pre-compression may increase the density of unburnt mixture and contribute to an earlier choke of the flow.

The most significant pressures coupled with the largest velocities from all tests might support the theory of a fast turbulent deflagration that wants to transition to detonation but can't, due to the low-diameter pipes at 12 metres.

Previous work suggests that dusts of K_{St} > 200 bar·m/s need pipe lengths of 20 – 40 metres to be able to achieve explosion pressures and velocities in the range of quasi-detonation regime (Bartknecht, 1981; Proust, 1996; Zhang et al., 2001). The results presented in this thesis indicate that nozzles and reducers strongly influence the propagation mechanism of dust explosions in pipes.

Given the evident influence that nozzles have on the pressure developed within the configuration, it is imperative to include their presence when performing system risk assessments.

4.7.3 Sources of error

Most tests share the same sources of error, though some errors might have a larger impact for some configurations.

- *Pressure wave velocities:* All the pressure wave velocities are calculated from manually selected data points, which can introduce subjectivity to the results. The investigator's choices in selecting data points can impact the accuracy and reliability of the resulting velocities.
- *Test samples:* The apparatus to measure the mass of the samples is calibrated and has an error of ± 0.01 g. This error is considered negligible as it is so tiny that it would not impact the precision of the results obtained in the tests.
- *Test samples:* The samples had to be extracted from containers ranging from 20 to 50 litres and might be subjected to segregation. The containers were rotated and mixed according to best practices, and samples were collected by scooping from the top of the containers (Allen, 1997). There is no way of knowing if the test samples represented the bulk of the dust, but the sampling was done as accurately as possible.
- *Instrumentation:* There can be significant errors in the measured pressure time histories due to faulty signal from the transducers, induced by vibration in the pipes.

  Given the limited number of pressure transducers, there is considerable uncertainty regarding pressure history – leading to the fact that average velocities of pressure waves might be vastly

different. This also leads to difficulty in deciding the impact that nozzles and diffusers have on combustion and pressure wave propagation.

- *Dust distribution:* Distribution of dust to give a correct nominal concentration. First, the dust was distributed as evenly as possible in the angled iron, utilizing a plastic mold that ensured a uniform distribution. This method ensures that the volume of dust is distributed evenly in the iron, so one must assume a uniformly distributed mass of the particles to give a correctly distributed nominal concentration. Secondly, the angled iron was inserted into the pipe and turned upside-down, then the iron was used to smudge the dust from side to side. It was distributed as uniformly as the method allowed.
- *Environmental factors:* Due to the location and time of the year, the experiments were executed in varying weather conditions and a range of temperatures, resulting in variable test conditions. Wind could agitate the dust, and moisture and humidity had the potential to impact the experimental results.
- *Unburnt dust:* After tests, there was always an amount of burnt and unburnt dust left in the pipes. The amount of dust present after combustion increased with an increasing amount of distributed dust, leaving a range of uncertainty to the actual concentration suspended and reacted during the experiments.
- *Dispersed dust cloud:* There is no way of knowing the actual nominal dust concentration present at any location at any time in the pipe.
- *Test data:* More tests should have been conducted. A larger amount of data would have made it easier to draw conclusions, observe trends and patterns, and understanding the different phenomenon observed.
- *Manual selection of datapoints:* All flame and pressure wave velocities are based on manually selected points in the pressure histories. The selection of the signals is a major source of error, another researcher would potentially find completely different velocities.

5. Conclusion

Explosion experiments with layered silicon dust have been conducted using various pipe configurations that simulated an industrial dust extraction system. A 32-litre ignition chamber was constructed to facilitate the experiments, and pipes were machined and equipped with pressure transducers and thermocouples. The pipes had lengths ranging from 6 metres to 24 metres and diameters from 245 mm to 62 mm. The analysis of the experimental data was focused on understanding the explosion propagation mechanisms of layered silicon dust in pipes and investigating the effect of nozzles and diffusers in the geometry.

Reference explosion experiments to decide the explosion indices of the dust have been performed in the standardized 20-liter USBM apparatus located at the dust explosion lab at UiB.

Attempts to utilize thermocouples to measure the propagation velocities of silicon flames have been unsuccessful. This is primarily the result of the high temperatures involved in silicon combustion, which causes the thermocouple wire to melt during combustion.

Given a pipe length of six meters and diameter of 245 mm, the overdriven initial explosion proved to lift the layered dust sufficiently. Subsequently, most of the dust ignited on the outside of the pipe, resulting in the formation of fireballs. The size of the fireballs increased as the nominal concentration of dust layers within the pipe increased. A distinction was noted for Si-2 in configuration 1, where the fireballs did not increase along with the nominal concentration of dust.

Consistent with theoretical predictions, reducing the diameter to 157 mm resulted in a notable increase in the overall explosion pressures and indications of Si-1 reacting inside the pipe and not just outside. However, Si-2 did not exhibit any signs of flame acceleration within the pipe, most likely due to its larger particle size distributions.

Introducing nozzles and diffusers to the configurations increased the maximum pressures and velocities of pressure waves. Their presence introduces complex interaction involving turbulence, pre-compression, shock reflections and pressure waves, and the interactions between them all. The configuration of 24 meters, consisting of four pipes of gradually reducing diameter, resulted in peak explosion pressures surpassing 50 barg and shock velocities above 2000 m/s. Velocities and pressures of such magnitude indicate that the combustion mechanism might be categorized as a quasi-detonation or an unstable fast deflagration.

Comprehensive work has previously been done regarding dust explosions in pipes. However, no previous experiments conducted in pipe configurations with varying diameters could be located. The results presented in this thesis indicate that nozzles and diffusers strongly influence the propagation characteristics of dust explosions in pipes, which should be accounted for when designing safety measures for dust-extraction systems. These observations warrant further investigation.

6. Future work

- Continued experimental studies in the configurations used in this thesis should investigate other techniques for flame detection, like optical detection systems. Thermocouples are not suited to measure the flame speed for metallic dusts because of the elevated temperature that metallic dusts burn with.
- A high-speed camera should be used. With high enough frames per second, the flame velocity can be measured with the camera, to be compared against other techniques for flame detection.
- Given the strength of the primary explosion, there was little to no difference in the dust's ability to propagate a flame through the pipes. This is because all the dust was "thrown" out of the pipes by the primary explosion. The primary explosion alone could propagate the first six metres in all the pipe dimensions. Downsizing the violence of the primary explosion (decreasing the amount of dust, the ignition time delay, and downsizing to 1kJ igniter) would allow for investigating low nominal concentrations to study the lowest concentration of dust that could propagate a flame.
- Further work should implement a better way to distribute dust inside the pipe, to give a higher accuracy of the dust layer.
- Moreover, it should include additional pressure transducers in and around the nozzles. An increased number of transducers would provide more data and allow for a deeper understanding of the behaviour of pressure and reflections.
- Most explosions in configurations of two pipes were evaluated without layered dust in the first section of pipes, intended to dampen the initial explosion. The tests demonstrated that a layer of dust in the first section of the pipe gave rise to significantly higher pressures. Given the time to do so, this should have been investigated with more tests. Comparing the influence of nozzles and expanders with tests in pipes of the same dimensions without nozzles would give an excellent reference to investigate the nozzle's contributions.
- The experimental results should be compared against computational fluid dynamics (CFD) simulations when available. To see if the high pressures and shock velocities can be reproduced by the CFD simulations.

List of references

Abbasi, T., & Abbasi, S. A. (2007). Dust explosions–Cases, causes, consequences, and control. *J Hazard Mater*, *140*(1), 7-44. https://doi.org/10.1016/j.jhazmat.2006.11.007

Allen, T. (1997). *Particle Size Measurement* (Vol. 5). Chapman & Hall.

Analog Devices, I. (1998). *Data Sheet, Thermocouple Conditioner and Setpoint Controller*. Retrieved 01.05 from https://www.analog.com/media/en/technical-documentation/data-sheets/AD596_597.pdf

Arymbayeva, A., & van Hees, P. (2020). *Variables impacting the probability and severity of dust explosions in dust collectors* (FPRF-2020-15). NFPA. https://www.nfpa.org/-/media/Files/News-and-Research/Fire-statistics-and-reports/Hazardous-materials/RFVariablesDustExplosionDustCollectors.ashx

Association, N. F. P. (2012). NFPA guide to combustible dusts. In *NFPA 72*. Quincy, Massachusetts.

Bartknecht, W. (1971). Brenngas- und Staubexplosionen. *Forschungsbericht F45, Bundesinstitut fur Arbeitsschutz, Koblenz*.

Bartknecht, W. (1981). *Dust explosions: Course, prevention, protection*. Springer. https://doi.org/https://doi.org/10.1007/978-3-642-67747-2

Barton, J. (2002). *Dust explosion prevention and protection*. Gulf Professional Publishing.

Ben-Dor, G., Igra, O., Elperin, T., & Lifshitz, A. (2001). Handbook of shock waves.

Bidabadi, M., Zadsirjan, S., & Mostafavi, S. A. (2013). Radiation heat transfer in transient dust cloud flame propagation. *Journal of loss prevention in the process industries*, *26*(4), 862-868. https://doi.org/10.1016/j.jlp.2013.03.002

Borissov, A. A. (1991). *Dynamic Structure of Detonation in Gaseous and Dispersed Media*. Springer.

Cashdollar, K. L., & Zlochower, I. A. (2007). Explosion temperatures and pressures of metals and other elemental dust clouds. *Journal of loss prevention in the process industries*, *20*(4), 337-348. https://doi.org/10.1016/j.jlp.2007.04.018

Cengel, A. Y., & Boles, A. M. (2006). *Thermodynamics an engineering approach* (5th ed.). McGraw-Hill College

Chan, C. K., & Greig, D. R. (1989). The structures of fast deflagrations and quasi-detonations. *Symposium, International, on Combustion*, *22*(1), 1733-1739. https://doi.org/10.1016/S0082-0784(89)80186-9

Chu, B.-T. (1953). On the generation of pressure waves at a plane flame front. *Symposium, International, on Combustion*, *4*(1), 603-612. https://doi.org/10.1016/S0082-0784(53)80081-0

CSB. (2006). *Combustible dust hazard study* (2006-H-1). https://www.csb.gov/file.aspx?DocumentId=5733

Eckhoff, K. R. (2016). *Explosion hazards in the process industries* (Second Edition ed.). Gulf Publishing Company. https://doi.org/https://doi.org/10.1016/B978-0-12-803273-2.01001-X

Eckhoff, K. R., Alfert, F., & Fuhre, K. (1988). Venting of dust explosions in a 5.8 m^3 bag filter under realistic conditions of dust cloud generation. *VDI berichte Nr. 701*.

Eckhoff, R. K. (2003). Dust explosions in the process industries.

Eckhoff, R. K. (2020). Fighting dust explosion hazards in the process industries. *Journal of loss prevention in the process industries*, *67*, 104225. https://doi.org/10.1016/j.jlp.2020.104225

Eckhoff, R. K. P., S. J. Gruvin, B. Hatcher, M. Johansson, T. (1986). Ignitability and Explosibility of Silicon Dust Clouds: Influence of Dust Fineness. *Journal of The Electrochemical Society*, *133*(12), 2631-2637.

El-Sayed, A. F. (2016). Fundamentals of Aircraft and Rocket Propulsion.

Enstad, G. A. (2009). Experimental Investigation of the Impedance Measurement Method for Detecting Dust and Gas Flames in a Flame Acceleration Tube. Development of Experimental Apparatus.

Glassman, I. (1960). Combustion of metals: physical considerations. *Solid Propellant Rocket Research, Progress in Astrronautics and Aeronautics*, 253-258.

Glassman, I. (2008). Combustion.

Hussaini, Y. M., Kumar, A., & Voigt, G. R. (1992). Major Research Topics in Combustion. In: Springer.
Jinzhang, J., & Xiuyan, T. (2022). *Propagation and attenuation characteristics of shock waves in a gas-coal dust explosion in a diagonal pipeline network*. S. nature.
Kalvatn, I. B. (2009). Experimental investigation of the optical measurement method for detecting dust and gas flames in a flame acceleration tube : development of experimental apparatus.
Kauffman, C. W. (1982). Agricultural dust explosions in grain handling facilities. *Fuel-air Explosions, Ontario, Canada*, 305-347.
Krehl, P. O. K. (2008). History of Shock Waves, Explosions and Impact: A Chronological and Biographical Reference. https://doi.org/10.1007/978-3-540-30421-0
Lee, S., H, John. (1984). Dynamic parameters of gaseous detonations. *Fluid mechanics*, *16*, 311-336.
Lee, S. H. J. (2008). *The detonation phenomenon*. Cambridge University Press.
Li, G., Yang, H. X., Yuan, C. M., & Eckhoff, R. K. (2016). A catastrophic aluminium-alloy dust explosion in China. *Journal of loss prevention in the process industries*, *39*, 121-130. https://doi.org/10.1016/j.jlp.2015.11.013
Li, Y.-C., Kauffman, C. W., & Sichel, M. (1995). An experimental study of deflagration to detonation transition supported by dust layers. *Combustion and Flame*, *100*(3), 505-515.
Liu, Q., Bai, C., Jiang, L., Dai, W., & Niu, F. (2011). Deflagration-to-detonation transition process for spherical aluminum dust/epoxypropane mist/air mixtures in a large-scale experimental tube. *Science China. Physics, mechanics & astronomy*, *54*(3), 533-541. https://doi.org/10.1007/s11433-011-4252-x
Liu, Q., Li, X., & Bai, C. (2009). Deflagration to detonation transition in aluminum dust–air mixture under weak ignition condition. *Combustion and flame*, *156*(4), 914-921. https://doi.org/10.1016/j.combustflame.2008.10.025
Marmo, L., Riccio, D., & Danzi, E. (2017). Explosibility of metallic waste dusts. *Process safety and environmental protection*, *107*, 69-80. https://doi.org/10.1016/j.psep.2017.01.011
Martin, R. K. (2013). Silicon: The Health Benefits of a Metalloid. In *Interrelations between Essential Metal ions and Human Diseases* (Vol. 13, pp. 451-473). Springer. https://doi.org/https://doi.org/10.1007/978-94-007-7500-8_14
Matsuda, T. (1995). *8. Explosion hazard of metallic silicon dust* (UDC 546.28:614.23:661.8).
Matsuda, T., Yashima, M., Nifuku, M., & Enomoto, H. (2001). Some aspects in testing and assessment of metal dust explosions. *Journal of loss prevention in the process industries*, *14*(6), 449-453. https://doi.org/10.1016/S0950-4230(01)00033-X
Morozzo, C. (1795). *Account of a violent explosion which happened in a flour-warehouse, at Turin, December the 14th, 1785, to which are added some observations on spontaneous inflammations* (Vol. 2).
Norsk Standard, NS-EN 14034-1:2007+A1:2011 D*etermination of explosion characteristics of dust clouds - Part 1: Determination of the maximum explosion pressure* pm_{ax} *of dust clouds*, (2011a).
Norsk Standard, NS-EN 14034-2:2006+A1:2011 *Determination of explosion characteristics of dust clouds - Part 2: Determination of the maximum rate of explosion pressure rise (dp/dt)max of dust clouds*, (2011b).
Norsk Standard, NS-EN 14491:2012, *Dust explosion venting protective systems*. In S. Norge (Ed.).
Ogle, A. R. (2017). *Dust Explosion Dynamics*. Elsevier.
Proust, C. (1996). Dust explosions in pipes: A review. *Journal of loss prevention in the process industries*, *9*(4), 267-277. https://doi.org/10.1016/0950-4230(96)00010-1
Ragland, K. W. B., Kenneth M. (2011). *Combustion Engineering* (Second ed.). Taylor & Francis Group.
Rockwell, S. R., & Rangwala, A. S. (2013). Modeling of dust air flames. *Fire safety journal*, *59*, 22-29. https://doi.org/10.1016/j.firesaf.2013.03.006
Rudinger, G. (1980). *Fundamentals of gas-particle flow*. Elsevier.
Rumble, R. J., Lide, R. D., & Doa, J. M. (2022). *CRC Handbook of Chemistry and Physics* (103th Edition ed.). CRC Press.

Shepherd, E. J., & Lee, S. H. J. (1992). On the transition from deflagration to detonation. *Major Research Topics in Combustion*, *ICASE/NASA LaRC Series.* https://doi.org/https://doi.org/10.1007/978-1-4612-2884-4_22

Skjold, T. (2003). Selected aspects of turbulence and combustion in 20-litre explosion vessels : development of experimental apparatus and experimental investigation.

Skjold, T. (2007). Review of the DESC project. *Journal of loss prevention in the process industries*, *20*(4), 291-302. https://doi.org/10.1016/j.jlp.2007.04.017

Skjold, T., Castellanos, D., Olsen, K. L., & Eckhoff, R. K. (2014). Experimental and numerical investigation of constant volume dust and gas explosions in a 3.6-m flame acceleration tube. *Journal of loss prevention in the process industries*, *30*, 164-176. https://doi.org/10.1016/j.jlp.2014.05.010

Skjold, T., Kalvatn, B. I., Enstad, A. G., & Eckhoff, K. E. (2009, 27-31 Juli 2009). *Experimental investigation of the influence of obstacles on flame propagation in propane-air mixtures and dust-air suspensions in a 3.6 m flame acceleration tube* Twenty-second International Colloquium on the Dynamics of Explosions and Reactive Systems (ICDERS), Minsk, Belarus.

Taveau, J., Vingerhoets, J., Snoeys, J., Going, J., & Farrell, T. (2015). Suppression of metal dust deflagrations. *Journal of loss prevention in the process industries*, *36*, 244-251. https://doi.org/10.1016/j.jlp.2015.02.011

Taveau, R., Jerome., Lemkowitz, M., Saul., Hochgreb, S., & Roekaerts, J. E. M., Dirk. (2019). Metal dusts explosion hazards and protection. *Chemical engineering transactions*, *77*. https://doi.org/https://doi.org/10.3303/CET1977002

Turns, S. R. (2000). An introduction to combustion : concepts and applications. (McGraw-Hill series in mechanical engineering)

van der Wel, P. L., Saul. Scarlett, Brian. van Wingerden, Kees. (1991). A Study of Particle Factors Affecting Dust Explosions. *Particle and Particle Systems Characterizations*, *8*(1-4), 90-94.

Warnatz, J., Maas, U., Dibble, R. W., & Warnatz, J. (2006). Combustion: Physical and Chemical Fundamentals, Modeling and Simulation, Experiments, Pollutant Formation. https://doi.org/10.1007/978-3-540-45363-5

Wiemann, W. (1987). Influence of Temperature and Pressure on the Explosion Characteristics of Dust/Air mixture and Dust/Air/Inert Gas Mixtures. In *Industrial Dust Explosions"* (K.L. Cashdollar and M. Hetzberg ed., pp. 33 -45). ASTM Special Technical Publication 958.

Yetter, A. R., & Dryer, L. F. (2001). Metal Particle Combustion and Classification. In E. D. Ross (Ed.), *Microgravity Combustion: Fire in Free Fall* (pp. 419-478). Academic Press.

Young, D. H., Freedman, A. R., & Ford, L. A. (2004). Sears and Zemansky's University Physics with Modern Physics, 11th Ed. *SciTech Book News*, *28*(1), 46.

Yuan, Z., Khakzad, N., Khan, F., & Amyotte, P. (2015). Dust explosions: A threat to the process industries. *Process safety and environmental protection*, *98*, 57-71. https://doi.org/10.1016/j.psep.2015.06.008

Zhang, F., Gronig, H., & van de Ven, A. (2001). DDT and detonation waves in dust-air mixtures. *Shock waves*, *11*(1), 53-71. https://doi.org/10.1007/PL00004060

Zhang, F., Murray, S. B., & Gerrard, K. B. (2010). Aluminium dust-air detonation at elevated pressures. 795-800. https://doi.org/10.1007/978-3-540-27009-6_119

Østgård, T. (2022). En eksperimentell studie av partikkelstørrelsesfordelingens innvirkning på utvalgte eksplosjonsparametere for silisiumstøv. *An experimental study of the effect of particle size distribution on selected silicon dust explosion parameters*.

APPENDIX A

Figure A-1 illustrate the ignition chamber in its two different forms, the chamber on the top is connected directly to DN250, whilst the one on the bottom is connected to a crossover, so it can be connected to DN160.

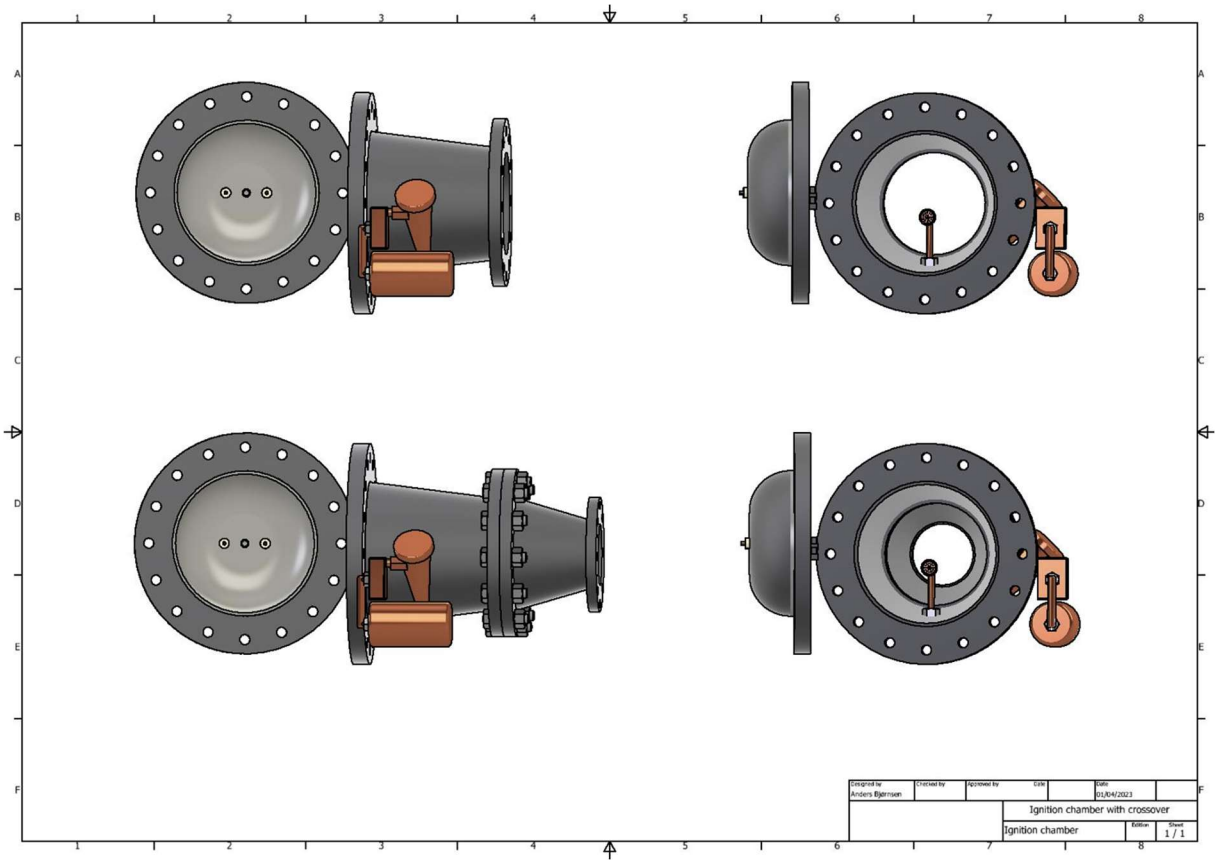

Figure A-1 : Ignition chamber configurations used during the experiments.

APPENDIX B

Malvern reports of the particle size distributions are presented in Figures B-1 and B-2. Some selected reports from the KSEP 7.1 software is presented in Figure B-3 to B-8.

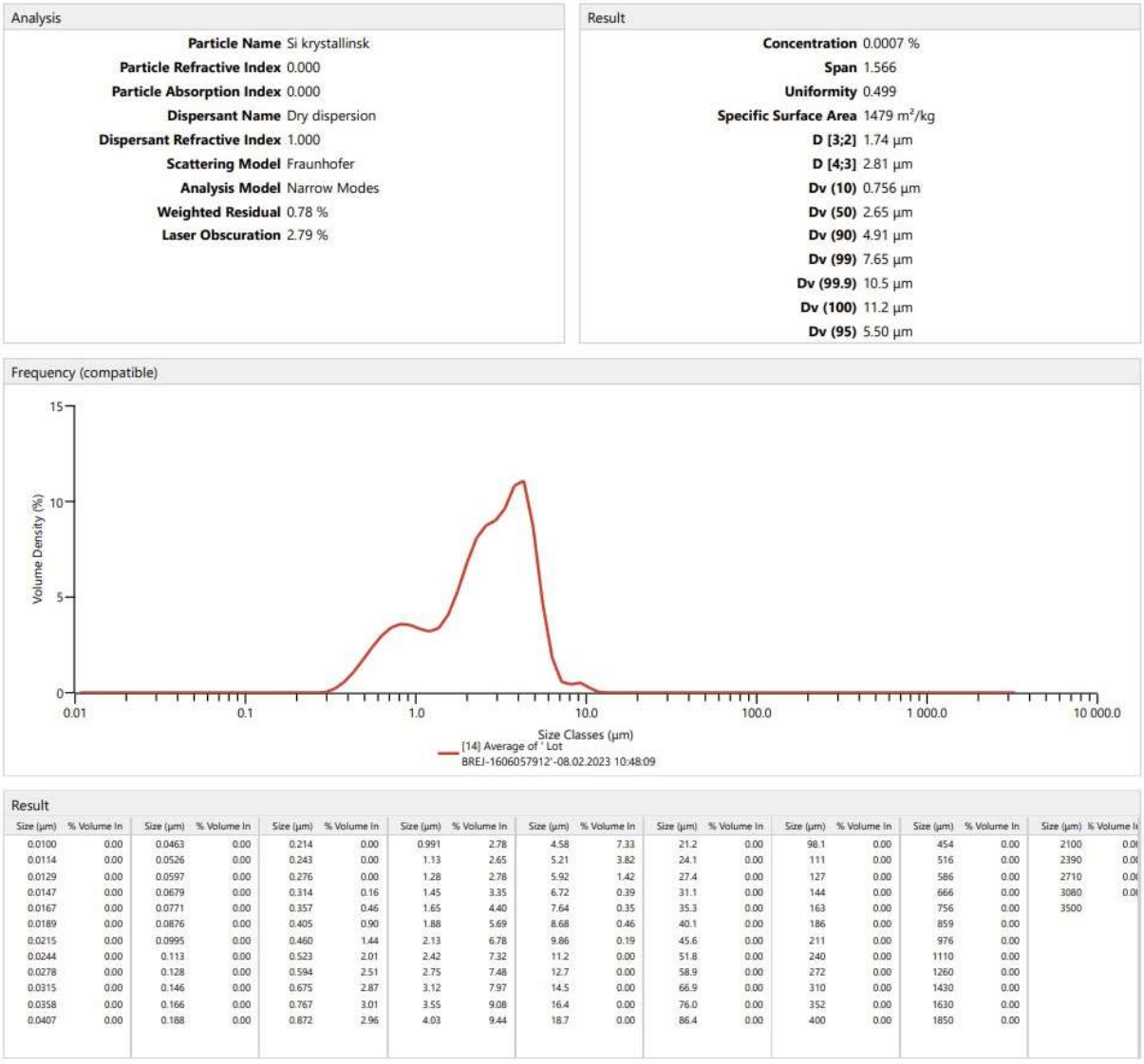

Analysis

Particle Name	Si krystallinsk
Particle Refractive Index	0.000
Particle Absorption Index	0.000
Dispersant Name	Dry dispersion
Dispersant Refractive Index	1.000
Scattering Model	Fraunhofer
Analysis Model	Narrow Modes
Weighted Residual	0.78 %
Laser Obscuration	2.79 %

Result

Concentration	0.0007 %
Span	1.566
Uniformity	0.499
Specific Surface Area	1479 m²/kg
D [3;2]	1.74 µm
D [4;3]	2.81 µm
Dv (10)	0.756 µm
Dv (50)	2.65 µm
Dv (90)	4.91 µm
Dv (99)	7.65 µm
Dv (99.9)	10.5 µm
Dv (100)	11.2 µm
Dv (95)	5.50 µm

Frequency (compatible)

Result

Size (µm)	% Volume In	Size (µm)	% Volume In	Size (µm)	% Volume In	Size (µm)	% Volume In	Size (µm)	% Volume In	Size (µm)	% Volume In	Size (µm)	% Volume In	Size (µm)	% Volume In	Size (µm)	% Volume In
0.0100	0.00	0.0463	0.00	0.214	0.00	0.991	2.78	4.58	7.33	21.2	0.00	98.1	0.00	454	0.00	2100	0.0
0.0114	0.00	0.0526	0.00	0.243	0.00	1.13	2.65	5.21	3.82	24.1	0.00	111	0.00	516	0.00	2390	0.0
0.0129	0.00	0.0597	0.00	0.276	0.00	1.28	2.78	5.92	1.42	27.4	0.00	127	0.00	586	0.00	2710	0.0
0.0147	0.00	0.0679	0.00	0.314	0.16	1.45	3.35	6.72	0.39	31.1	0.00	144	0.00	666	0.00	3080	0.0
0.0167	0.00	0.0771	0.00	0.357	0.46	1.65	4.40	7.64	0.35	35.3	0.00	163	0.00	756	0.00	3500	
0.0189	0.00	0.0876	0.00	0.405	0.90	1.88	5.69	8.68	0.46	40.1	0.00	186	0.00	859	0.00		
0.0215	0.00	0.0995	0.00	0.460	1.44	2.13	6.78	9.86	0.19	45.6	0.00	211	0.00	976	0.00		
0.0244	0.00	0.113	0.00	0.523	2.01	2.42	7.32	11.2	0.00	51.8	0.00	240	0.00	1110	0.00		
0.0278	0.00	0.128	0.00	0.594	2.51	2.75	7.48	12.7	0.00	58.9	0.00	272	0.00	1260	0.00		
0.0315	0.00	0.146	0.00	0.675	2.87	3.12	7.97	14.5	0.00	66.9	0.00	310	0.00	1430	0.00		
0.0358	0.00	0.166	0.00	0.767	3.01	3.55	9.08	16.4	0.00	76.0	0.00	352	0.00	1630	0.00		
0.0407	0.00	0.188	0.00	0.872	2.96	4.03	9.44	18.7	0.00	86.4	0.00	400	0.00	1850	0.00		

Figure B-1: Particle size distribution for Si-1.

Analysis	
Particle Name	Si krystallinsk
Particle Refractive Index	0.000
Particle Absorption Index	0.000
Dispersant Name	Dry dispersion
Dispersant Refractive Index	1.000
Scattering Model	Fraunhofer
Analysis Model	Narrow Modes
Weighted Residual	0.74 %
Laser Obscuration	1.67 %

Result	
Concentration	0.0026 %
Span	3.769
Uniformity	1.154
Specific Surface Area	219.6 m²/kg
D [3;2]	11.7 µm
D [4;3]	78.7 µm
Dv (10)	5.55 µm
Dv (50)	50.3 µm
Dv (90)	195 µm
Dv (99)	373 µm
Dv (99.9)	701 µm
Dv (100)	754 µm
Dv (95)	251 µm

Frequency (compatible)

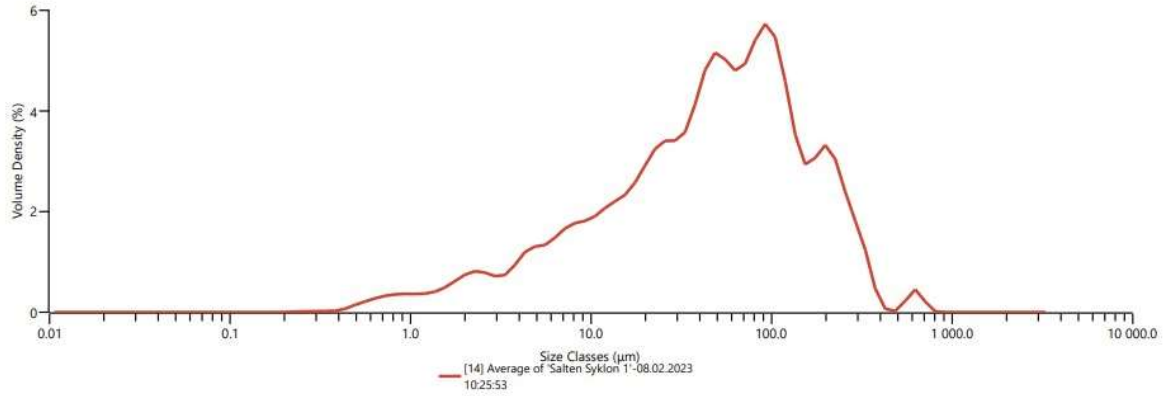

Result

Size (µm)	% Volume In	Size (µm)	% Volume In	Size (µm)	% Volume In	Size (µm)	% Volume In	Size (µm)	% Volume In	Size (µm)	% Volume In	Size (µm)	% Volume In	Size (µm)	% Volume In	Size (µm)	% Volume In
0.0100	0.00	0.0463	0.00	0.214	0.01	0.991	0.30	4.58	1.09	21.2	2.72	98.1	4.61	454	0.00	2100	0.0
0.0114	0.00	0.0526	0.00	0.243	0.01	1.13	0.31	5.21	1.10	24.1	2.85	111	3.84	516	0.19	2390	0.0
0.0129	0.00	0.0597	0.00	0.276	0.02	1.28	0.34	5.92	1.23	27.4	2.83	127	2.91	586	0.42	2710	0.0
0.0147	0.00	0.0679	0.00	0.314	0.02	1.45	0.41	6.72	1.39	31.1	2.95	144	2.39	666	0.17	3080	0.0
0.0167	0.00	0.0771	0.00	0.357	0.02	1.65	0.51	7.64	1.48	35.3	3.43	163	2.55	756	0.00	3500	
0.0189	0.00	0.0876	0.00	0.405	0.05	1.88	0.63	8.68	1.51	40.1	4.04	186	2.81	859	0.00		
0.0215	0.00	0.0995	0.00	0.460	0.12	2.13	0.69	9.86	1.58	45.6	4.34	211	2.57	976	0.00		
0.0244	0.00	0.113	0.00	0.523	0.18	2.42	0.66	11.2	1.73	51.8	4.20	240	1.98	1110	0.00		
0.0278	0.00	0.128	0.00	0.594	0.23	2.75	0.59	12.7	1.84	58.9	3.98	272	1.51	1260	0.00		
0.0315	0.00	0.146	0.00	0.675	0.27	3.12	0.60	14.5	1.94	66.9	4.09	310	1.05	1430	0.00		
0.0358	0.00	0.166	0.00	0.767	0.30	3.55	0.78	16.4	2.14	76.0	4.52	352	0.36	1630	0.00		
0.0407	0.00	0.188	0.00	0.872	0.30	4.03	1.01	18.7	2.43	86.4	4.82	400	0.03	1850	0.00		

Figure B-2: Particle size distribution of Si-2.

Universitetet i Bergen - Dust lab

Sample:	**Silgrain micron cut 8**
Customer:	
Reason:	
Data to sample origin:	
Preparation of sample:	
Median value:	

Explosion Characteristics

Max. explosion pressure:	Pmax	=	**9,5**	bar	± 10%
Max. rate of pressure rise:	(dP/dt)max	=	**716**	bar / s	± 12%
Product specific constant:	Kmax	=	**194**	m·bar / s	± 12%

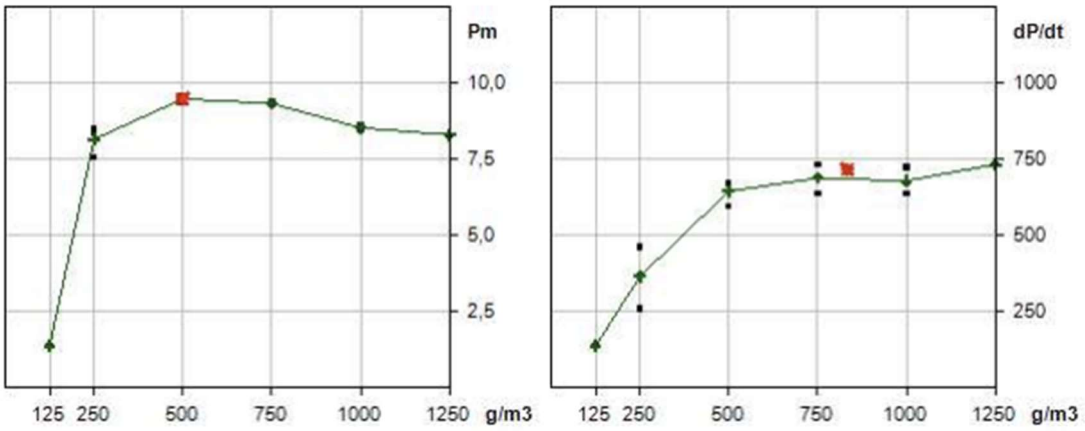

Figure B-3: KSEP 7.1 report, P_{max} and K_{St} of Si-1 series 1/2

Dust: Pmax, Kmax **Silgrain micron cut 8**

Test	Series	Conc. [g/m3]	Pm [bar]	dP/dt [bar/s]	tv eff [ms]
1	1	125	1,4	136	60
2	1	250	7,6	260	60
3	1	500	**9,5**	665	60
4	1	750	9,4	**733**	59
5	1	1000	8,6	674	60
6	1	1250	8,3	732	60
7	-	250	,0	0	60
8	-	500	,0	188?	60
9	2	250	8,4	461	60
10	2	500	**9,6**	673	60
11	2	750	9,3	637	60
12	-	1000	8,7	887	60
13	2	1000	8,5	**724**	61
14	3	250	8,5	370	61
15	3	500	**9,4**	594	60
16	3	750	9,3	**691**	60
17	3	1000	8,4	636	60

Figure B-4: KSEP 7.1 report, P_{max} and K_{St} of Si-1 series 2/2

Universitetet i Bergen - Dust lab

Sample:	**Si Salten**
Customer:	
Reason:	
Data to sample origin:	
Preparation of sample:	
Median value:	

Explosion Characteristics

Max. explosion pressure:	Pmax	=	**7,9**	bar	± 10%
Max. rate of pressure rise:	(dP/dt)max	=	**299**	bar / s	± 20%
Product specific constant:	Kmax	=	**81**	m·bar / s	± 20%

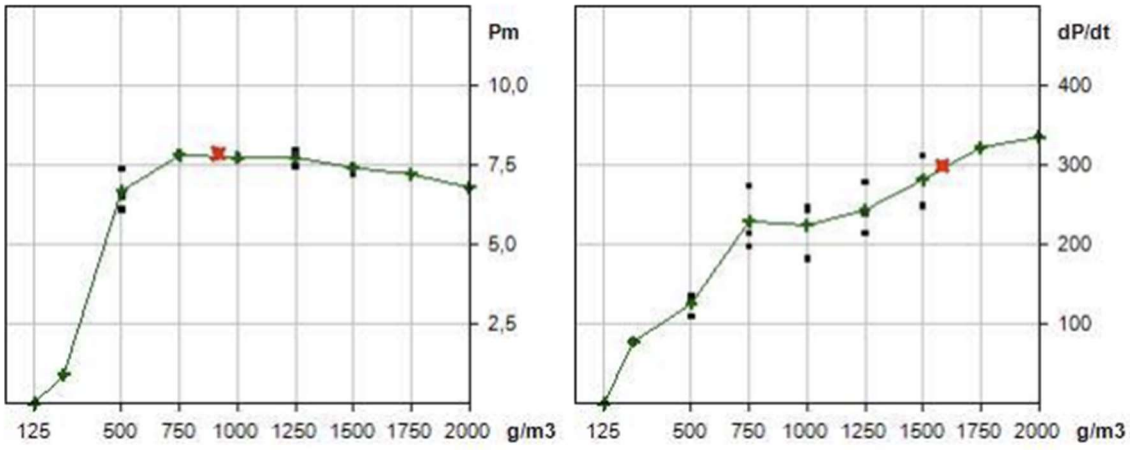

Figure B-5: KSEP 7.1 report, P_{max} and K_{St} of Si-2 series 1/2

Dust: Pmax, Kmax **Si Salten**

Test	Series	Conc. [g/m3]	Pm [bar]	dP/dt [bar/s]	tv eff [ms]
1	1	125	,0	0	60
2	1	250	,9	78	60
3	1	500	6,1	136	61
4	1	750	**7,8**	198	60
5	1	1000	7,7	247	60
6	1	1250	7,5	214	60
7	1	1500	7,2	312	61
8	1	1750	7,2	322	60
9	1	2000	6,8	**335**	60
10	2	500	7,4	130	60
11	2	750	7,7	215	60
12	2	1000	7,8	182	60
13	2	1250	**7,9**	238	60
14	2	1500	7,5	**284**	61
15	3	500	6,5	109	60
16	3	750	**7,9**	274	60
17	3	1000	7,7	243	60
18	3	1250	7,8	**278**	60
19	-	1500	,0	0	60
20	-	1500	8,0	327	60
21	3	1500	7,5	249	60

Figure B-6: KSEP 7.1 report, P_{max} and K_{St} of Si-2 series 2/2.

Universitetet i Bergen - Dust lab

Sample: **Silgrain microncut 8**
Customer:
Reason:
Data to sample origin:
Preparation of sample:
Median value:

Explosion Characteristics

Lower explosion limit: LEL = **100** g/m3 ± 10%

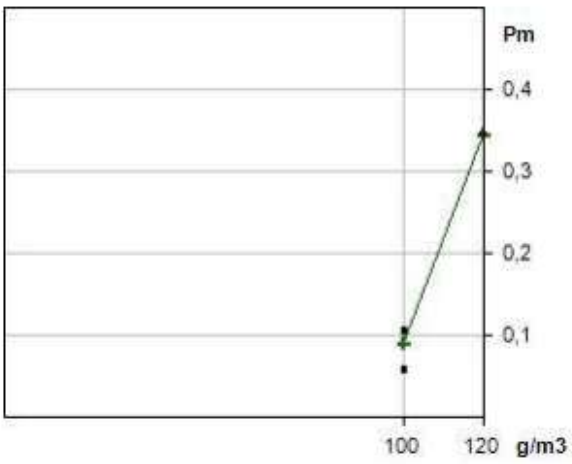

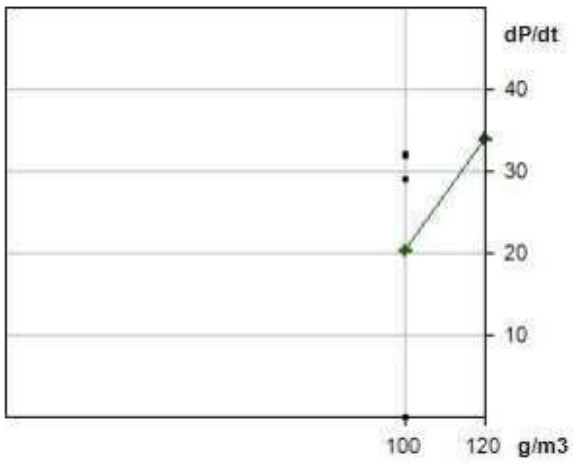

Dust: LEL **Silgrain microncut 8**

Test	Series	Conc. [g/m3]	Pm [bar]	dP/dt [bar/s]	tv eff [ms]
1	1	100	,1	32	59
2	1	100	,1	29?	60
3	1	100	,1	0	60
4	1	120	**,3**	**34**	60

Figure B-7: KSEP report , LEL of Si-1.

Universitetet i Bergen - Dust lab

Sample: **Si salten**
Customer:
Reason:
Data to sample origin:
Preparation of sample:
Median value:

Explosion Characteristics

Lower explosion limit: LEL = **180** g/m3 ± 10%

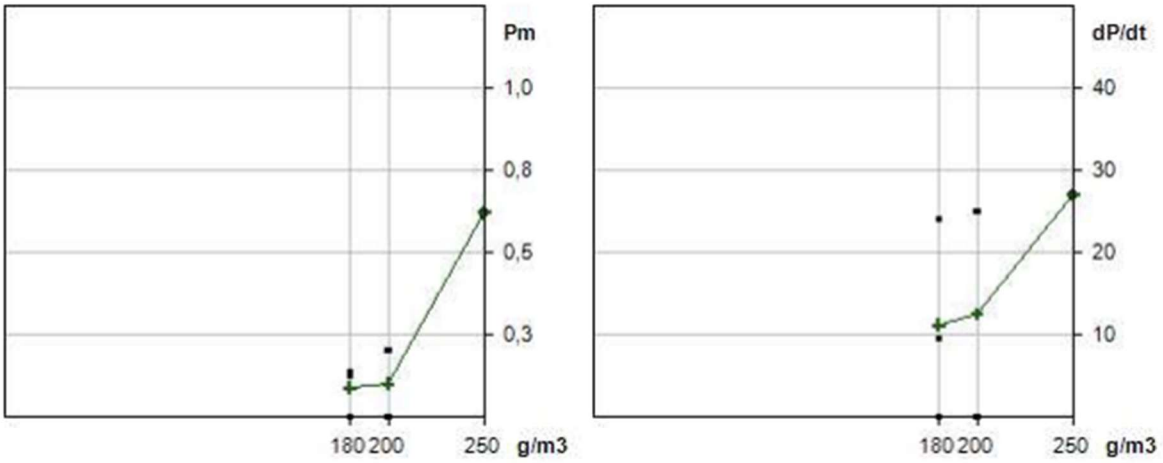

Dust: LEL **Si salten**

Test	Series	Conc. [g/m3]	Pm [bar]	dP/dt [bar/s]	tv eff [ms]
1	1	250	**,6**	**27**	60
2	1	200	,0	0	60
3	1	200	,2	25	60
4	1	180	,1	24	60
5	1	180	,1	10	60
6	1	180	,0	0	60

Figure B-8: KSEP report, LEL of Si-2.

APPENDIX C

The manually selected thermocouple signals are presented in Figure C-1 to C-7. All the velocities are presented in Table C-1 to C-7. The orange cells in the tables illustrate faulty thermocouple signals and velocities based on the saturated datapoints. These values are only included to illustrate thermocouple signal delay and uncertainty of the manual selection of data points.

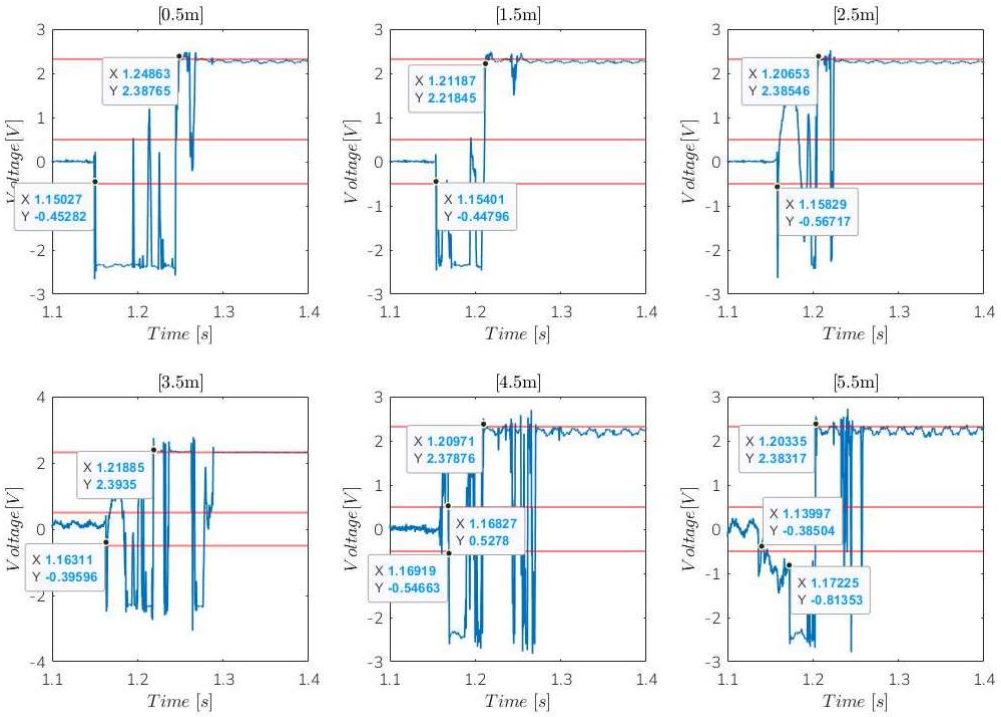

Figure C-1: Selected datapoints from the thermocouple signals for Si-1, 250 g/m^3.

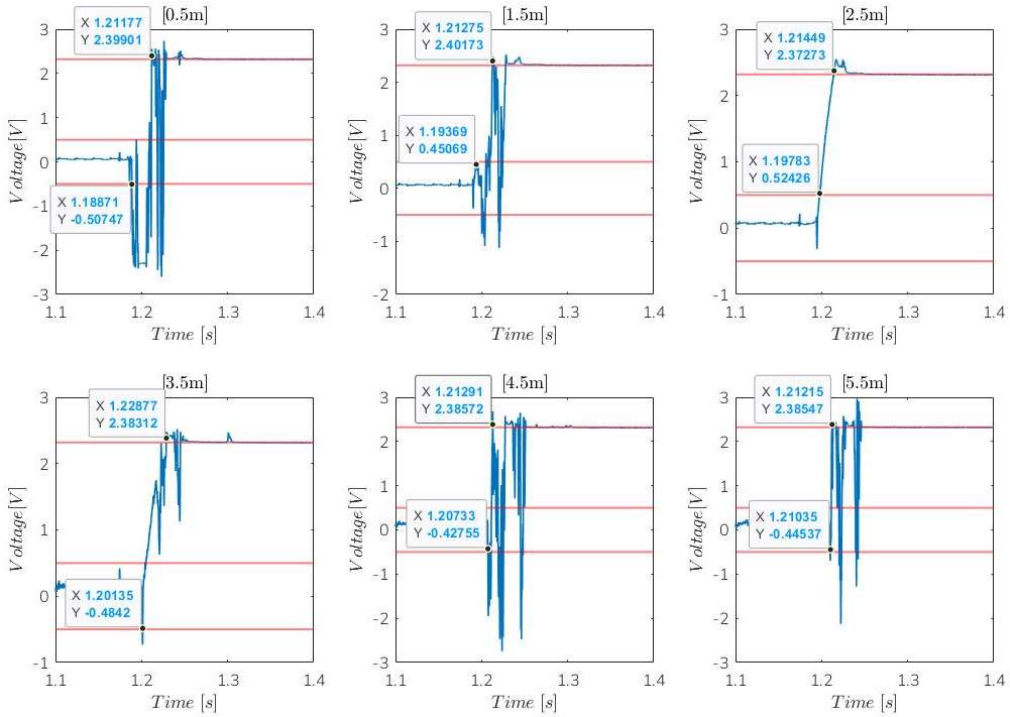

Figure C-2: Selected datapoints from the thermocouple signals for Si-1, 500 g/m³

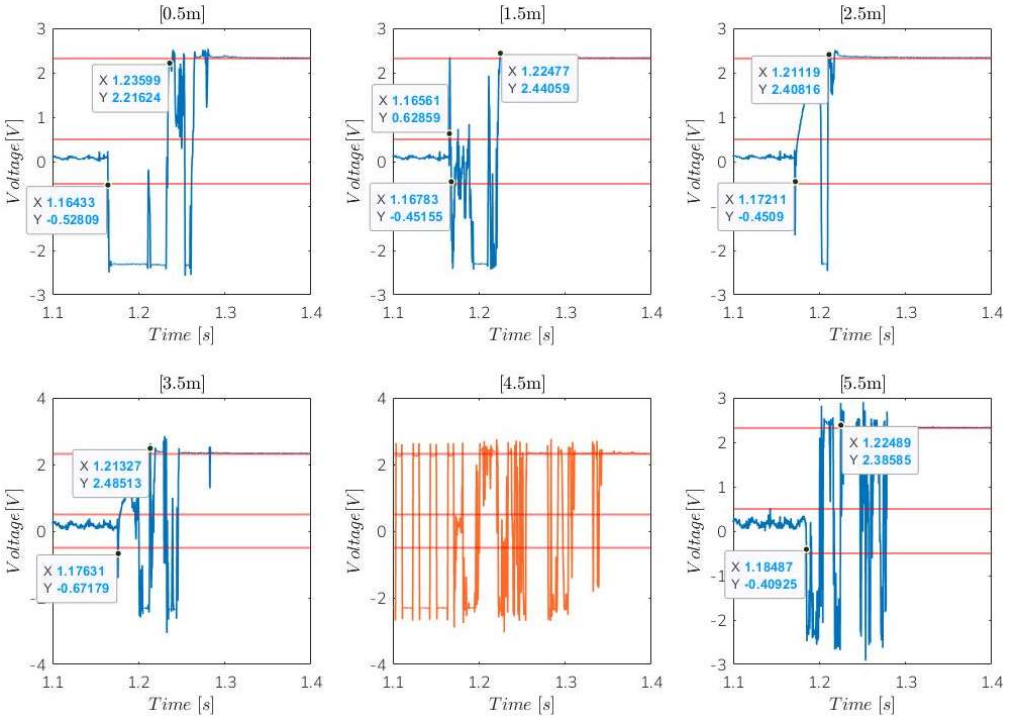

Figure C-3: Selected datapoints from the thermocouple signals for Si-1, 750 g/m³.

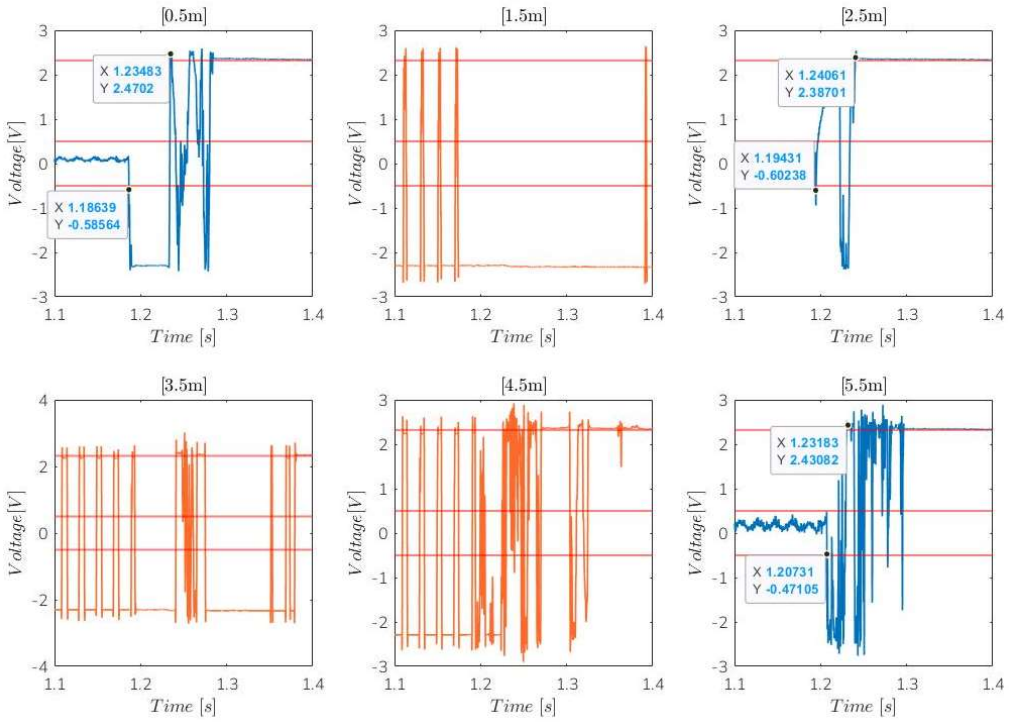

Figure C-4: Selected datapoints from the thermocouple signals for Si-1, 1000 g/m³.

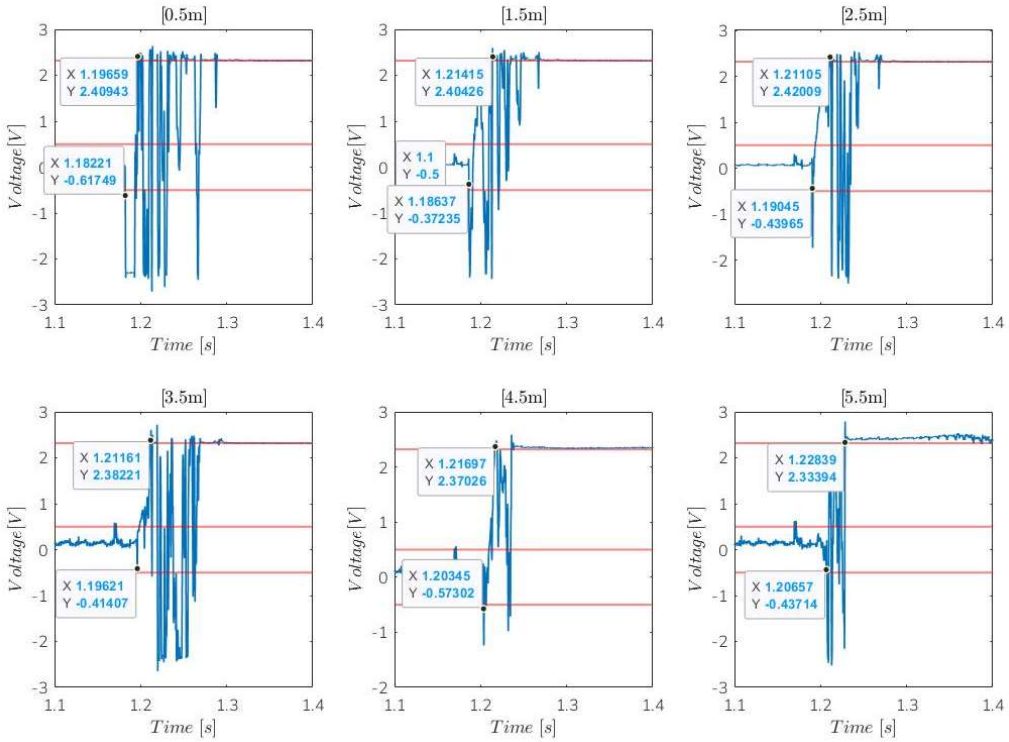

Figure C-5: Selected datapoints from the thermocouple signals for Si-1, ignition chamber first test.

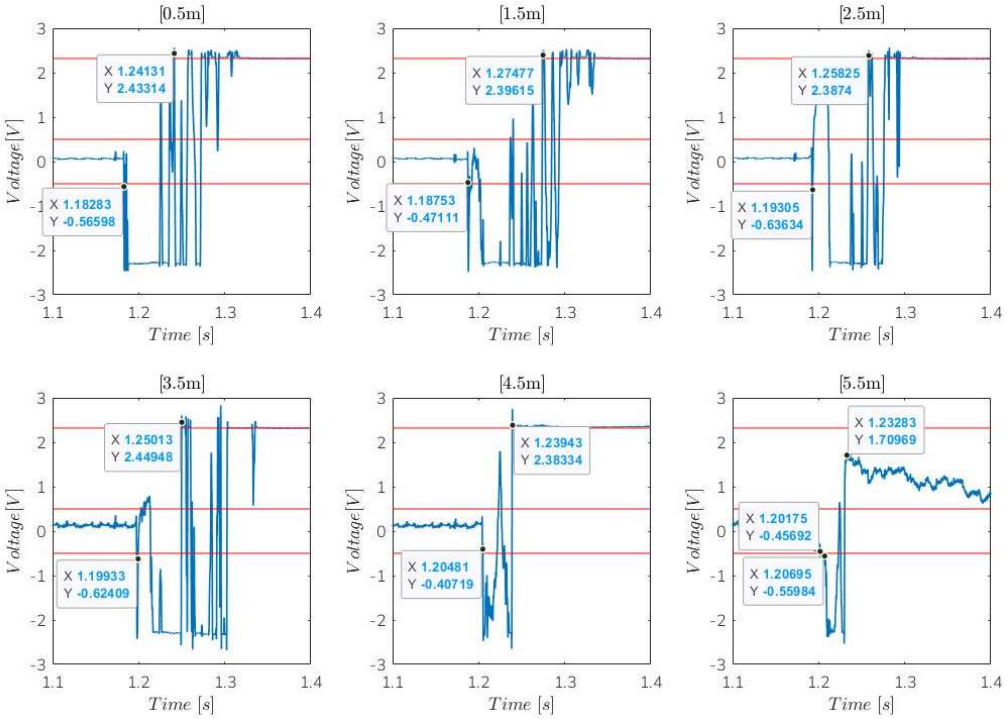

Figure C-6: Selected datapoints from the thermocouple signals for Si-1, ignition chamber second test.

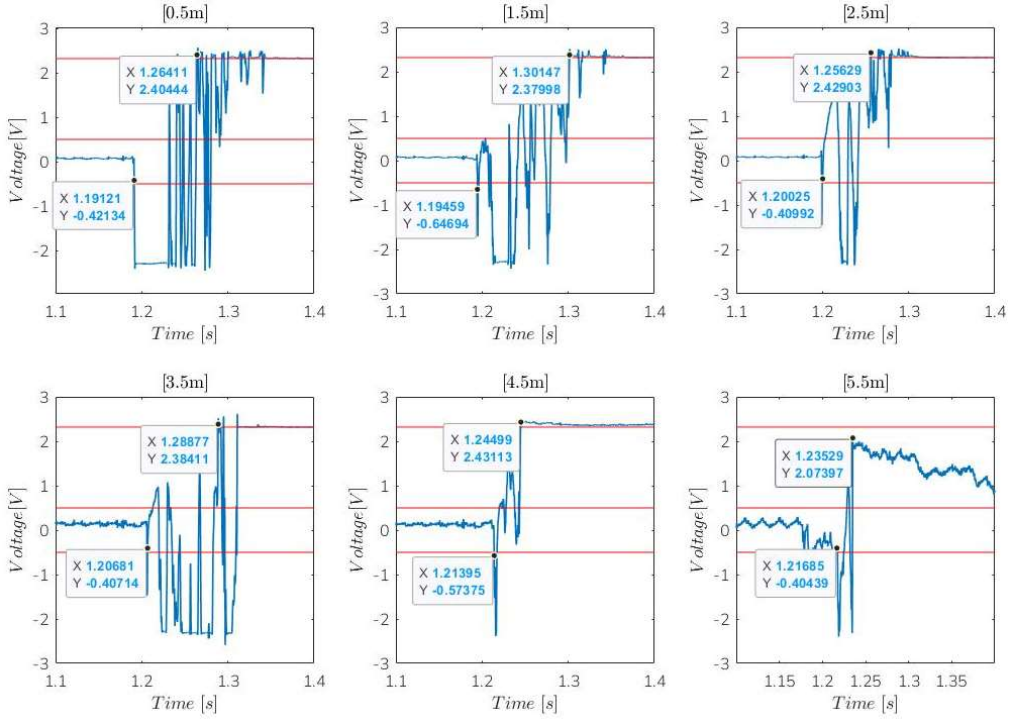

Figure C-7: Selected datapoints from the thermocouple signals for Si-1, ignition chamber third test.

Table C-1: Datapoints and velocities, configuration 1, Si-1 250 g/m³.

Location	Time	Velocity	Time saturated	Saturated Velocity
0.5	1.15027		1.24863	
1.5	1.15401	267.38	1.21187	-27.20
2.5	1.15829	233.64	1.20653	-187.27
3.5	1.16311	207.47	1.21885	81.17
4.5	1.16919	164.47	1.20971	-109.41
5.5	1.17225	326.80	1.20335	-157.23

Table C-2: Datapoints and velocities, configuration 1, Si-1 500 g/m³.

Location [m]	Time [s]	Velocity [m/s]	Time saturated [s]	Saturated velocity [m/s]
0.5	1.18871		1.21177	
1.5	1.19369	200.80	1.21275	1020.41
2.5	1.19783	241.55	1.21449	574.71
3.5	1.20135	284.09	1.22877	70.03
4.5	1.20733	167.22	1.21291	
5.5	1.21035	222.22	1.21215	-120.34

Table C-3: Datapoints and velocities, configuration 1, Si-1 750 g/m³.

Location [m]	Time [s]	Velocity [m/s]	Time saturated [s]	Saturated velocity [m/s]
0.5	1.16433		1.23599	
1.5	1.16783	285.71	1.22477	-89.13
2.5	1.17211	233.64	1.21119	-73.64
3.5	1.17631	238.10	1.21327	480.77
4.5				
5.5	1.18487	233.64	1.22489	172.12

Table C-4: Datapoints and velocities, configuration 1, Si-1 1000 g/m³.

Location [m]	Time [s]	Velocity [m/s]	Time saturated [s]	Saturated velocity [m/s]
0.5	1.18639		1.23483	
1.5				
2.5	1.19431	252.53	1.24061	346.02
3.5				
4.5				
5.5	1.20731	230.77	1.23183	-341.69

Table C-5: Datapoints and velocities, configuration 1, only ignition chamber test 1.

Location [m]	Time [s]	Velocity [m/s]	Time saturated [s]	Saturated velocity [m/s]
0.5	1.18221		1.19659	
1.5	1.18637	240.38	1.21415	56.95
2.5	1.19045	245.10	1.21105	-322.58
3.5	1.19621	173.61	1.21161	1785.71
4.5	1.20345	138.12	1.21697	337.84
5.5	1.20657	320.51	1.22839	87.57

Table C-6: Datapoints and velocities, configuration 1, only ignition chamber test 2.

Location [m]	Time [s]	Velocity [m/s]	Time saturated [s]	Saturated velocity [m/s]
0.5	1.18283		1.24131	
1.5	1.18753	212.77	1.27477	29.89
2.5	1.19305	181.16	1.25825	-60.53
3.5	1.19933	159.24	1.25013	-123.15
4.5	1.20481	182.48	1.23943	-93.46
5.5	1.20695	467.29	1.23283	-151.52

Table C-7: Datapoints and velocities, configuration 1, only ignition chamber test 3.

Location [m]	Time [s]	Velocity [m/s]	Time saturated [s]	Saturated velocity [m/s]
0.5	1.19121		1.26411	
1.5	1.19459	295.86	1.30147	26.77
2.5	1.20025	176.68	1.25629	-22.13
3.5	1.20681	152.44	1.28877	30.79
4.5	1.21395	140.06	1.24499	-22.84
5.5	1.21685	344.83	1.23529	-103.09